NTNU – Trondheim
Norwegian University of
Science and Technology

Analysis of the radiant heating and cooling System in the Green Energy Laboratory

Ludvig Nielsen

Master of Energy and Environmental Engineering
Submission date: March 2015
Supervisor: Vojislav Novakovic, EPT
Co-supervisor: Laurent Georges, EPT
Yanjun Dai, SJTU

Norwegian University of Science and Technology
Department of Energy and Process Engineering

NTNU
Norwegian University
of Science and Technology

Department of Energy
and Process Engineering

EPT-M-2014-76

MASTER THESIS

for

Student Ludvig Nielsen

Autumn 2014

Analysis of the radiant heating and cooling system in the Green Energy Laboratory

Analyse av systemet for oppvarming og kjøling basert på stråling i Green Energy Laboratory

Background and objective

Super-insulated envelopes of modern buildings put new demands on performances of heating and cooling installations. Radiant heating and cooling systems are promising techniques that could contribute to enhanced efficiency of energy utilisation and improved indoor environment in modern buildings. Combination of these two techniques with the use of renewable energy (e.g. solar, ground) and heat storage give also many advantages.

The goal for this collaborative activity is to analyse the radiant heating and cooling system installed at the Green Energy Laboratory (GEL) of the Jiao Tong University in Shanghai (SJTU), China, by use of simulations and laboratory measurements. The necessary background for this work was partly developed through the project assignment accomplished at NTNU. The major part of the work on analysis and development of design methods will be performed during this Master thesis work that will be accomplished at the GEL of the Jiao Tong University in Shanghai. This collaborative assignment is realised as a part of the Joint Research Centre in Sustainable Energy of NTNU and SJTU.

The following tasks are to be considered:

1. Establish/Select an appropriate model for simulation the GEL installation for radiant heating and cooling using the simulation tool TRNSYS.
2. Verify the established model by use of measured data from the GEL radiant heating and cooling system.
3. Conduct analysis of the GEL radiant heating and cooling systems focusing on their integration, design procedures, as well as the optimal use of renewable energy sources and heat storages.
4. Make a draft proposal (8-10 pages) for a scientific paper based on the main results of the work performed in the master thesis.
5. Make proposal for further work on the topic.

-- " --

Within 14 days of receiving the written text on the master thesis, the candidate shall submit a research plan for his project to the department.

When the thesis is evaluated, emphasis is put on processing of the results, and that they are presented in tabular and/or graphic form in a clear manner, and that they are analyzed carefully.

The thesis should be formulated as a research report with summary both in English and Norwegian, conclusion, literature references, table of contents etc. During the preparation of the text, the candidate should make an effort to produce a well-structured and easily readable report. In order to ease the evaluation of the thesis, it is important that the cross-references are correct. In the making of the report, strong emphasis should be placed on both a thorough discussion of the results and an orderly presentation.

The candidate is requested to initiate and keep close contact with his/her academic supervisor(s) throughout the working period. The candidate must follow the rules and regulations of NTNU as well as passive directions given by the Department of Energy and Process Engineering.

Risk assessment of the candidate's work shall be carried out according to the department's procedures. The risk assessment must be documented and included as part of the final report. Events related to the candidate's work adversely affecting the health, safety or security, must be documented and included as part of the final report. If the documentation on risk assessment represents a large number of pages, the full version is to be submitted electronically to the supervisor and an excerpt is included in the report.

Pursuant to "Regulations concerning the supplementary provisions to the technology study program/Master of Science" at NTNU §20, the Department reserves the permission to utilize all the results and data for teaching and research purposes as well as in future publications.

The final report is to be submitted digitally in DAIM. An executive summary of the thesis including title, student's name, supervisor's name, year, department name, and NTNU's logo and name, shall be submitted to the department as a separate pdf file. Based on an agreement with the supervisor, the final report and other material and documents may be given to the supervisor in digital format.

☒ Work to be done in lab (Green Energy Laboratory, Shanghai Jiao Tong University, China)
☒ Field work

Department of Energy and Process Engineering, 14. August 2014

Olav Bolland
Department Head

Vojislav Novakovic
Academic Supervisor

Research Advisors:
Prof. Yanjun DAI, Shanghai Jiao Tong University, e-mail: yjdai@sjtu.edu.cn
Prof. Tianshu GE, e-mail: baby_wo@sjtu.edu.cn
Prof. Laurent Georges, NTNU

PREFACE

This master thesis is written at the Norwegian University of Science and Technology, in collaboration with the Shanghai Jiao Tong University. The work consists of an analysis of a hydronic radiant heating system installed at the Green Energy Laboratory at SJTU. The main part of the master work was conducted in Shanghai.

I would like to thank my main supervisor, Professor Vojislav Novakovic for his guidance and for giving me the opportunity to conduct this work in collaboration with SJTU.

I would also like to express my gratitude to my supervisor at SJTU, Professor Yanjun Dai for supervising me during my stay in Shanghai.

I express my sincere thanks to my co-supervisor, Associate Professor Laurent Georges for helping and supporting me during the master thesis process. His contributions towards a final result have been of major importance.

Finally, I want to acknowledge the fellow students and researchers at the Green Energy Laboratory. They have helped greatly during my stay there.

Ludvig Nielsen *Trondheim 2015*

ABSTRACT

Climate change and energy scarcity put higher requirements on the use of energy in the society today. Buildings are a major contributor to the energy use and much attention is placed on energy efficient solutions in building services. One promising technology is hydronic radiant heating systems (RHS), which use moderate temperature water that can be supplied efficiently by "green" energy sources such as heat pumps, solar collectors and district heating. However, complexity in design and operation often makes RHS less competitive to traditional heating systems. Proper design procedures and control strategies should be developed in order to make this an economic solution for the future. In this work, a RHS installed at the Green Energy Laboratory (GEL) at the Shanghai Jiao Tong University (SJTU) is analyzed with the use of the simulation tool TRNSYS. A simulation model is built and validated against measurements from the actual system. The goal is to analyze the performance of the installed RHS for Chinese apartments in a Shanghai climate, with a focus on energy efficiency. The heat source is assumed to be an air source heat pump. Simulations are performed for different control strategies, insulation levels, heat pump sizes and thermal storages. Results show that the installed RHS can supply the entire heat load for a typical building in Shanghai. It is shown that for a colder climate a greater level of insulation is required, as the floor has a maximum heat output of about 50 W/m^2 at a supply temperature of 45°C. On/off thermostat control of the flow to each zone is confirmed to be sufficient. A stable heat pump operation is achieved with a storage tank, as cycling time is increased. Simulations are performed on fan coil units (FCU) as an alternative heat emitting system and results show that total heat demand is reduced by 11 %. However, the heat pump performance is reduced due to higher supply temperatures and the total electricity consumptions for the two systems are similar. RHS is here affirmed as a good solution for Chinese residential buildings, but a more detailed analysis of thermal comfort and a financial analysis should be conducted to assess its market competitiveness.

SAMMENDRAG

Klimaendringer og energiknapphet setter høyere krav til bruk av energi i dagens samfunn. Bygninger er en stor bidragsyter til energibruken og mye oppmerksomhet er gitt til energieffektive løsninger i bygg. En lovende teknologi er vannbårne oppvarmingsystemer basert på stråling (VOS), som bruker lav vanntemperatur som effektivt kan leveres fra "grønne" energikilder som varmepumper, solfangere og fjernvarme. Imidlertid kan kompleksiteten i forbindelse med dimensjonering og drift gjøre VOS mindre økonomisk konkurransedyktig i forhold til tradisjonelle oppvarmingssystemer. Gode dimensjoneringsprosedyrer og reguleringsstrategier burde utvikles for å gjøre VOS til en økonomisk bærekraftig løsning for fremtiden. I dette arbeidet har et VOS, installert i gulvet på Green Energy Laboratory ved Shanghai Jiao Tong University i Kina, blitt analysert ved bruk av simuleringsverktøyet TRNSYS. En simuleringsmodell er utviklet og validert i mot målinger fra det installerte systemet. Hensikten med arbeidet er å analysere oppvarmingssystemets ytelse for kinesiske boliger i Shanghai, med fokus på energieffektivitet. Varmekilden er antatt å være en luft-vann varmepumpe. Det er kjørt simuleringer for forskjellige reguleringsstrategier, isolasjonsnivåer, varmepumpe- og varmelagrings-størrelser. Resultatene viser at hele varmelasten og -behovet kan dekkes av det installerte systemet for en typisk kinesisk leilighet i Shanghai. For kaldere klima må isolasjonsnivået oppgraderes, da gulvet har en maksimal varmeytelse på 50 W/m^2 ved en tilførselstemperatur på 45°C. Av/på termostatregulering av vanntilførselen til hver enkel sone er bekreftet å være tilstrekkelig. Mer stabile driftsforhold for varmepumpen oppnås ved bruk av varmelagringstanker. Simuleringer av viftekonvektorer som alternativ varmeavgivelsessystem er gjennomført og viser at det total varmebehovet da er redusert med 11 %. Varmepumpens ytelse er imidlertid forringet p.g.a. høyere tilførselstemperatur på vannet og det totale elektriske forbruket er omtrent det samme for begge systemene. VOS er i dette arbeidet bekreftet som en god løsning for kinesiske boliger, allikevel anbefales en mer detaljert analyse av både termisk komfort og økonomi for å fastslå dens konkurransekraft i markedet.

CONTENTS

List of appendices:

TABLE OF FIGURES

NOMENCLATURE

θ	Temperature	[°C]
T	Temperature	[K]
R	Thermal resistance	[m^2K/W]
$\dot{q}$	Heat transfer rate per square meter	[W/m^2]
$\dot{Q}$	Heat transfer rate	[W]
k	Conductivity	[W/mK]
α	Thermal diffusivity	[m^2/s]
h	Heat transfer coefficient	[W/m^2K]
ε	Radiation Emissivity	-
α	Radiation Absorptivity	-
τ	Radiation Transmissivity, Time constant	-
σ	Stefan-Boltzman constant	[$5.67 * 10^{-8}$ W/m^2K^4]
C_p	Specific heat capacity	[kJ/kgK]
ρ	Density	[kg/m^3]
$\dot{m}$	Mass flow	[kg/s]
E	Emissive power	[W]
E_b	Black body emissive power	[W]
Re	Reynolds number	-
Pr	Prandtl number	-
Δt	Simulation time-step	[h]

ABBREVIATIONS

ASHP	Air source heat pump
RHS	Radiant heating system
TABS	Thermo-active building systems
GEL	Green Energy Laboratory

SUBSCRIPT

MR	Mean Radiant
c	Convective
r	Radiative
e	Evaporator
c	Condenser

1 INTRODUCTION

1.1 OBJECTIVE

The goal for this work is to analyze the hydronic radiant heating floor installed at the Green Energy Laboratory (GEL) of the Shanghai Jiao Tong University (SJTU) in China. For the analysis, a simulation model will be established in the simulation tool TRNSYS and validated with the use of measurements from the specific system in the laboratory. The analysis seeks to examine to which degree the radiant heating system (RHS) is suited for implementation into Chinese residential buildings. Accordingly, the analysis will dive into RHS design procedures, as energy efficiency and occupant thermal comfort are the overall purposes of building heating systems.

This work is a collaborative activity of the Joint Research Centre Agreement in Sustainable Energy between SJTU and the Norwegian University of Science and Technology (NTNU). The main findings will be incorporated in a draft proposal for a collaborative scientific paper. The draft is included at the end of this report.

1.2 BACKGROUND

About 40% of current worldwide primary energy use is consumed by buildings [1]. As literally billions of people are coming out of poverty and the world population increases, more buildings are needed for housing, schooling, working, etc. At the same time the climate changes are getting increasingly severe, which calls for a reduced use of fossil fuels. China is the biggest energy consuming and CO_2-emitting country in the world. Coal boilers mainly supply space heating in China today [2]. Problems of local pollution in the cities, together with a rapidly growing economy and urbanization, result in major incentives for a shift towards low-grade renewable energy sources. Energy efficiency of building envelope and HVAC (Heating, Ventilation and Air Conditioning) systems is a prerequisite for good performance of the entire heat chain. Thermal comfort for occupants is the

goal of heating systems and the quality of the indoor environment is getting more attention with the realization that e.g. sick building syndrome can become a serious expense for the society. This contributes to even higher requirements on the proper design and operation of the HVAC systems.

The recent progress in building envelope insulation techniques has severely reduced the demand for heating in buildings. It has opened doors for the utilization of low-temperature heat emitting systems, such as hydronic radiant floors. This low-exergy system has the ability to make renewable energy sources more viable, ensure a high degree of thermal comfort and provide architectonic freedom as the pipes are embedded into the floor. However, hydronic radiant floors are considered to be more complex in both design and operation and are often opted out for more straightforward systems for financial reasons. Knowledge about the behavior of radiant heating systems in different conditions is crucial, and comprehensive simulations are being done today to learn more about this. Scrutiny of the utilized computer models is required in order to trust the simulations which will be the design tools for building HVAC systems of tomorrow.

Radiant heating has been in use since the Chinese "Kang" and Korean "Ondol" were developed over 3000 years ago [3]. Flue gas from fires was led in passages underneath the floor to heat the floor surface so that the occupants could sit and sleep on them without getting cold. In Europe the "Hypocaust" was developed 1000 years later by the romans [4], and also used flue gas from fires as heat transportation medium. With the development of hydronic heating systems in the 19th century, radiant heating gained popularity. In the early 1950's cross-linked polyethylene (PEX) tubes were used for the first time in a radiant floor, which was another milestone as it mitigated the problems concerned with the old pipe materials. However, PEX tubes did not flourish in the commercial market. The investment cost of RHS was high, and at the same time oil prices were low, which made radiators a cheaper alternative. The 1970s energy crisis and the following global recession of the 80s led to an increased focus on energy efficiency and radiant floors gained popularity again. Some technical barriers still

existed, however. For instance, oxygen permeation through the plastic tubes was causing corrosion problems. This was solved with oxygen barriers on the tubes. Today, RHS is a mature technology in the Nordic countries and is known for excellent thermal comfort. As shoes are not worn inside at home, heated floors are especially popular in residential buildings compared to commercial ones. Up to 95 % of all buildings in Korea have radiant floors installed, in Northern China the number is 80 %. The high prevalence is caused by the "Kang" and "Ondol" traditions tracing back thousands of years. Other parts of China also report a fast-growing tendency towards using radiant floors both for commercial and residential buildings [4]. However, due to problems with design and operation, a need for better design procedures and total system energy performance research were called for by Hu et al. [5], who did a review on the utilization of radiant heating and cooling systems in China.

Enova SF, a public enterprise created to promote sustainable energy solutions and owned by the Norwegian Ministry of Petroleum and Energy, gives economical support to building owners if they change from direct electrical heating to hydronic heating. This reflects the Norwegian Governments ambitions for a transition to hydronic heating systems and highlights the importance of doing research in this area.

1.3 Outline

Chapter 2 contains the theory behind the analyzed technologies. Heat transfer mechanisms are presented. Building heating demand as well as human thermal comfort will be explained. An introduction to common hydronic radiant heating systems is included together with a comparison between radiant and convective heating systems. Control theory of RHS is presented. In the final section, heat pump theory is briefly introduced.

Chapter 3 presents the computer simulation and experimental theory. The utilized simulation tool TRNSYS and its models will be explained. Information

about the Green Energy Laboratory and heating system installed in the specific lab and the modelling of this in TRNSYS is given. The conducted experiments are explained in detail and uncertainties involved with simulation and measurements are noted.

Chapter 4 comprises the experiment results and the validation of the simulated model against the measured data. The calibration of the initial simulation model towards a final validation will be explained.

Chapter 5 explains how the analysis of the validated model is conducted and presents the analysis results. The radiant floor model is implemented into a typical Chinese apartment model, as given to the author by GEL researchers. Based on simulation results, a logical sequence showing why and how to control a RHS is presented. The floor is then simulated in a super-insulated building model and connected to a heat pump and buffer tank to assess the system performance together with heat source and storage.

Chapter 6 contains results from simulations of fan coil units (FCU) as an alternative heat emitting system, for comparison to RHS. The same storage, heat pump and building models are used as in the last part of chapter 5. The last section of the chapter compares the simulation results of the two heat emitting systems.

Chapter 7 is a design proposal for a radiant underfloor heating system in the typical Chinese building model used in the first part of chapter 5. The design is based on the results of the simulations performed in the previous chapters.

Chapter 8 summarizes the results of this work and presents conclusions based on the findings.

Chapter 9 presents ideas for further work on this system based on the scope and limitations of this work.

1.4 DELIMITATIONS

The purpose of this thesis is to analyze the RHS with respect to energy and thermal comfort. Initially it was assumed that the installed RHS system in GEL was used for cooling as well. However, this is not the case, as fan coil units are used for this purpose. Consequently, the analysis of the radiant floor does not consider cooling. Only hydronic radiant heating is handled, while electrical radiant systems are left out of the scope. Domestic hot water is not taken into account. Investment and operative costs are not considered.

TRNSYS does not capture local thermal comfort parameters, such as solar irradiation, radiation asymmetry, air temperature gradient and air movement in a zone. As a result, the analysis is limited with regard to detailed thermal comfort assessment, especially for the simulation of the fan coil units.

The outdoor climate is an important boundary condition for heating analyses. The analyses in this thesis are based on typical Shanghai climate. The effects of solar irradiation into zones are not handled and shading is assumed to be close to 100 % for all windows in the models, except for some windows in first simulations.

TRNSYS is not an easy simulation tool to use. Dealing with problems of convergence of the simulations, limitations on the TRNSYS models, and result interpretation is very time consuming. As a consequence, the system simulation models used in the analysis of this thesis are not built very complicated. Focus has been on a careful analysis of the simulation outputs.

The report contains a long theory section and a detailed description of the utilized TRNSYS models. The first part of the analysis (section 5.2) consist of a thorough explanation of why and how to control RHS, based on simulation results. It reflects the attention of the author on a deep understanding of the system behavior. However, much of this information is not directly related to the

main findings of the analysis. Central results are found in sections 5.2.7, 5.3 and Chapters 4 and 6.

2 RADIANT HEATING TECHNOLOGY

The physical nature of radiant heating systems (RHS) is complex and involves many different heat and mass transfer mechanisms. An understanding of these mechanisms is needed to be able to evaluate system behavior and eventually impose improvements for design and operation. The first sections of this chapter seek to explain the basics of the physical phenomena of RHS. Heating systems exist to cover a certain need. What are these needs and how can RHS cover them in an efficient way? The basics of heating demand in a building as well as human comfort are described. Important parameters to consider when designing RHS are presented together with a selection of RHS technologies and their properties. Some information on systems using air as a heat transport medium is presented. Control theory of RHS is covered. An introduction to air source heat pumps is added in the last section. Heat and mass transfer is represented by theory from the book by Çengel [6]. In sections 2.4 and 2.6 most of the theory covered comes from the work of Siegenthaler [7].

2.1 HEAT AND MASS TRANSFER EFFECTS

There are three different modes of heat transfer within heat and mass transfer theory. These are conduction, convection and radiation. In RHS, all three modes are active and important for system performance. When a material changes state from liquid to gas, it absorbs heat. This heat is called condensation heat or latent heat. Stratification is another effect to be considered, as it affects thermal comfort and heat transfer. Thermal mass stores heat and can have major impacts on the heat transfer processes. Figure 2.1 shows how heat transfer occurs through a building wall element.

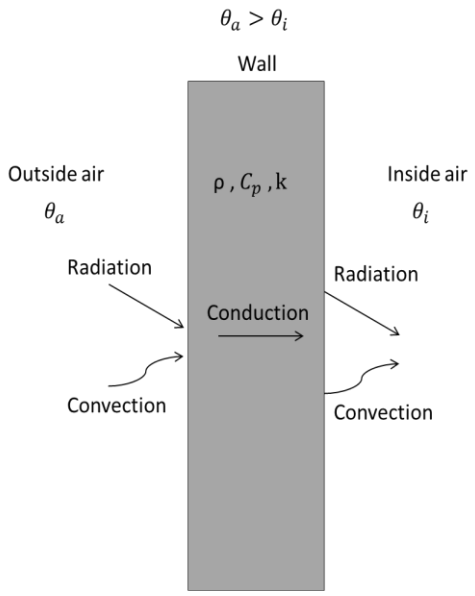

Figure 2.1: The three modes of heat transfer through a wall element. Heat flows to the outside surface through convection and radiation, is conducted and stored in the wall before being convected and radiated from the inside surface to the interior.

The overall rule of heat transfer is analogous to Ohms law in electricity. It states that current is equal to potential over resistance. In heat transfer theory the heat transfer rate is analogous to current and temperature difference to potential. Equation 1 outlines the heat transfer process. For radiation heat transfer the potential is different, cf. equation 8.

$$\dot{Q} = \frac{\Delta\theta}{R} \tag{1}$$

Each mode of heat transfer can be represented by a thermal resistance R. In the next sections the modes of heat transfer as well as stratification and thermal storage will be explained.

2.1.1 Conduction

Heat is molecular vibrations in a material. The vibrations will propagate through the material and to other materials in physical contact with the heated material. The molecules collide and dissipate the energy to surrounding molecules. Heat always flows from higher temperature to lower temperature because of this dissipation of the heat energy. This process is called heat conduction. The speed of the conduction is decided by the temperature gradient and the material property called conductivity. The higher the conductivity the higher the heat transfer. The Fourier's law encapsulates these two postulates in equation 2 and describes heat flow per area in the direction normal to a surface.

$$\dot{q} = -k \frac{d\theta}{dx} \tag{2}$$

This equation only applies to 1D steady state heat transfer. When considering transient heat conduction equation 12 must be employed due to heat storage in the mass, which greatly complicates calculations. Several methods exist to assess the transient conduction heat transfer and are beyond the scope of this work, although some of them are mentioned in section 3.2.1.

2.1.2 Convection

Conduction happens within and between materials at rest. When one of the materials flow, e.g. air flowing over a plate, heat is also transferred by the bulk flow (advection) of the material. The molecules close to the surface are heated up and transported away and are replaced by colder molecules. Heat transfer is increased compared with the stationary state where only conduction occurs because the temperature gradient at the surface is higher. This is the reason why air feels colder if there is movement, i.e. wind, present. Newton's Law of Cooling describes convection in equation 3.

$$\dot{q} = h\,(\theta_{surf} - \theta_{air}) \tag{3}$$

Heat transfer per area is proportional to the temperature difference between the surface and air temperature. *h* is the heat transfer coefficient and is of major importance for convectional heat transfer. The equations for heat transfer are derived from a similarity analysis of the continuity, momentum and energy equations. In most applications however, the fluid motion is too complex and correlations for the heat transfer coefficient h must be found empirically. A wide series of correlations for different flow schemes exists and are of the form of equation 4. *c* and *exp* are constants that vary according to flow scheme and geometry. Because air velocity, and therefore the Reynolds number, greatly affects these parameters a detailed fluid dynamic simulation should be utilized for high precision assessment of these correlations, but this is not necessary for the considerations done in this work.

$$\mathrm{h} = \mathrm{c}(\theta_{\mathrm{surf}} - \theta_{\mathrm{air}})^{\mathrm{exp}} \tag{4}$$

There are three different branches of convection: external forced convection, internal forced convection and natural convection. Forced convection means that the fluid motion is forced, e.g. by a fan or a pump. External refers to the situation where there is a free stream velocity or temperature outside of their respective boundary layers. A fan blowing cold fresh air over a warmer floor is an example for external forced convection. Internal refers to the situation where there is boundary layer development from two sides that meet. The free stream nature of the flow is thus eliminated. A pump pumping water through a pipe for hydronic heating would be an example of forced internal convection. Natural convection, also called free convection, is not spiked from a device forcing mass movement, but from buoyancy forces. When a fluid heats up it expands and its density decreases. In an environment of fluids with a higher density, the heated fluid bulk will start to rise. Similarly, when a fluid is cooled it will become more dense and sink. Temperature differences in fluids thus induce a flow within the fluid and cause higher heat transfer rates. The buoyancy forces also give arise to the stratification effects seen in buildings (see section 2.1.4).

When air with one temperature is replaced by air of a different temperature, as is usually the case of ventilation, this can also be viewed as heat transfer by advection, thus convection. In this case, equation 5 must be employed.

$$\dot{Q} = \dot{V}\,\rho C_p(\theta_{in} - \theta_{out}) \tag{5}$$

2.1.3 Radiation

The third mode of heat transfer is thermal radiation. Unlike conduction and convection, radiation does not need a medium to propagate through. This is because thermal radiation is electromagnetic waves that can travel through vacuum. Over 50% of heat transfer from radiative systems is from radiation and is thus of big importance when considering RHS.

As the charged particles of a material vibrate due to their temperature and collide they emit radiation. The higher the temperature is, the greater the kinetic energy of the molecules and the higher is the frequency of the electromagnetic waves. The radiation from the sun has a higher frequency than the terrestrial radiation because it has a lot higher surface temperature and therefore it is called short-waved and the terrestrial long-waved, cf. Planck's law. All surfaces emit thermal radiation as long as they have a temperature. The balance between absorbed and emitted radiation decides whether or not the surface is a net heat source or sink to the surroundings. The emitted radiation is given by the Stefan-Boltzman law (equation 6). However, this is for an ideal body called a black body, which has an emissivity of 1. Emissivity is the ratio of the emitted radiation of a real body and that of a black body of the same temperature and is therefore less than 1 for real bodies. To get the real emissive power E of a surface equation 7 must be computed. Emissive power is equal to radiative heat transfer to the surroundings per square meter.

$$E_b = \sigma\, T_{surf}^4 \tag{6}$$

$$E = \varepsilon E_b \tag{7}$$

To calculate the radiative heat balance between two surfaces a thermal resistance network as shown in Figure 2.2 can be used. F is the view factor and is defined as "the fraction of the radiation leaving surface 1 that strikes surface 2 directly" [6].

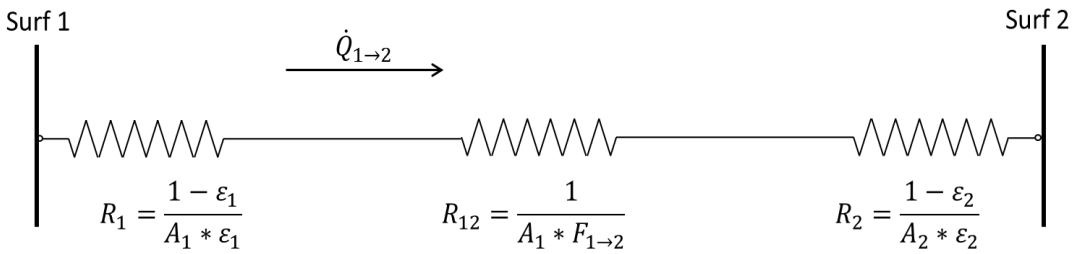

Figure 2.2: Thermal resistance network model for thermal calculations between two surfaces. The impact on heat transfer from emissivity of the surfaces as well as the view factor is visible in the resistance equations.

Following the convention that flow equals potential divided by the sum of the resistances we end up with equation 8 for radiative heat transfer between to surfaces. A common simplification is that surface 2 is a black body that totally encompasses surface 1, and with much bigger area. This means that both the view factor $F_{1\to2}$ and the surface 2 emissivity are equal to one, thus yielding equation 9 which is used in simplified analysis. For a more detailed analysis an extension of equation 8 with all present surfaces must be employed, which gives a system of equations that are hard to solve without a computer. As well as the surface properties also the 3D geometry must be known to be able to compute the view factors between all surfaces.

$$\dot{Q}_{1\to2} = \frac{\sigma(T_1^4 - T_2^4)}{\frac{1-\varepsilon_1}{A_1\varepsilon_1} + \frac{1}{A_1F_{1\to2}} + \frac{1-\varepsilon_2}{A_2\varepsilon_2}} \tag{8}$$

$$\dot{Q}_{1\rightarrow 2} = A_1 \varepsilon_1 \sigma (T_1^4 - T_2^4) \tag{9}$$

Incident radiation, called irradiation, can be absorbed, reflected or transmitted. The sum of these is therefore equal to one, as showed by the equation

$$\rho + \alpha + \tau = 1 \tag{10}$$

where ρ is the reflectivity, α is the absorptivity and τ the reflectivity of the material surface. These properties are dependent on both radiation frequency and direction, but a usual simplification is that a surface is both diffuse and grey which implies that its radiative properties are independent on direction and frequency, respectively. If the temperature of a surface and its surroundings are close to equal, which is often the case when considering long-wave radiation transfer of building surfaces, the Kirchhoff's law of thermal radiation can be assumed. In other words, the emissivity can be assumed to be equal to the absorptivity. An opaque surface has transmissivity equal to zero. Applying Kirchhoff's law to an opaque surface thus yields

$$\rho + \varepsilon = 1 \tag{11}$$

When a gas influences the radiative heat transfer between two surfaces it is called a participating medium. For high temperature processes, especially if particles are present, this can be of major importance. One example is combustion in a furnace. Another situation where participating medium must be considered is if the radiation travels long distances through a gas, e.g. the atmosphere. However, for most situations gases between surfaces can be neglected in radiative heat transfer calculations.

2.1.4 Stratification of Room Air

The same buoyancy forces discussed in section 2.1.2 cause warm air to rise and colder air to sink. In an enclosure, these forces lead to a stratification effect where the warmer air is stuck under the ceiling and the colder air at the floor. This effect can create a sensation of a cold draft along the floor when e.g. a door is open. Stratification effects might lead to a considerable vertical temperature gradient, which might have negative effect on thermal comfort. Another negative effect could be that during heating the warm air rises to the vicinity of the ceiling, which in effect is an unoccupied zone where warm air is not necessary, thus leading to an ineffective heating. Stratification might also be desirable. The airport in Bangkok has a radiant cooling floor installed throughout the terminal [8]. Here the cool air along the lower part of the terminal, which is the occupancy zone, maintains the thermal comfort in hot climate conditions.

2.1.5 Thermal Mass

For transient analysis the heat storage in materials must be taken into account. The 1D heat conduction equation without internal heat generation is showed in equation 12. With the assumption of a temperature independent conductivity of the material, equation 12 is rewritten to equation 13.

$$\rho C_p \frac{\partial \theta}{\partial t} = \frac{\partial}{\partial x} k \left(\frac{\partial \theta}{\partial x}\right) \tag{12}$$

$$\frac{\partial \theta}{\partial t} = \alpha \frac{\partial^2 \theta}{\partial x^2} \tag{13}$$

α is the thermal diffusivity of a material. It reflects the ability of the material to lead temperature and is equal to conductivity divided by the specific heat capacitance and density. These three parameters thus affect how the temperature changes over time within a material that experiences heat conduction. With a low conductivity and high heat capacitance the temperature will change slowly over time. The opposite are materials of high conductivity and low heat capacity. One good example of this is aluminum, which quickly become

warm and lead heat very well. Thin sheets of Aluminum are hence frequently used in hydronic radiant underfloor heating to diffuse the temperature evenly over the surface.

2.2 Occupant Thermal Comfort

Occupant comfort is the primary goal of building HVAC systems. Humans spend a significant part of their lives inside and there are vital incentives for individuals, companies and the society to safeguard personal health. Recent studies show that a good indoor environment increases human productivity [9], which implies a close link comfort and economy. A major part of occupant comfort is linked to the thermal environment. When a human is thermally satisfied with his/her surroundings he/she is said to be thermally comfortable. This differs from person to person because it also involves personal factors such as health, psychosocial and mechanical environment, not only the physical heat balance of the body. The human body loses heat through perspiration, conduction to surfaces in direct contact with the body, radiation to surrounding surfaces, convection to the ambient air and breathing. To be in thermal equilibrium it needs to produce as much heat through the metabolic processes as it transfers to its surrounding by the mentioned means. Radiation together with convection accounts for the most of this heat transfer under normal conditions. The body senses not only the air temperature, but also the radiative temperature of its surrounding. To assess this, an operative temperature θ_{op} is defined in equation 14 and is a combination of the radiant and convective heat transfer. For air velocities under 0.2 m/s and a difference between the mean radiant temperature and air temperature of 4°C this equation can be simplified to equation 15. The operational temperature is the temperature that humans sense and the one that needs to be controlled by a HVAC system.

$$\theta_{op} = \frac{h_c\theta_{air} + h_r\theta_{MR}}{h_c + h_r} \tag{14}$$

$$\theta_{op} = \frac{\theta_{air} + \theta_{MR}}{2} \tag{15}$$

The mean radiant temperature is the surface temperature a completely surrounding black body would have so that the same radiant heat transfer would take place as in the actual case, e.g. a person sitting in a room. Another instrument to assess thermal comfort is the Predicted Mean Vote and Predicted Percentage of Dissatisfaction (PMV-PPD) scale, wherein the operative temperature is an input. PMV values are in Figure 2.3 given verbal meaning and the PPD is plotted against these. The PPD can never reach zero and thus reflects the human nature of the assessment: Everybody will never be completely satisfied, even though the mean vote is at perfect comfort (PMV equal to zero).

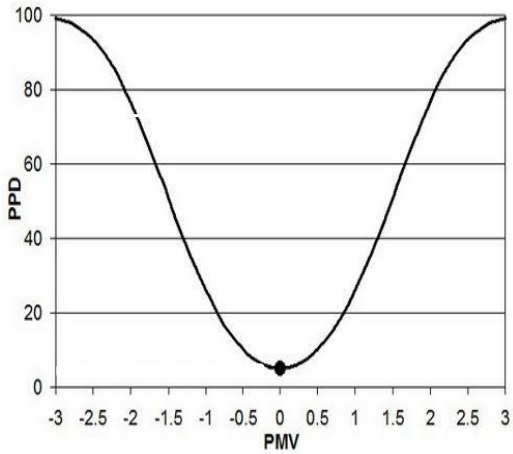

-3	Very cold
-2	Cool
-1	Slightly cool
0	Comfortable
1	Slightly warm
2	Hot
3	Very hot

Figure 2.3. The PMV and PPD indices.

This scale and its underlying equations were made in the 70s by Professor P. O. Fanger. Despite of some weaknesses of the model due to the complexity of human thermal comfort, it is widely used in the literature [10],[11]. It is also an output of simulations in TRNSYS, and will be used in this work for thermal comfort considerations.

The parameters for thermal comfort are many and include psychosocial and mechanical parameters as well as the thermal ones. Local parameters include draft, radiation symmetry, vertical air temperature gradient, operative temperature and air humidity. All of these are results of the outside climate condition, i.e. weather, through the building envelop and HVAC system, as illustrated in Figure 2.4. Internal loads of heat, humidity and air pollutants can also be significant. Planning and design of the HVAC system is thus of utmost importance for good indoor thermal comfort.

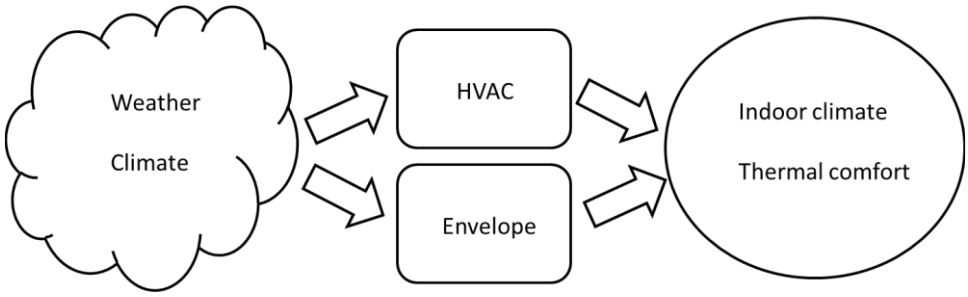

Figure 2.4: The weather affects thermal comfort through the building envelope and HVAC system.

Example: The radiators of a room are normally placed directly underneath the windows. This has two purposes. One is to mitigate the cold draft coming from the windows due to the natural convection occurring at the cold window surface by heating up this surface. The other is to even out the surface temperatures in the room to abate the radiation asymmetry caused by a cold window surface. With modern high thermal resistance windows both these problems with the cold window surface are abolished and the warm radiator thus becomes redundant and can be replaced by alternative heating systems such as radiant. This is how the thermal comfort requirements dictate how the conventional HVAC systems were built. Modern super-insulated building envelops together with improved HVAC components create a higher flexibility in choosing HVAC system for contemporary buildings.

2.3 HEAT BALANCE OF BUILDINGS

Buildings are subjected to various energy flows. The thermal energy flows are labeled gains and losses, where gains depict a positive flow of heat into the building and a loss a negative flow. Gains consist of internal gains and external gains. Examples of internal gains are heat emitted by a person, by a computer or by the lights. An external gain example is the short-waved thermal irradiation from the sun incident on the building. Typical losses are heat loss through the wall in the winter and the heat loss due to the substitution of warm indoor air with cold outdoor air, i.e. ventilation.

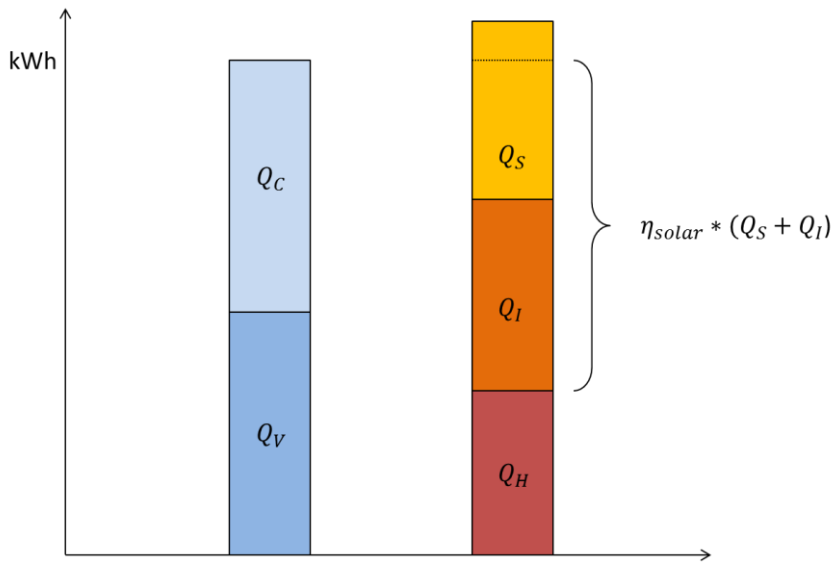

Figure 2.5. Energy balance of a building. The blue bars are losses while the orange are gains. The red is the heat demand of the building, i.e. what we must add to maintain the desired operative temperature.

To maintain the desired operative temperature and thermal comfort of a room all these heat flows must be balanced to make sure that the net heat flow into the room is zero. If this is not equal to zero we would experience either a drop or rise in operative temperature. Figure 2.5 shows this energy balance. Q_C and Q_V are the conduction and ventilation heat losses, respectively. Q_S and Q_I are the solar and internal heat gains. Not all of the gains can be used for heating purposes as some

of it is present in periods of the year where we do not need heating. η_{solar} is the solar efficiency, i.e. how much of the gains can actually be used for heating. Q_H is the heat demand for the building. From the figure a heat demand equation can be formed. This is done in equation 16.

$$Q_H = Q_C + Q_V - \eta_{solar}(Q_I + Q_S) \tag{16}$$

The same procedure is followed to obtain the heat balance equation for cooling. The heat demand must be covered by the HVAC system of the building. A heating source provides the heat before a distribution network (ducts, pipes, etc.) distributes the heat out to the different parts of the building. Finally a heat emitter transfers the heat into each room. Different controlling strategies exist to control the system and its components. A wide range of different heat sources, distribution techniques and heat emitters are available. With an exception of fan coil units, which are simulated as an alternative to radiant heating, only hydronic radiant types of heat emitters will be considered in this thesis. The next section covers the main characteristics of RHS.

2.4 Hydronic Radiant Heating Systems

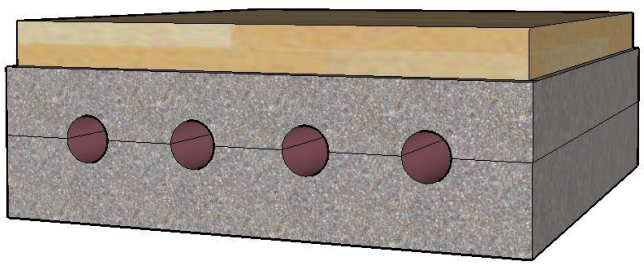

Figure 2.6: A radiant underfloor heating element. Water flows through the pipes and heat is emitted to or absorbed from the zone above. Simplified model for illustrative purposes.

Hydronic radiant heating system is a heat emitting system with complex dynamics. All modes of heat transfer as well as heat storage effects are very important. Figure 2.6 shows a section of an underfloor RHS. It is the end device

in the heating system of the building, and the device in direct contact with the environment in which the occupants reside. Water is distributed in pipes within structures such as panels, walls, ceilings, floors or the building concrete skeleton and heats them.

Being a radiant system it intrinsically has a large portion of radiant heat transfer. It also has a considerable portion of convectional heat transfer, so both modes must be taken into consideration. Radiant heating systems increase the mean radiant temperature of the room so that the operative temperature can be achieved with a lower air temperature, cf. equation 14. A lower air temperature increases the perceived indoor air quality [12]. In this way colder air can be provided to the occupants and the indoor climate improved accordingly.

Big surfaces are a characteristic of a radiant system. Equation 17 is a heat emission equation for heat emitters:

$$\dot{Q} = h_{conv+rad} A_{surf} (\theta_{surf} - \theta_{op}) \tag{17}$$

The heat transfer coefficient h is now consisting of both the radiative and the convective heat transfer. $\dot{Q}$ is the heat rate provided to the zone. The big surface of a radiant system means that we can provide the same amount of heat with a lower surface temperature, as compared to a system with a smaller surface. Conventional radiator systems have a smaller surface and consequently need a higher surface temperature to provide the same amount of heat, cf. equation 17. The high temperature drives natural convection and increases the convectional part of heat transfer. Convectional heat transfer enhancements such as fins and plates are frequently used in conventional heat emitting systems, thus creating even higher convectional heat transfer. As a result, these systems are not referred to as radiant systems. Because of their complexity radiant systems are still considered a more innovative solution, especially for cooling [13]. Radiant heating systems are used considerably more in residential buildings because of its thermal comfort properties [14]. The Norwegian government has ambitions of increasing the share of hydronic heating in Norway, and is mentioning radiant

heating as a suitable technology to help reach the energy efficiency goals of the future [15].

The major advantages of radiant systems are improved indoor climate and thermal comfort, energy efficiency and low exergy destruction due to smaller temperature differences. The latter improves the efficiency of environment friendly energy sources, such as solar thermal power, district heating, heat pumps powered by photovoltaic cells for heating and district cooling or solar powered absorption chillers for cooling. COP of heat pumps and chillers are higher with smaller temperature differences. The feasible options for choosing energy source in buildings are increased. With presumably rising energy prices in the future a change of heat source can become economically reasonable as well as technically possible with a robust heat distribution and heat emitting system. Smaller temperature differences also lead to reduced heat losses in distribution and heat production. Architectonic freedom is ensured as the pipes are imbedded in the building structure and big ventilation ducts and unaesthetic radiators become superfluous.

To make best use of the advantages of RHS a sophisticated control system must be implemented, especially for the slow reacting TABS (see section 2.4.2) [16]. A dedicated outdoor air system (DOAS) is needed in a combination with radiant system to take care of the latent loads and to aid during maximum heat load conditions. Control strategies must take into account both these systems at the same time.

Complexity in designing and implementing such systems leads to a higher investment cost and with relatively cheap fossil fuels the economic incentives to build RHS are not always strong enough. Fossil fuel and electrical boilers produce high temperatures, thus making cheaper high temperature heat emitting systems the most economical option. Plenty of attention is put into RHS research to find the best options for design, construction and control to make it an economically feasible solution for heating of commercial buildings in the future.

Hydronic radiant systems have a short-term self-regulating property. The system provides a temperature to the building element in which the water flows through. This is in contrast to an electric radiant system that provides a certain power, where the electric current decides the power output. Equation 17 shows that the emitted heat is proportional to the temperature difference between the room and the RHS surface. As the operative temperature of the room sinks when the heat load increases, the power output increases because this difference is growing. In the long run the average water temperature in the system will drop and create a demand for more heat to keep the set point water temperature at the desired level.

Hydronic radiant heating systems have tubes embedded in layers of different materials, such as gypsum or concrete. There are several options on how to install the tubes, with regards to how deep the tubes are embedded, how far it is between each tube, etc. These design parameters will be explained in the following section.

2.4.1 Important Design Parameters

The surface temperatures in a room decide how much heat will flow between the surface and the room. RHS control these surface temperatures. Water flows through the tubes and heat is diffused through the pipe and wall materials and into the room. Heat is transferred by forced internal convection inside the pipes, conduction from the pipes to the surface, by radiation and external forced or natural convection to the room, depending on ventilation type. Figure 2.7 shows these modes of heat transfer that takes place in a RHS element.

The heat transfer coefficient h together with the temperature difference between the surface and the zone air decide the amount of heat that is convected per square meter, cf. equation 3. This coefficient is usually taken from standards, but because it is a function of air velocity, temperature and surface geometry there might be some discrepancies between the real value and the standardized value [17]. Thought should be put into deciding this parameter.

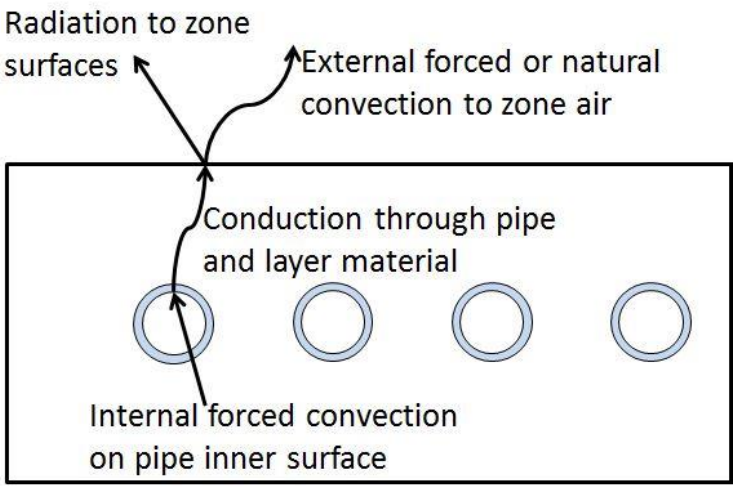

Figure 2.7: Heat transfer effects from water to zone of a radiant heating element. Heat storage effects occur in the material layers and can be decisive.

The design and layout of the tubes in a RHS includes different parameters, which have different effects on thermal performance. Tube size does not have a significant effect on thermal performance and are designed with regards to head loss considerations. Tube depth from the floor surface does effect thermal performance because the deeper the tubes are laid the more thermal resistance and thermal mass exists between the warm water and the zone, thus reducing and delaying heat transfer. Tube depth is therefore an important parameter when considering RHS. Tubes spacing is also of importance because a smaller distance between the tubes (measured center to center) means more tubes per square meter, consequently raising the average surface temperature as well as lowering the surface temperature gradient. Small distance between tubes signifies a higher heat transfer rate, but is also mechanically limited by flexibility of the tubes. Smaller tubes can be laid with smaller distance between them, but cause a higher head loss at the same time. Heat capacity, density and conductivity of the material layers between the tubes and zone surfaces significantly effects heat transfer, see sections 2.1.1 and 2.1.5.

Input parameters are water flow and temperature and are obviously of importance for the heat transfer, as depicted by equation 18, which gives the heat transfer rate to a hydronic heat emitter. Flow and temperature are usually

controlled to match the thermal losses and gains to maintain a set-point temperature of a zone and is covered in section 2.6.

$$\dot{Q} = \dot{m}\, C_p(\theta_{inlet} - \theta_{outlet}) \tag{18}$$

2.4.2 Thermo-Active Building Systems (TABS)

TABS is a system where the thermal mass of the RHS is significant (see section 2.1.5). It can be water tubes embedded in the concrete slab of a building or in a concrete layer inside the building. The main point is that the thermal mass affects the thermal performance of the system significantly. From equation 13 it can be read that a high heat capacity leads to a slow temperature change of a material and TABS will thus react slowly to sudden changes in load. Rapid changes in load conditions might be tough to meet because of this. In such an environment it is necessary with an additional fast responsive heating system to aid the TABS. This secondary system also becomes necessary at high loads because TABS does not have a high heating capacity due to its low surface temperature. Research does show that TABS have a self-regulating property because of its thermal mass, thus dampening the peak temperature oscillations [18]. This is analogous to coastal climates that are cool in the summer and mild in the winter because of the high heat capacity of the ocean.

Because it only handles the sensible load there is always a need for an air system to take care of the latent load. For modern buildings with super insulated envelopes TABS has been found to be especially promising considering thermal efficiency and comfort [19]. It is also expected that with the progress of predictive control strategies TABS have good prospects for future buildings.

2.4.3 Radiant Underfloor Heating

A hot floor is a thermally comfortable one, as the optimal vertical temperature gradient for thermal comfort is higher temperature on the floor and lower temperature higher up, see Figure 2.8. To heat the floor a TABS can be used, or a system with a smaller heat capacity and thus quicker to respond, such as in a wooden floor or a thin layer of concrete. A warm floor drives natural convection and lessens stratification problems. On the other hand, a cold floor would drive stratification because it cools the air, which stays along the surface, and air movement is minimal. A heated ceiling would cause the same effects as a cold floor.

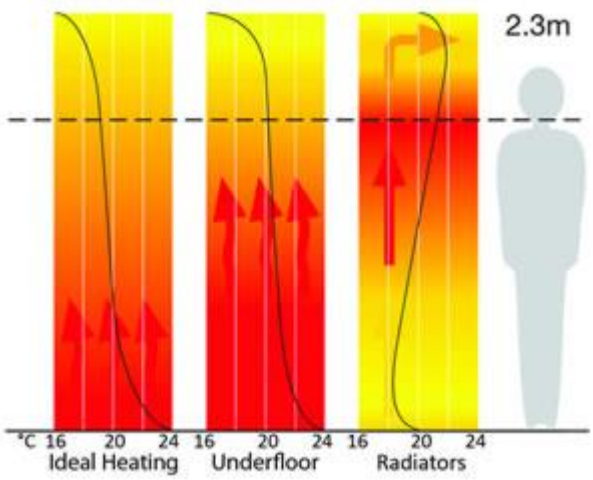

Figure 2.8: Ideal gradient vs gradients for underfloor and radiator heating. Source: http://www.chelmerheating.co.uk

Numerous designs, construction and layout possibilities for radiant floor heating exist and are in use. In this work the focus is on the system installed in the GEL. It is a radiant underfloor heating consisting of tubes embedded in a thin layer of concrete on top of an original floor. It has a certain amount of thermal mass due to the concrete layer, but is not considered heavy enough to be a TABS.

2.5 RADIANT VERSUS AIR HEATING SYSTEMS

Ventilation is required, as radiant heating systems do not handle latent loads. The question is whether or not the ventilation system should also supply the heat. Studies show that radiant systems use less energy and provide better thermal comfort than conventional all air systems [19]. A dedicated outdoor air system (DOAS) for use in combination with RHS does not need the same dimension as a conventional all air system that also covers the sensible load. Water can transport much more heat than air because of a much higher heat capacity, cf. equation 18. Pumping water will save energy compared to blowing air with fans. With a lower volume flow demand, the duct space requirements are reduced. Draft risks in the occupancy zones are moderated. Air movement in the rooms becomes easier to predict. Due to higher surface temperatures the risk of condensation and mold growth is reduced using radiant heating.

Ventilation systems can have severe problems of pollution and microbial contamination when not properly maintained [20]. By lowering the size of the air system and air flow rates it might be easier to maintain a healthy quality of the indoor air through the DOAS.

To achieve the same operative temperature an all air system for heating must provide a higher air temperature because the surface temperatures are lower. This high air temperature is produced in an air handling unit (AHU) that uses a heat source with higher supply temperature, i.e. more exergy. This reduces the performance of renewable energy sources, chillers and heat pumps. A RHS uses lower temperature and there is therefore a higher flexibility in choosing heat source.

Radiant systems are more complex in design and challenging to control especially in combination with a DOAS. This leads to both economic and technological barriers towards investing in and constructing radiant systems. An all air system might be more reasonable. Dokka et al. [21] explain that an all air system is very simple and leads “to a potential cost reduction” in their zero

emission office building concept. There are also knowledge barriers impeding the usage of TABS and guidelines for design and operation must be made to ease the work of the entrepreneurs.

2.5.1 Fan Coil Units

An alternative heat emitting systems (HES) to the radiant floor is a fan coil unit, which emits heat primarily through convection. A radial fan sucks air from the zone through a filter and blows it across a heating coil and back to the zone, see Figure 2.9. Supply water temperature must be higher when using an FCU instead of a radiant floor, which is essentially caused by the lower heat capacity of the air versus water. To supply the same amount of heat, a higher temperature is required, which in turn causes air stratification in the zones. Higher air mass flow could be used to enhance heat supply to the zone, but would lead to high air movement problems (draft, dust spreading) in the zones. The air temperature gradient caused by convectors is similar to that of radiators (see Figure 2.8). Modern FCUs have enhanced heat transfer and can hence be operated with lower water temperatures, but the outlet air temperatures which cause the stratification remain the same.

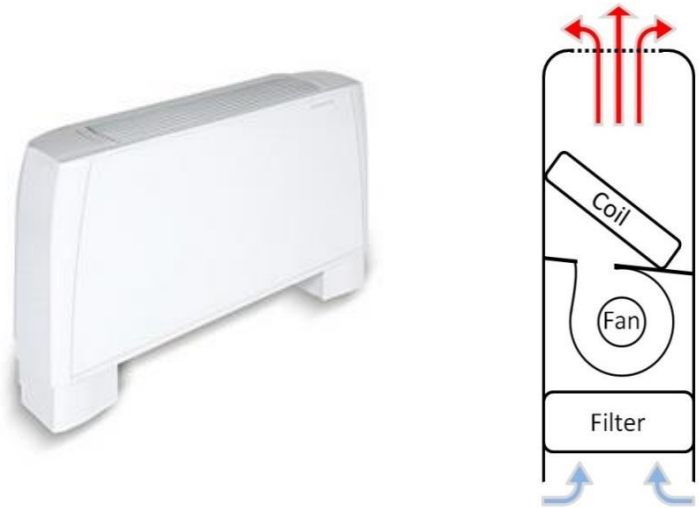

Figure 2.9: Fan coil unit. Source: sabiana.it. To the right is a sketch of the internal construction of the FCU and its operation principle.

2.6 CONTROL OF HYDRONIC RADIANT FLOORS

To ensure thermal comfort for the occupants of a building the operational temperature must be kept at a desired level. Overheating and coldness occurs when the heat gains to a zone is different from its heat losses over time. The heat delivered or removed by the heating system must match this gap for the indoor temperature to be stable and at a desired value. Hydronic heating systems carry heat by the means of water and have two changing parameters of importance: Flow and temperature. Equations 19, 20 and 21 show how these two parameters change the heat transfer from a heat emitter to a zone. Equation 19 calculates how much heat the water has delivered through the heat emitter and equation 20 how much heat the heat emitter has delivered to the zone by radiation and convection. Given that no heat is stored in the heat emitter and that there are no external losses these two values are the same and the equations can be combined to an equation for surface temperature. Assuming that the heat capacity of water, surface area of the emitter, heat transfer coefficient and operative temperature of the zone are all constant, the surface temperature, and thus heat delivered to zone, is a function of inlet temperature and flow (equation 21). Therefore, these are the two parameters to manipulate for control of a hydronic heating system.

$$\dot{Q} = \dot{m}C_{p,w}(\theta_{in} - \theta_{out}) \tag{19}$$

$$\dot{Q} = hA(\theta_{surf} - \theta_{op,zone}) \tag{20}$$

$$\theta_{surf} = f(\theta_{in}, \dot{m}) \tag{21}$$

Figure 2.10 shows the block diagram of a simple control system for the hydronic heating. It is called a closed-loop feedback control system because the operative temperature is measured from the zone and fed back to the controller, creating a closed loop. The controller reads the gap between the set-point temperature and the measured temperature of the zone and sends an electrical signal to an actuator or pump accordingly. The actuator opens or closes a valve to

manipulate flow to the heat emitter or to mix two water flows for supply temperature manipulation. In the zone-box of the figure the heat balance decides the change of zone temperature according to equation 26. A temperature sensor measures the new temperature and the process is repeated.

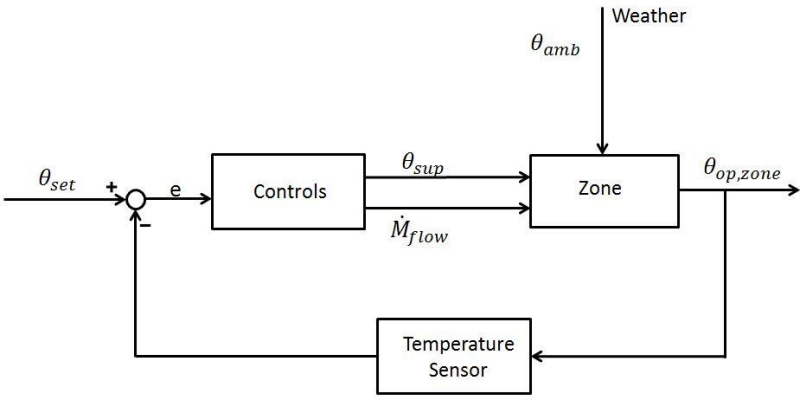

Figure 2.10: Block diagram showing the feedback control system for heating or cooling.

The controls box is exploded in Figure 2.11 and Figure 2.12 to show a more detailed block diagram for valve- and pump control, respectively. To control a valve, a signal is sent to an actuator that moves the valve stem to manipulate the valve opening. For pumps the signal is sent to a pump motor that drives an impeller to manipulate flow and differential pressure. These signals can be analog or digital, even mechanical for some actuators, and are on/off or continuous.

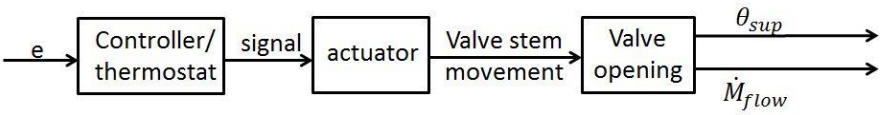

Figure 2.11: Exploded controls box from Figure 2.10. Control of a valve.

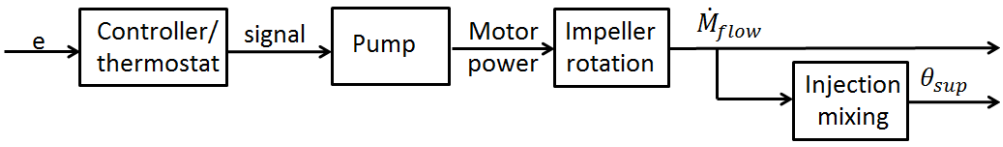

Figure 2.12: Exploded controls box from Figure 2.10. Control of a pump.

A thermostat can be viewed as a temperature sensor and on/off controller in one unit that opens and closes a switch when the difference between set-point temperature and measured temperature exceeds a limit called the differential. The on/off signal is either sent analogous through a wire to the actuator or, for modern systems, digitally through a communication bus or wire-less network to a system control center. Thermostats can be electromechanical or purely electric and can have several stages for heat source systems which have more stages of heat production.

Flow can be altered by controlling either a pump or a valve. When the flow decreases, the output temperature also decreases because it takes longer time for the fluid to pass through the heat emitter. The lower average temperature of the fluid leads to a lower surface temperature of the heat emitter and therefore a smaller heat transfer, c.f. equation 20. The relationship between heat output and flow is non-linear and valve characteristics should be chosen carefully to ensure good controllability. Different RHS loops are usually controlled as different thermal zones in the building, and installing a pump on each loop would not be economically viable. Valves, installed on the return manifold, control the flow to each loop by opening or closing following the signal from the zone thermostat. If there are significant differences in tube lengths or flow requirements between the loops, balancing valves installed on the supply manifold must be adjusted to ensure proper flow and control. Temperature is manipulated by the means of a mixing assembly, which mixes return and supply water. This can be achieved through a 3-way mixing valve that measures the supply and return temperatures and modulates the valve opening according to the supply set-point temperature. Another option is to inject hot water from the source into the radiant heating loop in an injection mixing assembly, using either a 2-way valve or a pump. A presentation of all the different components and systems used in hydronic heating systems is not in the scope of this work and the reader is encouraged to look in the literature for more details in this regard.

The heat losses from a zone and heat transfer to the zone are approximately proportional to the outside temperature and the surface temperature of the heat

emitters, respectively. The heat transfer coefficient (see sections 2.1.2 and 2.1.3) is a function of temperature difference, and hence not constant as temperatures change. However, for the narrow band of operative temperatures encountered in occupancy zones of buildings, it is assumed constant. Accordingly, heat transfer is proportional to the temperature difference, $\Delta\theta$. Heat loss can therefore be predicted by measuring ambient temperature, and the control system react to the changes in heat load before the operative temperature changes. This is done by changing the supply temperature to the heat emitters according to the ambient temperature, with the use of a curve called an outdoor reset line, see Figure 2.13. The colder the ambient air is the warmer the supply temperature of the heating system.

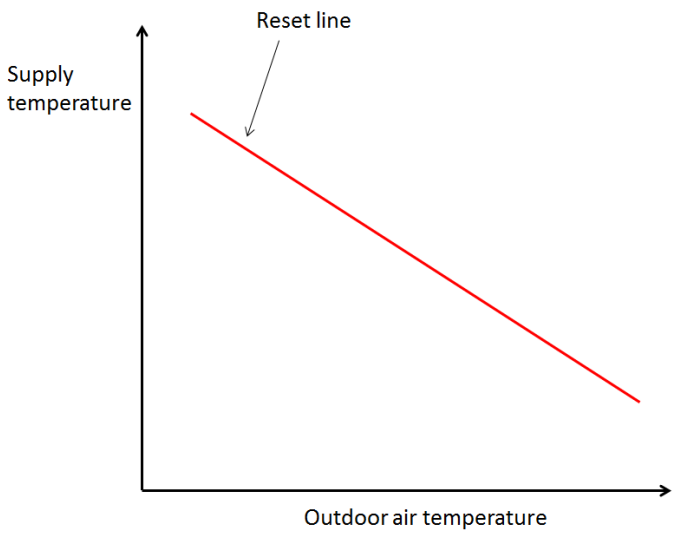

Figure 2.13: Reset line for supply temperature to radiant floors.

Figure 2.14 shows the block diagram of such a control system with a backward loop for the zone temperature and forward loop for the ambient temperature. It shows how modern heating control is done. Various solutions and strategies exist to effectively control the operative temperature to be as stable and thus comfortable as possible, and this figure encapsulates the basic ideas. Measurements of wind, solar irradiation and internal gains could be used as further forward loops together with intelligent controllers to better predict the heat balance of the zone and to control the temperature and flow accordingly.

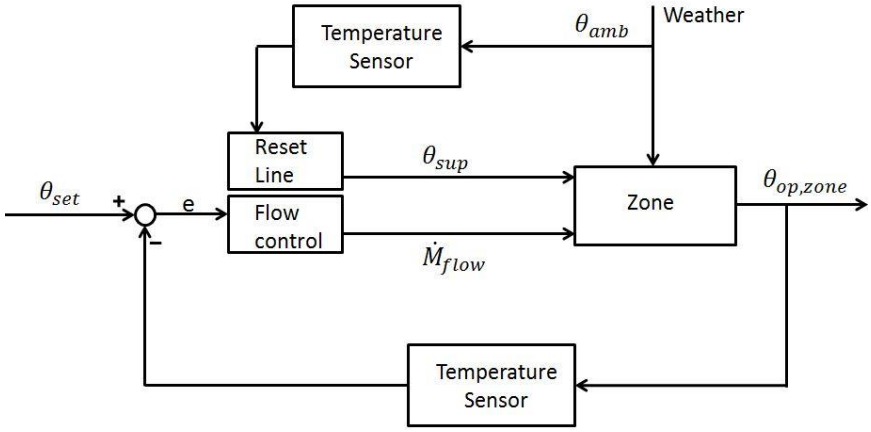

Figure 2.14: Block diagram showing how the reset line controls the supply temperature based on the weather conditions with a feedforward loop.

The output signal from the controller depends on the control mechanism and strategy. On/off is the simple form of a signal, but there are different strategies to when and how often a device should turn on and off. In a differential controller the switch is turned on or off whenever the value of the read variable is far enough from the set-point value and keeps this signal until the read variable reaches the opposite differential. This causes the controlled variable to undulate over and under the set-point. To keep a more stable controlled variable, strategies such as pulse width modulation (PWM) control and floating control can be utilized. These are methods that have more sophisticated on/off criteria than the simple differential method and turn the switch on and off more frequently, even when the controlled variable is within its differential.

The output signal can also be continuous, as an analog voltage or current, or as a digital signal. The magnitude of the signal depends on the size and behavior of the error between the measured and set-point value of the controlled variable. In a proportional (P) processing controller the signal is proportional to this error by a magnitude of the proportional gain constant K_p. Proportional control inherently causes a small deviation from set-point, even in steady state. In an integral (I) processing controller the signal is proportional to the integral of the error by a magnitude of the integral gain constant K_i. Integral control is used together with P control to eliminate the set-point deviation. In a derivative (D)

processing controller the signal is proportional to the derivative of the error by a magnitude of the derivative gain constant K_d. Derivative control is used together with P and I control to more quickly stabilize the control variable and to ameliorate problems of overshooting. I and D controllers are usually combined with a P controller to form PI, PD and PID controllers. A PID controller can be seen as a P, I and D controller connected parallel and their contribution to the signal can thus be added together as in equation 22. K_i is equal to K_p divided by a time constant called integral time T_i. K_d is equal to K_p multiplied by a time constant called derivative time T_d. M is a constant that is always present in the signal to avoid unstable operation when the error is close to zero.

$$\text{Signal} = K_p(y_{set} - y) + \frac{K_p}{T_i}\int (y_{set} - y)dt + K_p T_d \frac{d(y_{set} - y)}{dt} + M \tag{22}$$

If a process is easy to control and do not demand quick controlling, on/off or continuous modulating controllers using proportional action can be utilized. For systems which are harder to control, integral action can be added. For even tougher systems, where quick control is demanded, derivative action might be required. In hydronic heating systems derivative action is usually not required because of the high thermal capacity, of the water and building constructions. For radiant heating floors with higher thermal mass it is usually sufficient to use on/off type controllers. Continuous signal controllers are more expensive and must also be connected to actuators and valves which are suited for this kind of operation. On a mixing assembly sophisticated control is required as the changes in mixed temperature can be sensitive to valve positions.

2.7 HEAT SOURCE: HEAT PUMP

A heat emitting system does not work without a heat source. A usual heat source to a hydronic heating system is an air source heat pump (ASHP) that takes heat from the air and transfers it to the heating water. Such heat pumps are also called air-water heat pumps to specify the source and load media. Ground-water heat pumps work with a higher efficiency because of a more stable source temperature and lower temperature lift, but are associated with a much higher investment cost due to ground digging and drilling and are not considered here.

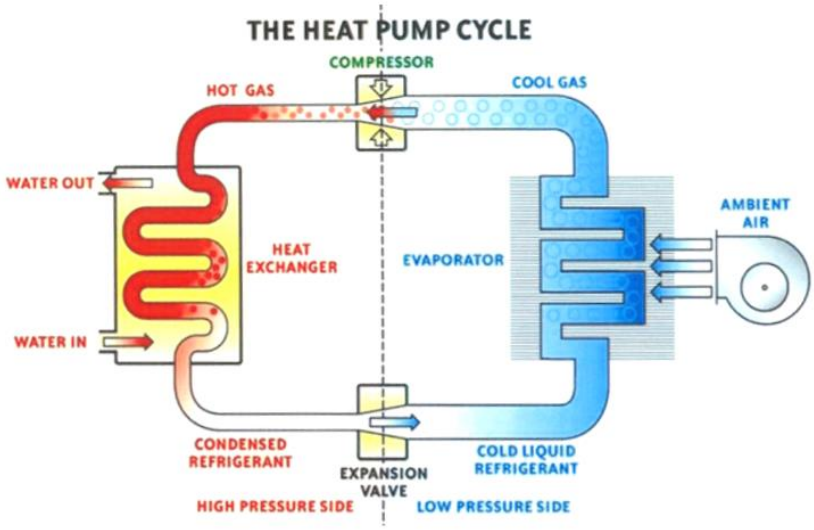

Figure 2.15: Air source heat pump cycle.
Source: http://deron.en.alibaba.com/

Figure 2.15 shows the working principle of an ASHP. A liquid refrigerant at low temperature is boiled in the evaporator, where heat is transferred from the outdoor air to the refrigerant through external forced convection, with the use of a fan. The temperature difference, which drives the heat transfer, between the two media is kept constant as the liquid is at its boiling temperature. The refrigerant is super-heating slightly, to avoid droplets in the compressor inlet, before the compressor adds energy and raises both temperature and pressure. The stored latent energy in the gas is then condensed in a condenser where heat is transferred from the refrigerant to the heating water. At last the refrigerant is expanded by an expansion valve to lower temperature and pressure and the

cycle is complete. It is important to select a working fluid (refrigerant) which can be boiled at ambient air temperature and condensed at the heating water temperature. The power input to a heat pump is electricity to the compressor and evaporator fan. The heat output is the heat transferred to the heating water in the condenser and is equal to the compressor power plus the evaporator heat input. Heat pump performance is assessed by the coefficient of performance (COP) and is equal to heat output over power input, shown in equation 23.

$$\mathrm{COP} = \frac{\dot{Q}_{\mathrm{cond}}}{W_{\mathrm{el}}} = \frac{\dot{Q}_{\mathrm{evap}} + W_{\mathrm{el}}}{W_{\mathrm{el}}} \tag{23}$$

The heat pump performance is dependent on many variables. The higher the temperature difference between source and load, the lower the performance, because the compressor has to work harder to supply the heat demanded at the condenser. For this reason ASHPs have higher COP at higher ambient temperatures. Thermal inertia creates an on/off cycle as the heat pump turns off and on. This is depicted in Figure 2.16. If the heat pump is oversized, the set-point temperature of the heating water will be reached quite quickly and the heat pump switches off. As the heat is emitted out to the heated zones the water temperature decreases until lower differential is reached and the heat pump switches back on. The more oversized the heat pump, the higher the frequency of this on/off cycle and thus bigger cycling losses. Lifetime of the components will be reduced by wear and tear.

The τ_{on} and τ_{off} represents the heat-up- and cool-down time constants, which are the time it takes an exponential functions value to reach 63% of its steady state value. It is thus a measure of thermal inertia of a system, whether it is a heat pump, radiant heating system or a whole building. This latency of the heat output can be viewed as a heat loss and is called cycling losses.

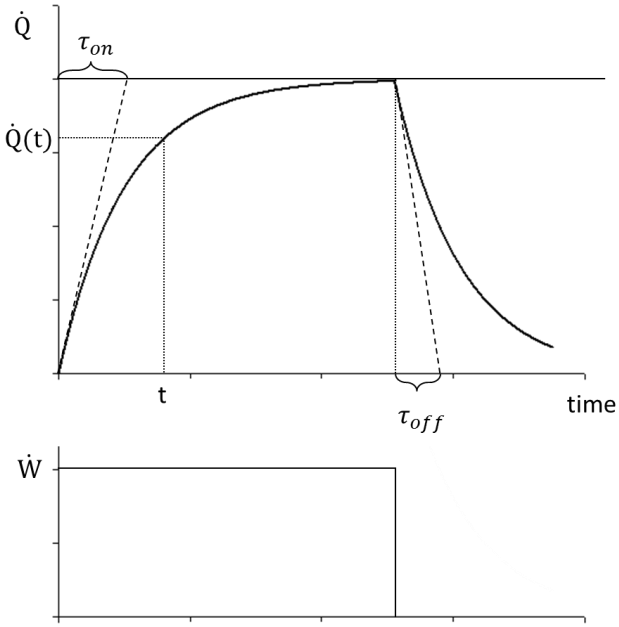

Figure 2.16: Start/stop cycle of a heat pump. The top shows the condenser heat output and the bottom shows compressor power, both as functions of time. The top line is the steady state condenser heat output.

Air is cooled at the source side of the evaporator and if surface temperature is lower than the air dew-point temperature, icing on the heat exchanger surface occurs. This ice is a thermal resistance and impedes heat transfer to the refrigerant. Therefore ASHP applied in such climates are equipped with a defrosting function, where either the cycle is reversed temporarily or an electric heating element heats the evaporator and melts the ice. Icing and defrosting as well as on/off cycles therefore cause a deterioration of COP that should be taken into account when performing energy analysis over time.

3 SIMULATION MODELING AND EXPERIMENTS

3.1 MODELING THE PHYSICS

The underlying physics of a buildings energy flows are very complex, as showed in chapter 2. Heat transfer is a combination of the three modes conduction, convection and radiation and each of these are further divided into different branches and are inherently difficult to assess for a given setting. The boundary conditions consist of weather and humans, which are both difficult to predict and to measure. Precise calculation is a very demanding task. The engineer needs to foretell both the thermal loads to size HVAC equipment and the energy use to assess its influence and at the same time secure occupant comfort. The researcher needs to analyze the different technologies, try new approaches and ultimately acquire a better understanding of the dynamics of the overall system performance. Building performance simulation (BPS) is therefore very important. When conducting a BPS some assumptions and simplifications must be made on account of the complexities involved. The process of making assumptions and simplifications to derive equations for general calculations of a certain physical phenomena or system is called modelling. There are many ways to model a buildings energy performance and its underlying physical phenomena. Different computer programs have been developed for assessing the energy flows of a building and they are using different models to do this. These programs are called simulation tools. There is a range of BPS tools available and they all have their own strengths and weaknesses [22]. The most basic models have many simplifications and are thus not very accurate and are not very flexible, but they require less computational power and are adequate for rough estimates. The more detailed models use numerical methods that include a discretization of the building for more accurate assessment such as local thermal comfort, but are likewise computationally expensive and require a bigger amount of knowledge to be used. The consequence of using different models in different tools is that the results of a simulation will vary from tool to tool. Behrendt et al. [23] simulated the same simple model with different tools and

showed significant discrepancies in the results. A good understanding of the tool at hand is thus required to assess the result in an adequate way.

Another reason to simulate is to challenge the current standardized values. Many coefficients and equations that are used in standards for load and energy calculation might not be completely reliable, and a detailed simulation study might challenge these and propose improvements. Le Dréau et al. did this for the Danish building regulation [24].

Simulation of RHS is recommended to ensure thermal comfort and energy efficiency and to avoid condensation on the surface of a radiant cooling system. The inputs to a RHS are mass flow and inlet water temperature. These two inputs need to be linked to the outputs of the system, namely surface temperature and heat flow to the zone. This is done by a RHS simulation model. In this work the active layer model implemented in the simulation tool TRNSYS will be considered (see section 3.2.2). Radiative heat transfer can be simulated by the use of simplified room geometry, while convection is a more intricate problem involving air flow in the room, thus requiring detailed information about the ventilation system. A comprehensive air flow and heat transfer analysis would involve a computational fluid dynamics (CFD) simulation, but this comes with a high computational cost and is not considered in this analysis.

3.2 Simulation Tool TRNSYS

To model and simulate the radiant heating system in this work, the simulation tool TRNSYS is used. TRNSYS is a TRaNsient SYstem Simulation program used to simulate any type of dynamic systems [25]. It solves algebraic and differential equations. The tool has a wide variety of models, called types, from different energy domains, which are mathematical descriptions of real life systems or structures such as buildings, fans, ducts, engines, etc. The source code of TRNSYS is provided to its users and is thus making it a very flexible tool that can be edited and programmed by the users themselves. The user can modify the

models, or even create entirely new ones. This also makes it a relatively advanced tool and is mostly used for academic purposes or by expert users. TRNSYS consists of a suite of programs, among others a visual user interface called the Simulation studio, an interface for inputs to the multi-zone building model called TRNBuild and an Editor called TRNSED for making simple stand-alone programs and for performing parametric runs. An executable calls a simulation engine, which is running the simulations. In this work only the Simulation studio and the TRNBuild interface will be concerned. TRNEdit will be used for parametric runs.

The types are solved separately in their own subroutines within the simulation engine, at every time-step. They consist of equations and require inputs and parameters for generating their results, or outputs. The outputs are averaged over the time-step. Inputs can change every time-step, but the parameters are fixed values such as size and constant material properties. An input is usually an output from another type. TRNSYS grants access to the source code and is therefore not a black box method. Figure 3.1 is a representation of how this works in TRNSYS. First the subroutine of type 1 is run in the solver, and the output from this becomes the input to the next subroutine, which is solved next. A loop would occur if one of the outputs of type 2 was one of the inputs of type 1, forcing the program to solve it iteratively.

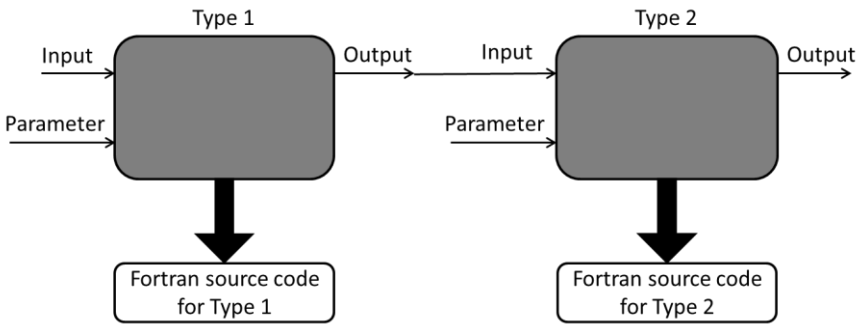

Figure 3.1: Representation of the simulation process between types in TRNSYS.

In the Simulation studio the types are connected together with lines, defining the input-output properties of the system. Figure 3.2 and Figure 3.3 show how this looks in the Simulation studio. It is seen how the outlet of the fan is the inlet of the duct. If the connections form a loop, TRNSYS will use a numerical method until convergence. Convergence of numerical simulations can be a complicated matter and deserves attention, but is not part of the scope of this work.

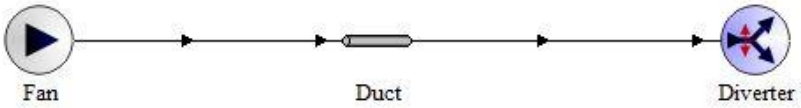

Figure 3.2: Connection of types in Simulation studio.

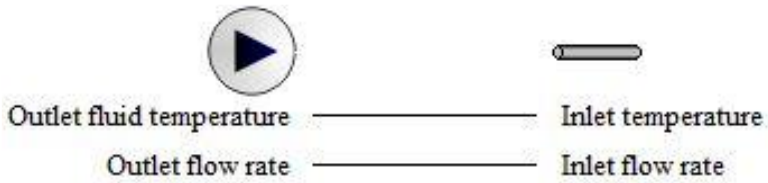

Figure 3.3: Outlet from fan to inlet of duct connection.

The types and their connections are implemented in the Simulation studio. The different parameters for the types are also defined by the user here. Equations and parameters that are not a part of a specific type can be implemented explicitly by the user in an equation box and used by all the types. The control cards are also implemented in the Simulation studio. This info controls the simulation parameters such as time-step, start time for the simulation, length of the simulation, convergence criteria, etc. The Simulation studio then creates an input file called the deck file, which contains all the information that is implemented in the simulation studio and that the solver uses to perform the simulations.

In this work a radiant heating system is modelled and simulated. The next section describes the calculations performed by the utilized types.

3.2.1 Type 56: Multi-zone Building Model

TRNSYS type 56 is used for simulating buildings. In the model it is possible to divide the building into different zones. Each zone can also be divided into several air nodes. These air nodes are mainly used to simulate stratification effects in large spaces. Each surface in the zone is modelled as a single node. The radiation zone is not affected by the air nodes and radiation beams can therefore travel unhindered between them. Figure 3.4 shows the different nodes and how the air nodes are distributed in a zone. The equations used in the simulation procedure calculate the heat flow between each node.

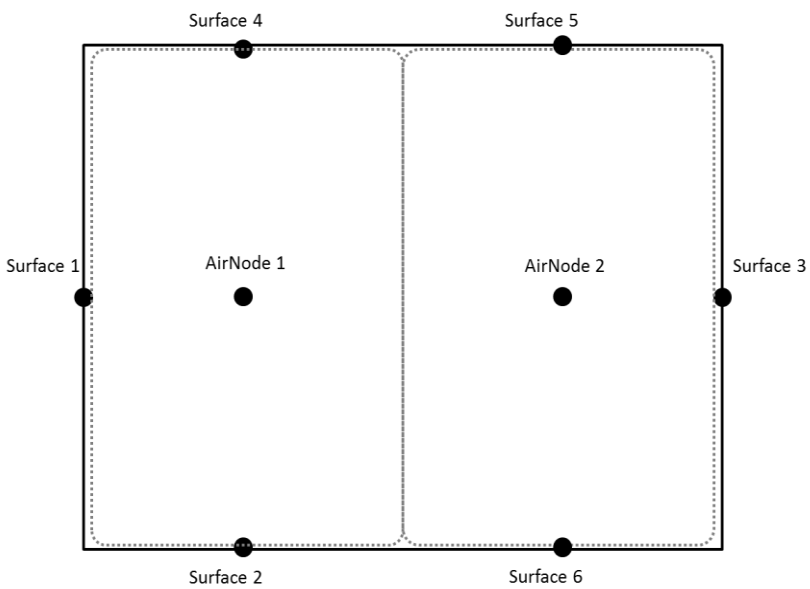

Figure 3.4: A zone and its surfaces and air nodes as modelled by TRNSYS.

Type 56 utilizes a heat balance method, which calculates heat flows from and between surface and air nodes and balances them. Surfaces are modelled homogenous over their area and the air homogenous over its air node volume. Heat flows through the building envelope to, or from, the outside boundary conditions. The outside surfaces exchange heat through convection with the air and radiation with its surroundings, as depicted in Figure 3.5. The net positive heat is then conducted through the wall into the zones of the building where radiation and convection occurs on the inside surfaces. The radiation heat

transfer occurs between the surface nodes, while the convection occurs between surfaces and the air node they face. Bulk convection from infiltration, ventilation and between zones or air nodes are only occurring on the air nodes. The air node heat flows are showed in Figure 3.6. The figure is explained on the next page.

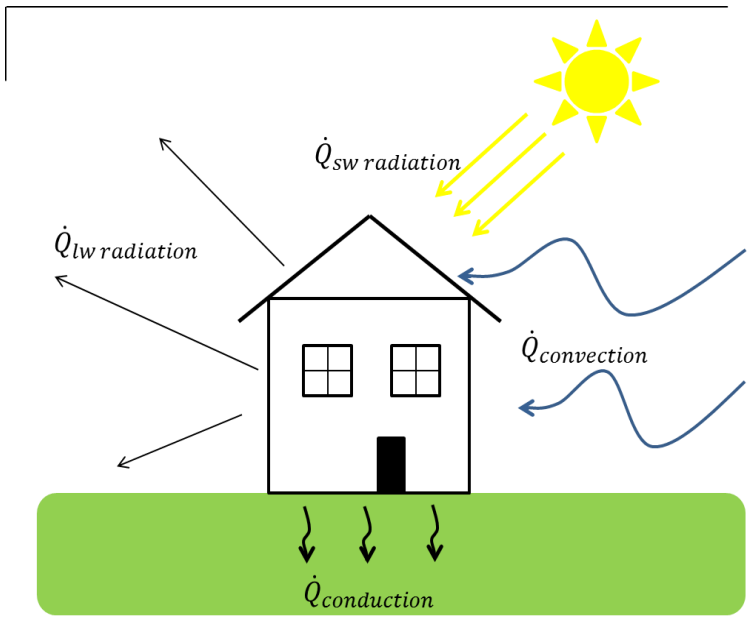

Figure 3.5: Exterior heat flows on a building. *lw* and *sw* stands for long- and short-waved.

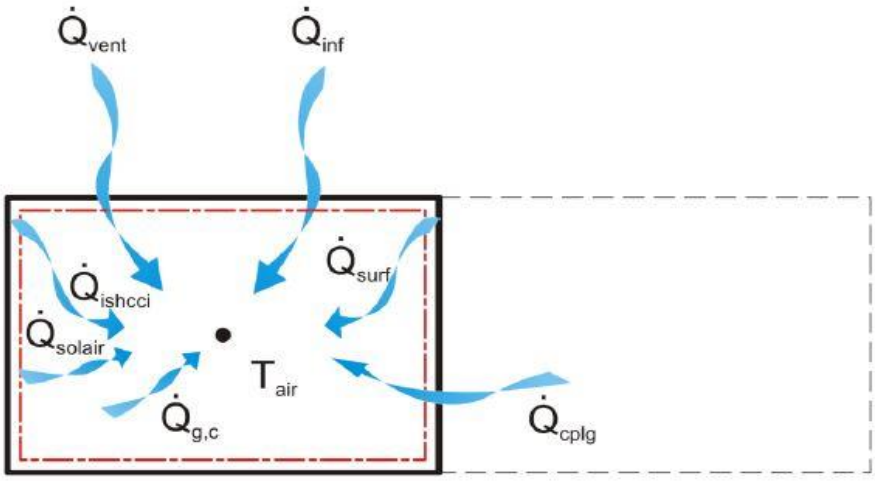

Figure 3.6: Heat balance of an air node. All the heat flows combine to a net positive or negative heat flow to the air node, which then changes temperature according to equation 26. Source: TRNSYS 17 manual.

The different heat flows in the figure are:

$\dot{Q}_{vent}$	Ventilation
$\dot{Q}_{inf}$	Infiltration
$\dot{Q}_{surf}$	Convection from surfaces
$\dot{Q}_{cplg}$	Bulk convection from adjacent air nodes
$\dot{Q}_{g,c}$	Internal gains from lights, computers and humans
$\dot{Q}_{solair}$	Part of transmitted solar irradiation that immediately becomes a convectional gain
$\dot{Q}_{ishcci}$	Part of solar irradiation absorbed by internal shading devices that immediately becomes a convectional gain

The heat flows are calculated and added together as in equation 24, and gives the net flow of heat to the air node: $\dot{Q}_{total}$. Equation 25 is then discretized into equation 26 and the result is the air node temperature at the next time-step.

$$\dot{Q}_{total} = \sum \dot{Q}_{in} - \sum \dot{Q}_{out} \tag{24}$$

$$\dot{Q}_{total} = \rho V C_p \frac{d\theta}{dt} \tag{25}$$

$$\theta^{t+1} = \theta^{t} + \Delta t \frac{\dot{Q}_{total}}{\rho V C_p} \tag{26}$$

These are the basics of the heat balance method. To derive the heat flows to the air node and the surface temperatures, different calculations are performed in the model. Some of them will be addressed below.

Walls

The thermal behavior of the walls is modelled in TRNSYS as one-dimensional heat conduction and calculated by the method of conduction transfer functions.

This is a black box method that models the dynamic thermal behavior of the wall and then uses this directly in the simulations. It utilizes the user-given properties of the wall to create a set of constants, which are used during calculation. In this way the computational time is shortened because the wall is modelled as a transfer function instead of a set of layers of different properties. Thermal mass effects are handled in this method. If the wall is very light, it will be simplified to a single resistance, thus neglecting thermal mass behavior. Each wall has two nodes: One for the exterior surface and one for the interior. It is a well validated method, but has some weaknesses when simulating very heavy and super-insulated walls with short time steps [26]. More details to this model are found in Appendix B.

Another approach to simulate conduction through walls is a numerical method where the wall is discretized into several resistances and capacitances. The method is more computational expensive than the transfer function method, but with contemporary computer power it is becoming the preferred model for BPS. It is not employed in TRNSYS type 56.

These methods are simplifications, and usually disregard heat transfer effects like thermal bridges, internal convection in the wall due to infiltration air flows, enhanced heat transfer due to moisture content of structures, internal heat generation and the complex nature of heat conduction to the ground [27].

Convection

Convective heat transfer to an air node occurs at the interior surfaces and due to bulk air transportation to and from the node, as well as from convective internal gains. There is also convective heat flows from the surroundings to the exterior surfaces. Peeters et al. [28] show that the heat transfer coefficients are very important for BPS tools. Imprecise values or faulty correlations lead to inaccurate results. There are two ways of obtaining the heat transfer coefficients in TRNSYS. One way is to use the standard values, already implemented in the program or given by the user. The other is to use an “internal calculation”. This is merely a calculation of a set of implemented heat transfer coefficient correlation

equations given in the program. For detailed heat transfer calculation and model considerations such as the one employed in this work the internal calculation should be used. Equation 27 gives the generic equation performed by Type 56 to calculate the coefficient. In the properties window of the building in TRNBuild the different values for *a* and *e* can be implemented, according to setting. The different settings are heated and cooled floors and ceiling, and vertical walls. A set of standard values are implemented. For the exterior surfaces no correlation is given, and TRNSYS will produce an error if "internal calculation" is marked for an exterior surface. This is because the nature of the exterior surface heat transfer coefficients are highly dependent on situation and should therefore be given by the user for the given situation. If no such correlation or value is available the standard value given in TRNSYS will be utilized.

$$h_{conv} = a(\theta_{surf} - \theta_{air})^{e} \tag{27}$$

The bulk convection to an air node is present in the ventilation, infiltration and air movement between the different nodes. Equation 28 gives the heat transferred by this bulk flow of air. The volume flow is given by one of the three mentioned effects. The flow and inflow temperature can be user-defined or given as inputs to type 56 from other types, such as specialized ventilation types.

$$\dot{Q} = \dot{V}\, \rho_{air}\ \ C_{p,air}\, (\theta_{inflow} - \theta_{air}) \tag{28}$$

Location of the air flows, such as ventilation outlets, is not given and is thus assumed to be homogenous throughout the air node. This simplification means that local heat transfer coefficients and draft effects are not considered in the model. To model such details an advanced numerical method such as CFD should be employed.

Radiation

Surfaces within the zone are modelled as grey surfaces at two different wavelengths, which mean that they have different properties for two wave lengths, namely long-wave and short-wave. Short-wave radiation is radiated from the sun because of its high temperature and is divided into diffuse and direct radiation within TRNSYS. There are thus three different types of radiation modelled in TRNSYS. Windows are assumed opaque to long-wave, and partially transparent to direct and diffuse short-wave radiation.

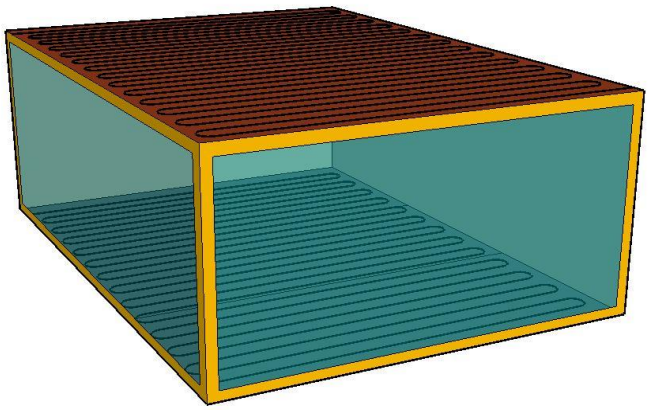

Figure 3.7: Example of how a zone looks in the Trnsys3d window.

TRNSYS 17 has the ability to use detailed radiation models using a detailed geometry. The building, room or zone can be sketched using a google SketchUp plugin called Trnsys3d and imported into TRNSYS as an .IDF file. Figure 3.7 shows how a room can be sketched in Trnsys3d. With this information the detailed models for direct and diffuse short-waved solar radiation and for long-wave radiation can be employed.

Figure 3.8 shows the difference between the standard long-wave radiation model and the detailed one. In the standard model an equivalent surrounding

temperature T_{star} is computed and the radiation transfer to each surface is area weighted. A radiation balance is calculated based on T_{star} and each surface gets its share of the heat according to area.

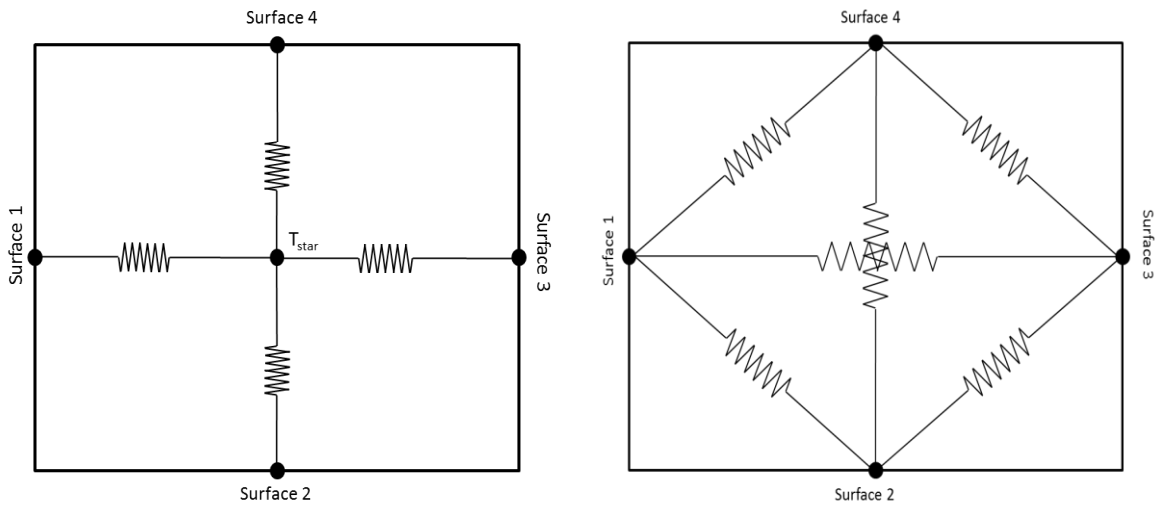

Figure 3.8: Left: Standard model for long-wave radiation within a radiation zone. Right: Detailed model.

In the simple model convective heat transfer is considered to the air node. Therefore it can only be utilized for zones with only one air node. The detailed model uses view factors to determine the heat transfer between all surfaces. Resistances between the surfaces consist of the same resistances as depicted in Figure 2.2. Gebhart factors are used for the calculations. The Gebhart factor is defined as the fraction of the emission from one surface A that reaches another surface B and is absorbed [25]. It is a function of the view factor between surface A and B as well as the reflectivity, emissivity and area of the surfaces, which are all constant during simulation. Thus, in the beginning of the simulation the view factor matrices and Gebhart factor matrices G^* are computed and throughout the simulation multiplied with the fourth power of the surface temperature vector:

$$\dot{Q} = G^* T^4 \tag{29}$$

The short-waved direct radiation, or solar beam radiation, is entering a zone through the exterior windows. This can be calculated by a standard or a detailed model in TRNSYS. The standard model takes in a user-defined parameter GEOSURF for each surface, which states how much of the incoming solar radiation that is incident on the surface. The trace of the solar beams on e.g. a floor during a day can be modelled with a schedule or input to this value. Another way of modeling this is to use the detailed model for short-wave direct radiation which uses the detailed geometry information to calculate how much of the direct radiation hits each surface at each time-step. This detailed calculation is only applied to external windows. For adjacent windows between zones the standard model is used.

The short-waved diffuse radiation standard model uses weighted area factors that take into account the surface properties reflectivity and absorptivity (walls are assumed opaque). For the detailed model uses the Gebhart factors method similar to the one for long-waved radiation. All surfaces are assumed to be transparent to be able to make the matrices, and are later defined with a transmitted solar radiation heat flux equal to zero.

According to the explanation given in section 2.1.3 and equations 10 and 11 the solar absorptivity and long-waved emissivity of the surface walls must be implemented. This is done in the wall type manager in TRNBuild.

Gains

Internal gains are modelled as source points within the geometry. Gains consist of latent and sensitive gains where the latter is divided into convective and radiative gains. Convective and latent gains directly influence the air node heat and moisture balances. For the radiative part there are two models, one standard and one detailed. The standard one employs area weighted factors for the distribution and does not consider the location of the gain in the geometry. This is considered in the detailed model where the 3D-location of the gains can be implemented as GeoPos in the Geo-Info window in TRNBuild. Source point view factors are computed and used to calculate how much of the radiative gain each

surface receives using the Gebhart factors. The location of the gain does not affect convectional and latent gain calculations within the air node is it located.

Comfort model

In the comfort type manager in TRNBuild the comfort model parameters clothing, activity, external work and air velocity must be user-defined. These are used together with the operative temperature to find the PMV-PPD values for the thermal comfort assessment. In the air node window of the zone in TRNBuild either a simple or detailed model for calculating the mean radiant temperature can be chosen. The simple model employs area-weighted factors of the surface temperatures, while the detailed model uses the Gebhart factors calculated by the point view factors of the actual location of the person in the room. The person is modelled as a point location in the room, given by the user as a GeoPos similar to the one for internal gains. Short-wave radiation is not taken into account. This leads to major uncertainties in thermal comfort calculations close to windows. Because local thermal comfort is a function of air velocities in the zone a detailed analysis is usually based on a CFD simulation. This is not a goal for this study and will therefore not be taken into account.

3.2.2 Active Layer Model In Type 56

To simulate RHS an active layer model is implemented in TRNSYS, whose aim is to simplify the complex 3D heat transfer of RHS into a 1D model that can be employed in the transient conduction transfer function method of TRNSYS.

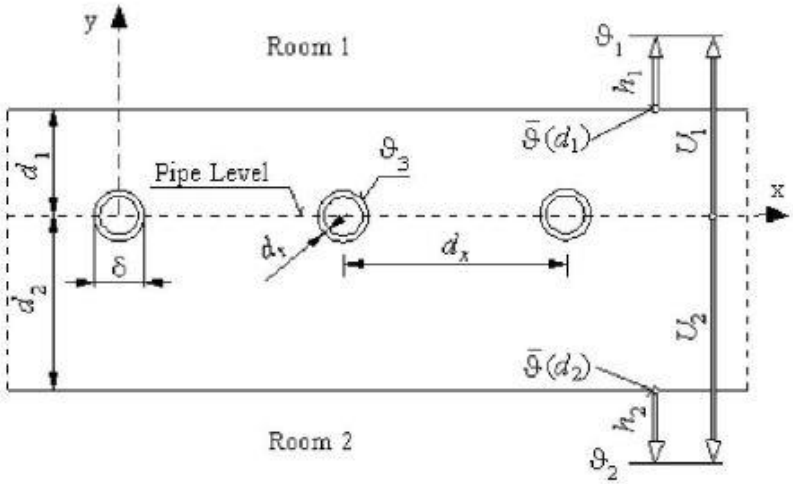

Figure 3.9: Thermo-active construction element. d_x is the distance between the pipes, d_r is the pipe wall thickness, δ is the pipe outer diameter. U_1 and U_2 are the thermal transmittance of layers, h_1 and h_2 are the heat transfer coefficients of room surfaces, d_1 and d_2 are the thicknesses of the layers, θ_1 and θ_2 are the room air temperatures and θ_3 is the pipe surface temperature. It is a 3D model because heat flows in both x and y directions while water flows in the z direction. Source: TRNSYS17 manual.

This model correlates the inlet temperature of the fluid with a simplified temperature called the average core temperature $\bar{\theta}_k$. It is a simplification from a 3D geometry of pipes to a 1D infinitely thin layer inside a structure. This layer has the homogenous temperature $\bar{\theta}_k$. Figure 3.9 shows a geometry layout of a typical radiant heating element. The modelled core layer is located at y = 0 in the figure. The *U's* are the thermal transmittance and can also be written as *1/R*, where *R* is the thermal resistance of the layers. A representation of this simplification is shown in Figure 3.10. The transformation from 3D to 1D is quite elaborate, and will only be briefly presented in this paper. For more details please refer to the TRNSYS 17 manual [25].

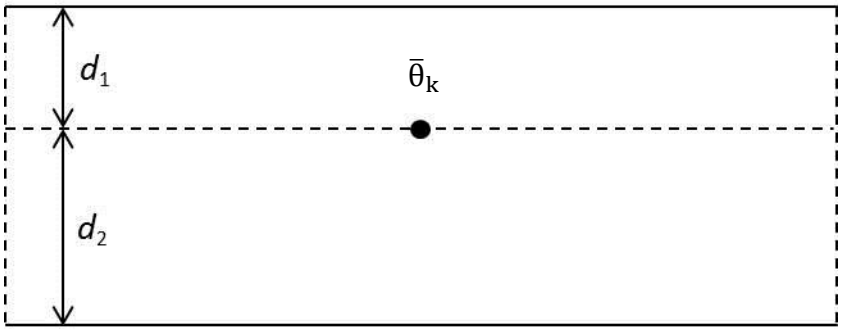

Figure 3.10: The 1D simplification of the 3D geometry of Figure 3.9.

Heat is transferred from the pipe to the two rooms as well as between the two rooms. This can be modelled as a triangular network of thermal resistances, which can be transformed into a star network (see Figure 3.11) to simplify calculation. This is equivalent to the standard method for the long-wave radiation thermal resistance network in TRNSYS (see Figure 3.8).

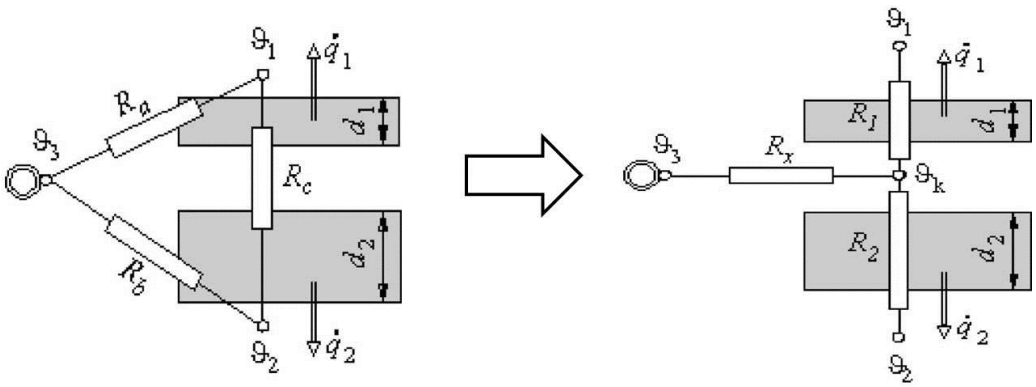

Figure 3.11: The delta-wye transformation of a thermal resistance network. The new temperature is simplified to an average temperature $\bar{\theta}_k$. Source: TRNSYS17 manual

θ_3 is the temperature of the pipe surface. R_x is the equivalent thermal resistance between pipe surface and the core temperature. Equations are needed to derive θ_3 from the user-defined inlet temperature θ_{in}. Heat transfer occurs from the

mean water temperature $\bar{\theta}_w$ in the pipes to the surface through convection at the inner surface and conduction through the pipe shell. This can be modelled as two thermal resistances in series. To relate the mean water temperature from the inlet temperature equations modelled as a thermal resistance R_z are used. Figure 3.12 depicts the total resistance network. Each resistance contains equations that are assembled to a total resistance formula (equation 30) for the total resistance between the inlet temperature and the core temperature of the active layer.

$$\mathrm{R_{total}} = \mathrm{R_z} + \mathrm{R_{conv}} + \mathrm{R_{cond}} + \mathrm{R_x} \tag{30}$$

The water temperature in the pipes is following an exponential curve. The final derivation of the formula for R_z contains a linearization of this curve which only holds if the specific mass flow rate $\dot{m}_{sp}$is sufficiently high. This is the water flow rate through the element per surface area. To make sure that $\dot{m}_{sp}$ is high enough common practice in TRNSYS is to split the surface of the thermo-active elements into smaller sections, thus decreasing the surface area and increasing the specific mass flow rate. After calculating the active layer temperature it is used in the transient conduction transfer function method of TRNSYS to calculate the heat flow and heat storage in the adjacent layers. Detailed thermal resistance formulas used in the simulations are presented in Appendix A:

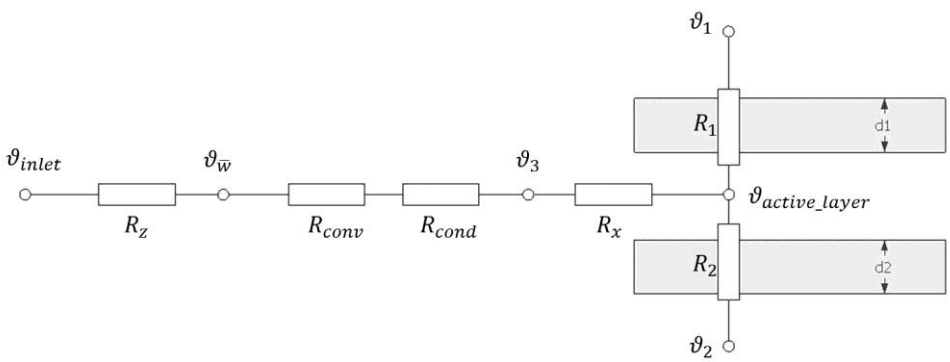

Figure 3.12: The total resistance network of the thermo-active construction element between inlet temperature and zone temperatures. Source: TRNSYS17 manual.

Another option is the type 653 “Simplified radiant floor” model, which utilizes an effectiveness approach in its calculations. This model is a part of the Thermal Energy System Specialists (TESS) libraries, for which the author has no license, and is therefore not considered. The active layer model in type 56 is nonetheless considered a more appropriate model for simulating the installed system in the laboratory, and is chosen as the simulation model for this work.

3.2.3 Weather Type

The ambient boundary condition for the simulations is the weather. Solar diffuse and direct irradiation, air temperature and humidity, wind, etc. are input parameters of huge importance. These inputs are given as a text file with a table of numbers normally given hourly for a whole year. Because of the relatively long data interval uncertainties arise, especially on partially cloudy days where the actual amount of direct solar irradiation might vary from minute to minute. When simulation time steps are shorter than one hour, a linear interpolation is used to derive data for each time step. There are many approaches to make weather input data. One such approach is called Typical Meteorological Year (TMY). It uses historical weather data to derive a typical year of a certain location. This type of weather file does not capture the worst case scenario, because such days are quite rare. The weather file is a file of type .tm2. An upgrade, .tm3, is available, but in TRNSYS the old type .tm2 has to be used. An important fact is that one of the most important parameters, solar irradiation, is usually not measured, it is estimated [27]. Another note is that the measurements are measured at a weather station. The local weather effects might be somewhat different at the actual building location. Caution must thus be taken when using weather data for detailed building energy estimation due to these uncertainties.

In this work the TMY file for Shanghai (CN-Shanghai-583670.tm2) is used in the simulations.

3.2.4 HEAT PUMP MODEL

Heat pump theory is introduced and briefly explained in section 2.7. Internally a heat pump is quite complex and a detailed simulation model of all its components is not computationally cheap. As a consequence, an approximation is required. Heat pump manufacturers provide characteristic power curves with their products that contain actual measurements done on the unit. These data are electrical power consumption and heating power (condenser power) for certain evaporator inlet temperatures and condenser outlet temperatures, from which COP can be computed according to equation 23. The powers are functions of two variables, which for ASHP are ambient air temperature and heating supply water temperature. An example of such curves can be seen in Figure 3.13. With the use of them in a simulation model it is possible to compute heat pump performance with the inputs inlet temperatures and mass flows to the condenser and evaporator. As the outlet temperature is a function of heating power and the heating power is a function of the outlet temperature, iteration is necessary. To simulate different heat pump sizes a linear scaling factor can be applied to both power curves. COP is then uninfluenced while the power input and output are increased or decreased.

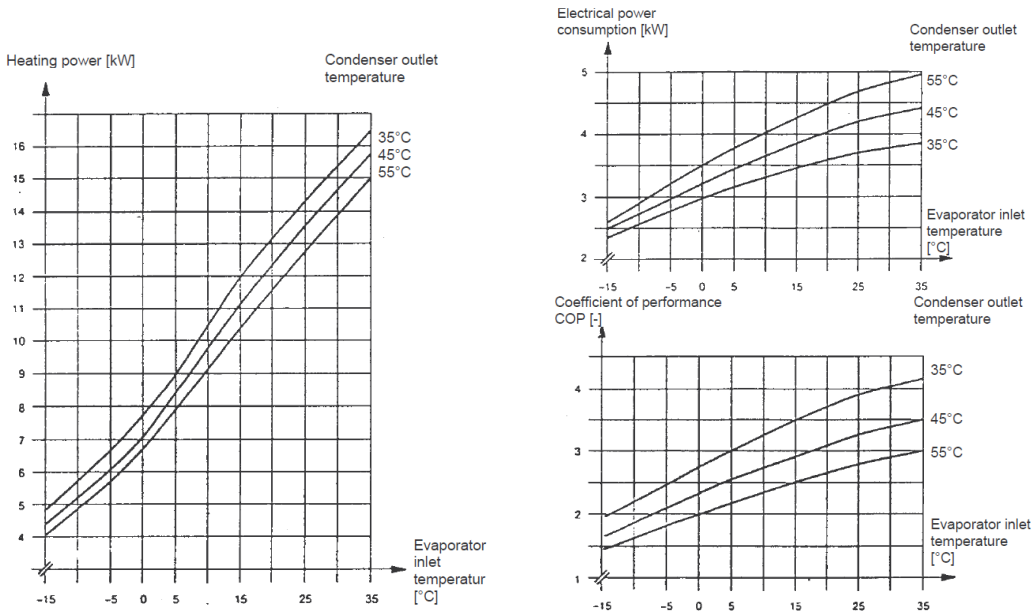

Figure 3.13: Typical performance curves of an air source heat pump. Source Type 401 manual [29].

This is exactly what TRNSYS type 401 "Compression heat pump" [29] does. With the inputs mass flow and inlet temperature to the two heat exchangers plus an externally computed heat pump on/off control signal it computes energy performance and outlet temperatures for the ASHP. The performance curves are put into the model as two sets of biquadratic polynomial coefficients of the form in equation 31, one for the electrical power consumption and one for the heating power capacity. These coefficients must be computed externally. An excel program provided together with the type 401 reads the performance curves and creates the biquadratic coefficients that is used in the model. The temperatures in the equation are normalized, marked by the subscript *n*.

$$\begin{aligned}\mathrm{Power} = {} & \mathrm{A} + \mathrm{B} * \mathrm{T}_{\mathrm{n,e,in}} + \mathrm{C} * \mathrm{T}_{\mathrm{n,c,out}} \\ & + \mathrm{D} * \mathrm{T}_{\mathrm{n,e,in}} * \mathrm{T}_{\mathrm{n,c,out}} + \mathrm{E} * \mathrm{T}_{\mathrm{n,e,in}}^2 + \mathrm{F} * \mathrm{T}_{\mathrm{n,c,out}}^2\end{aligned} \tag{31}$$

The model takes into account cycling- and icing losses. Equation 31 computes the steady state performance without losses. Cycling losses are then subtracted from this steady state value to calculate the real instantaneous heating power, which is integrated and averaged over the time-step to compute the outputs. Equation 32 comprises the whole calculation based on values from Figure 3.14 from the type manual. $\dot{Q}_{cycle}$ is the time-step averaged condenser power with the cycle losses accounted for.

$$\dot{\mathrm{Q}}_{\mathrm{cycle}} = \dot{\mathrm{Q}}_{\mathrm{ss,c}}(1 + \frac{\tau_{on}}{\Delta t} e^{-\frac{t_f}{\tau_{on}}} \left(e^{-\frac{t_{ub}}{\tau_{on}}} - e^{-\frac{t_{lb}}{\tau_{on}}} \right)) \tag{32}$$

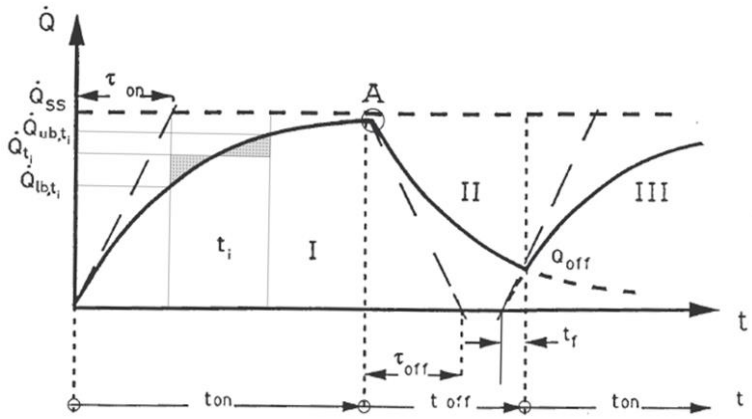

Figure 3.14: On/off cycle operation of a heat pump as presented in the TRNSYS model documentation [29].

COP is corrected for icing and defrosting losses according to the curve of Figure 3.15, which is a superposition of a straight line and a Gauss distribution curve. The Gauss curve reflects that icing occurrence is higher at around 0–5°C when the air contains more humidity than cold dry air, while the straight line represents the power needed to defrost the evaporator.

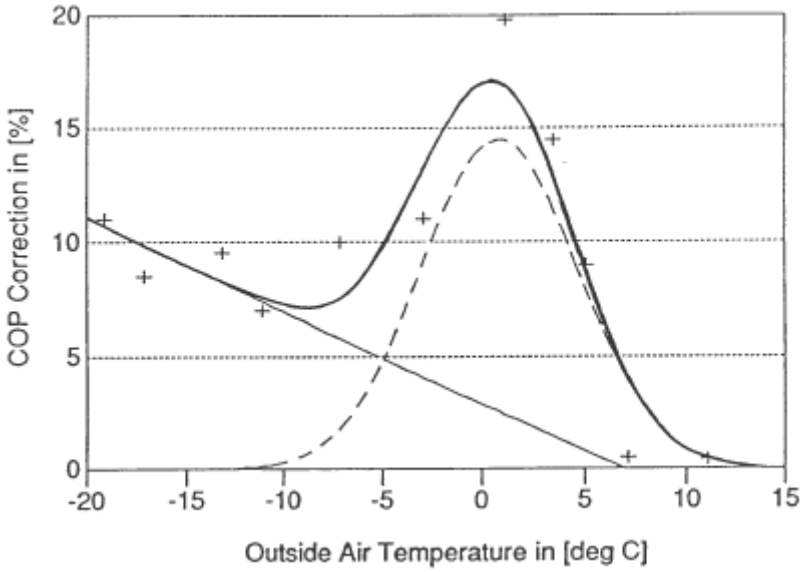

Figure 3.15: The COP correction curve due to de-icing used in the simulation model, as presented in the TRNSYS model documentation [29].

COP correction on the y-axis corresponds to the ΔCOP_{ice} in equation 34. Equations 33 - 35 show how the final condenser power is calculated in the model. With the compressor power and condenser power the evaporator power can be computed and from these the outlet temperatures of both heat exchangers. This completes the calculations performed by the model, see manual [29] for more detailed information.

$$\mathrm{COP_{cycle}} = \frac{\dot{\mathrm{Q}}_{\mathrm{cycle}}}{\mathrm{W_{el}}} \tag{33}$$

$$\mathrm{COP_{corr}} = \mathrm{COP_{cycle}}(1 - \Delta\mathrm{COP_{ice}}) \tag{34}$$

$$\dot{\mathrm{Q}}_{\mathrm{c,final}} = \mathrm{COP_{corr}} * \mathrm{W_{el,comp}} \tag{35}$$

3.3 MODELING THE SYSTEM IN GEL

The objective of this work is to build a simulation model of a radiant heating system that is installed in the Green Energy Laboratory at the Shanghai Jiao Tong University in China, see Figure 3.16. This model is then calibrated and validated to measurements done in the lab.

3.3.1 THE GREEN ENERGY LABORATORY

Figure 3.16: The Green Energy Laboratory building at the SJTU Minhang campus in Shanghai. The shading device surrounding the entire façade can be seen.

The GEL building was constructed at the Minhang campus in 2012 by SJTU in cooperation with the Italian Ministry for Environment, Land and Sea. It is a 1500 m^2 research center for energy-efficient solutions in buildings and contains many different laboratories and state of the art technologies for heating and cooling purposes. For its low-energy technologies it has been rewarded the LEED Gold certification. Amongst these is the radiant underfloor heating system installed in an office room which will be analyzed in this thesis.

3.3.2 The GEL Lab Room and Radiant Floor

The room is located in the south-east corner of the ground floor in the GEL building. Figure 3.17 shows a picture of the room taken at the time of writing and Figure 3.18 shows the lab as drawn in Google SketchUp. It is an empty room with different heating and cooling systems installed for experimental work. An air-water heat pump supplies heat and cool to the system. The two fan coil units (FCU) were tested by Chuan, et al. [30] for cooling conditions. From the schematic diagram in Figure 3.23 the hydronic location of the floor heating system can be seen. The hydronic system is explained in section 3.4.

Figure 3.17: Picture of the lab room at GEL. A fan coil unit can be seen on the floor to the left.

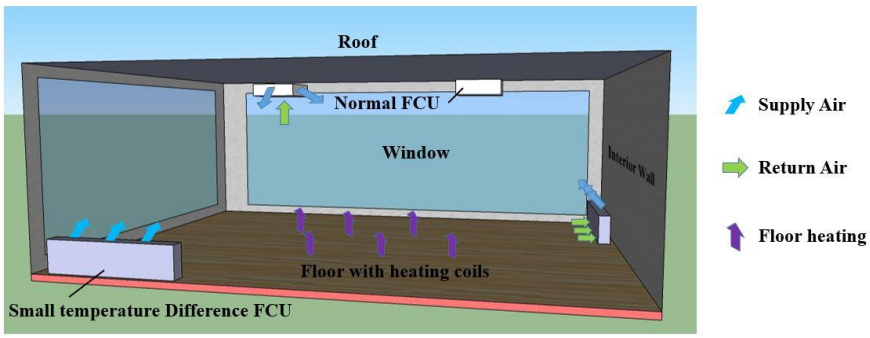

Figure 3.18: The office lab room. "Roof" is actually an adjacent room in the first floor. The fan coil units (FCU) provide both heating and cooling, while the floor is only used for heating. Source: Chuan, Z. [30]

Data on the room geometry, construction parameters and boundary conditions are presented below, together with necessary assumptions made.

Geometry		Area 53 m^2 and height 3 m. It has two exterior walls, one big facing south and another smaller facing east. Both have big windows, see Figure 3.18. For more details on walls and windows, refer to Appendix C.
Heating		Radiant underfloor heating and two different kinds of fan coil units, which all utilize hot water provided by the air-water heat pump. In this work only radiant underfloor heating was used. For details see Figure 3.19.
Cooling		Cooling is provided by two different kinds of fan coil units, which utilize cold water provided by the air-water heat pump.
Ventilation		Turned off during experiments. Not necessary to consider for the validation of the radiant floor model.
Shading		On the GEL building there is an exterior shading element encompassing the entire vertical façade. Assumed to block 100% of incoming radiation during experiments, the exterior shading parameter in Type56 was set to 1. Big trees are also blocking irradiation outside of the building.
Windows		Data provided by GEL students. U-value 2.83. A frame ratio of 0.3 is used in the simulations. See Appendix C.
Gains		No internal gains present during experiments
Infiltration		Not known, assumed to be 0.4 h^{-1} and constant. Adjusted as a part of the calibration process.
Boundary condition	*Adjacent rooms*	22°C.
	Ground	Data not given, so the average air temperature 17.2°C of Shanghai is used.
	Exterior	Shanghai TMY2 weather file. Hot and humid weather in the summer, cool and humid in the winter.

During the preliminary work for this thesis, it was assumed that the radiant floor in the laboratory provided cooling as well as heating. It later became clear that this was not the case, and that the analysis for this thesis should only focus on heating.

The tubes of the radiant floor are placed in a layer of concrete on top of an aluminum sheet with a layer of insulation underneath, all on the original floor of the building, see Figure 3.19. On top is a floor covering layer of wood, which serves an aesthetic purpose as well as reducing surface temperature and heat flow. Detailed layer properties used in the simulations are specific heat capacity, density and conductivity. No detailed information about these is available and standard values are employed in the TRNSYS simulations. These values are calibrated as a part of the validation process.

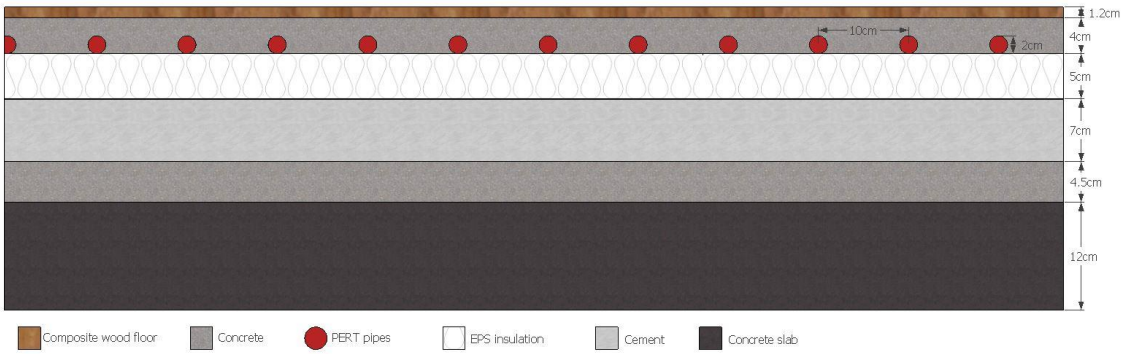

Figure 3.19: The floor construction in the x-z-plane. The bottom three layers is the original floor, with the radiant heating system installed on the top of it. Distance between pipes are provided in the system data, but were found to be inaccurate. The validated model contains a distance of 15 cm between the pipes. Pipe diameter is 20mm and pipe wall thickness is 2mm.

The detailed layout in the x-y-plane is not available, but some pictures from the time of construction were taken, and a rough sketch is made from these in Figure 3.20. Three different loops are connected to a single manifold, and the areas of the loops are all different. Loop 1 (the left loop in the figure) is assumed to have the biggest load due to its proximity to the large window surfaces. Because of the high u-value of the windows their surface temperature will be low during

heating conditions. Loop 1 has a higher total view factor to these windows surfaces than the other two loops and thus an increased heat transfer, cf. equation 8. Each loop contains a flow control valve, which are governed by a room thermostat. A rough estimate of the distance between pipes based on number of loops and length of the floor in x-direction is 15 cm.

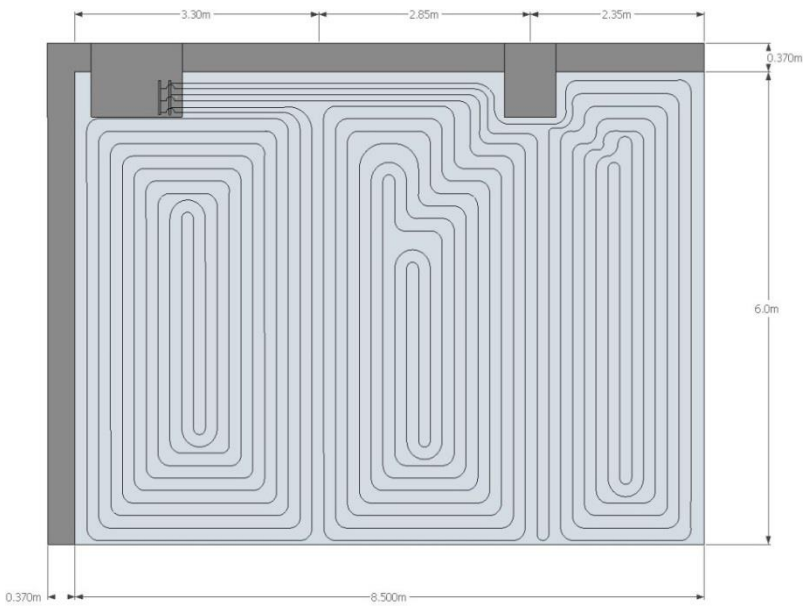

Figure 3.20: A rough drawing of the x-y-plane tube layout based on pictures taken at the time of construction. The thin dark areas are the windowsill. The three loops are numbered 1, 2 and 3 starting from the left.

3.3.3 Comparison To Typical Norwegian Radiant Floor Systems

The biggest difference between Norwegian and Chinese building practice is that more timber is used for residential buildings in Norway. In China, most residential buildings are concrete apartment complexes. The installed system in GEL is thought to be used in these types of apartments, and can be placed directly on top of an existing concrete floor. Many of the Norwegian radiant floor systems are developed for use in a timber construction and are thus inherently different in this regard. Systems which can be placed on top of an existing timber floor construction do exist. They rarely involve the concrete filling which is used

at the GEL, but rather gypsum or particle boards together with a temperature distribution plate of aluminum. Uponor has a good list of different Norwegian systems at their website [31].

In Norway, PEX tubes of diameters 12, 17 and 20 mm are used. As the tubes get bigger, the typical distance between them increases and is 125, 200 and 300 mm, respectively. Here a clear difference is noted, as the system installed in GEL has 20 mm tubes and a distance between tubes of about 15 cm. The tight bends caused by a close distance between the tubes are a limiting factor for the Norwegian systems. Why the Chinese system can have a closer distance when using 20 mm tubes is unknown to the author, but it could be that the tubes are of a more flexible material. As the layout information given to the author is found to be imprecise, their might also be a problem with the tube size data, but this is not further addressed here.

3.3.4 Model In TRNSYS

The active layer model described in section 3.2.2 is used to model the radiant floor installed at the GEL. This floor heating system model contains constraints depicted in Figure A-1, which limits the modelling capability. The system data given to the author is showed on the left side of Figure 3.21. However, the constraints hinder these exact data to be modelled, as distance between pipes d_x must be at least 5.8 times the tube diameter δ. With δ equal to 2 cm, d_x must be at least 11.6 cm. d_x equal to 10 cm will not run in TRNSYS and was thus set to 12 cm in the preliminary simulations. Another constraint is that the layer thickness d_1 from the center plane of the pipes upwards must be at least 0.3 times d_x, which with d_x equal to 12 cm is 3.6 cm. d_2 must be at least 0.5 times δ which is equal to 1 cm. In total the concrete layer must be at least 4.6 cm with d_x equal to 12 cm. The actual layer installed in GEL is only 4 cm thick. This problem was aggravated as d_x was shown to be around 15 cm, causing the concrete layer to be at least 5.5 cm in the simulation. As the author does not have access to TESS libraries of TRNSYS, which contains another radiant floor heating model, the problem is circumvented by changing the material properties of the concrete layer

surrounding the tubes, with a focus on conductivity. This is done in accordance with the supervising professor at SJTU. The values are calibrated to the measurements from the lab.

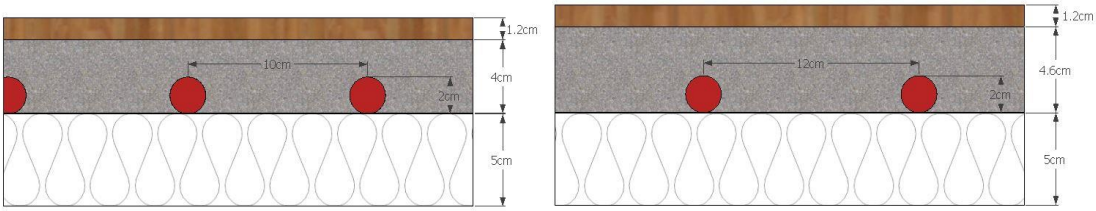

Figure 3.21: Limitation of the TRNSYS type 56 radiant floor model caused by the model constraints. The actual system data is to the left and the necessary adjustments for TRNSYS simulations to the right.

The lab room is modelled with the TRNSYS type 56, according to section 3.3.2 and Appendix C. Three different floor surfaces are created, each with an area corresponding to Figure 3.20 and modelled as radiant floor active layers in the building model. Distance between pipes was set to 15 cm. Inputs to the model are outside weather conditions provided by the typical meteorological year (TM2) file for Shanghai as well as radiant floor inlet temperature and water flow. For the validation simulations these inputs are from experimental measurements. Figure 3.22 shows how this is implemented in the TRNSYS simulation studio window. Measurements are averaged to time intervals of 12 minutes, the minimum time-step length for this system, before being printed to a text-file, which is imported into TRNSYS using a type 9 Data reader.

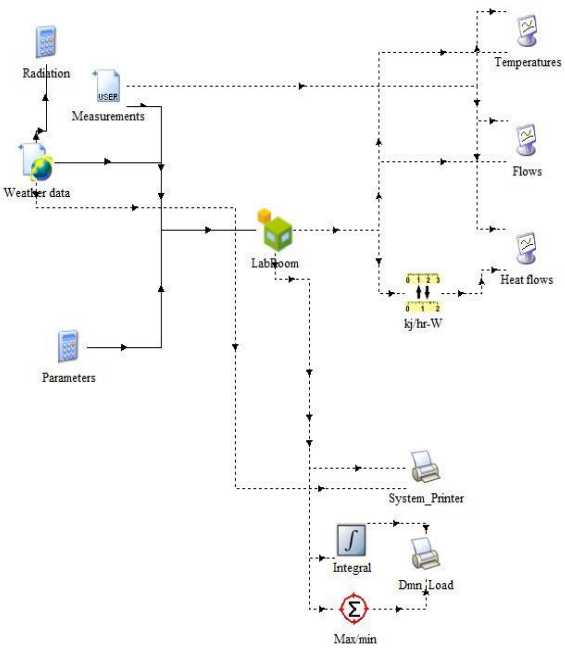

Figure 3.22: TRNSYS simulation studio screenshot of the lab room simulations.

3.4 EXPERIMENTS

Measurements are taken in the lab for comparison and validation of the simulation model. A hydronic schematic diagram of the heating and cooling system is depicted in Figure 3.23 and shows the location of the different measurement devices, from which most are placed outside of the actual GEL building, see Figure 3.24. For this work only the temperature measurements 103 and 104 as well as the flow meter 121 are of importance while the remaining measurements are used to monitor the entire system in operation.

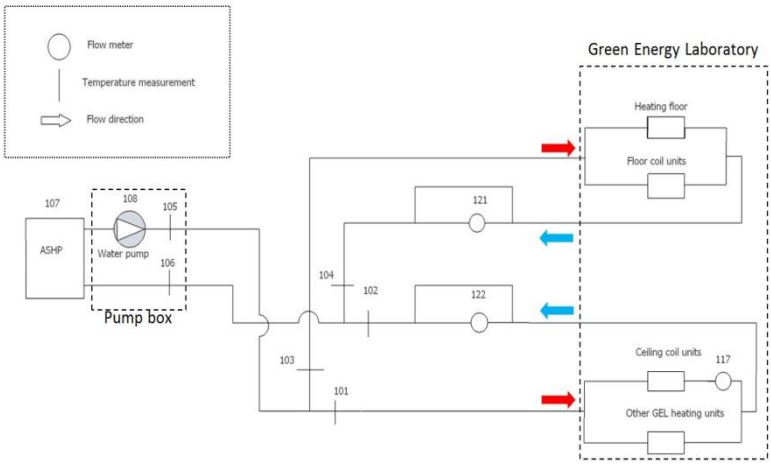

Figure 3.23: Schematic diagram of the system installed in the lab. Valves not included. 103 and 104 represent inlet and outlet water temperatures of the radiant floor respectively, while 121 measures the water flow through the floor.

Because these measurements are taken outside some uncertainty is expected. The distance from the floor loop manifold to the sensors is not significant however, and the discrepancies should not be critical. There are no detailed measurements per loop of the radiant floor and all measurements are taken for the entire floor as one. The floor heating fan coils and the radiant floor share the same sensors and to avoid any “leakage” through the fan coil loop the flow control valves to this are manually shut.

The sensors send the measurements to a data acquisition system (DAS) which samples and converts the signals to digital data at user-given time intervals, and sends it to an excel plug-in where they are printed as raw data. To convert the units from the raw data units of volts, mA and resistance Ω into normal units kW, °C and m^3/h, conversion equations provided by GEL students are utilized. The right side of Figure 3.26 shows the DAS and computer screen used in the experiments.

Figure 3.24: The outside part of the water loop. In the figure the air source heat pump, the pump box, flow meters 121 and 122 are easily seen. All thermal resistors are places close to the pump box. Compare to Figure 3.23.

No measurement is completely accurate and the sensors thus have a certain range of uncertainty. Table 3-1 is an overview of the sensors used in this experiment, their range of measurement and their uncertainty. More detailed information about the sensors is not available. Figure 3.25 shows pictures of the actual sensors installed. Because the measured data are directly used as inputs to the simulation, the uncertainty levels in the table can be used without any further error analysis.

Table 3-1
Sensors used in the experimental setup

Sensor type	Number of sensors	Measurement range	Uncertainty
Flow meters	3	0-40m³/h	5%
Thermal resistance	6	0-100°C	3%
Temperature logger	4	0-100°C	5%

The temperature loggers measure air temperatures inside the room and outside. Thermal resistors are of the type PT1000 and measure the temperature in the water loop at inlet and outlet of the different loads and the source. Figure 3.23 shows the placement of flow meters and thermal resistances. The information in this table is from the paper of Chuan [30].

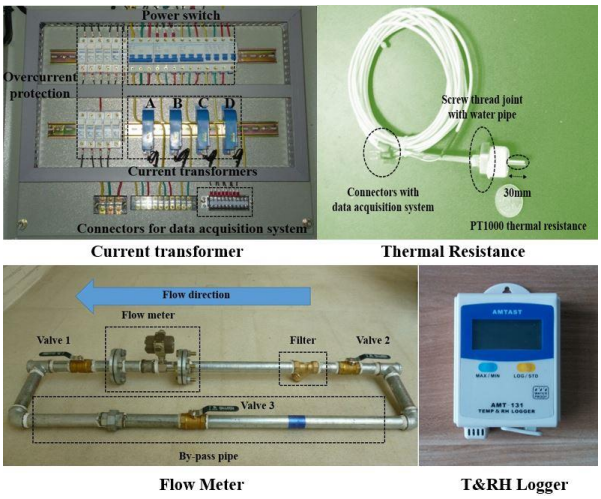

Figure 3.25: Pictures of the different sensors used in the experiments. Source: Chuan, Z.[30]

The DAS is set up by the user in the excel plug-in before conducting experiments. Which sensors to sample data from, their respective raw data format and time interval of the samples are the most important settings. Because of the time-step limitations of the TRNSYS wall transfer function method (see section 3.2.1), the time-step for the simulation model cannot be shorter than 0.2 hour, i.e. 12 minutes. It would be pointless to take measurements very often because of this, and a measurement interval of 1 minute is chosen and then averaged over 12 minute intervals for comparison.

The system is delivered by Carrier China, a part of the United Technologies Corporation, and is used for both heating and cooling. It comprises an air source heat pump with two compressors which use about 6-7 kW at stage 1 and 11-12 kW at stage 2, for heating. It delivers heat and cool to five different rooms in the GEL, four in the first floor and one on the ground floor, and is dimensioned accordingly. In all the first floor rooms, floor fan coil units are the end units. On the ground floor, in the laboratory room, there are fan coil units in the ceiling, on the floor as well as a radiant floor installed. A central operations control display (see Figure 3.26) governs each end unit of the system as well as the set-point temperature for the heat pump. Each end unit is controlled by a thermostat controller which has an on/off function as well as a set-point temperature for the zone, and controls an actuator on a 2-way valve on the water loop supplying the unit. These can be set manually in each room or centrally by the central controller.

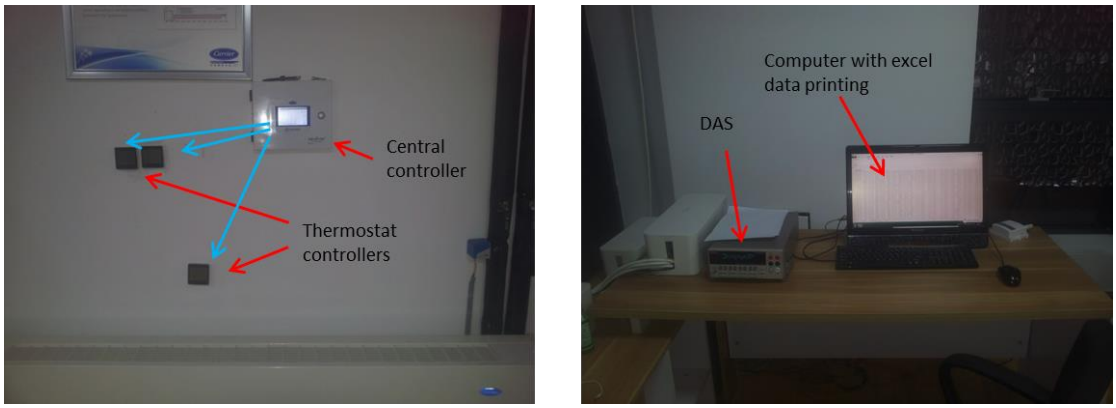

Figure 3.26: Pictures of controllers to the left and the data acquisition system with computer to the right. Each thermostat controller controls one unit, e.g. radiant floor. The central controller controls the whole system including the ASHP.

The goal of the experiments is to gather data for validation of a computer model of the radiant floor for heating. This fall was a warm one in Shanghai and heating conditions did not occur until ultimo November. As a consequence, the experiments were delayed by over a month. As the weather was stable and clear the temperature undulated significantly between night and day often being 15

degrees colder at night. Due to the big capacity of the ASHP and the low heat load of the laboratory room, other terminals in the building had to be on for the heat pump to function properly. Many trials were performed and due to the lack of information much time was spent analyzing the data to gain knowledge about the system operation. Power outages and voltage drops at the GEL caused some data to be corrupted. The computer depicted in Figure 3.26 was old and several experiments were corrupted by computer errors. Influence by occupants of the rooms in the first floor, where the fan coils were running during experiments, contributed to the time consuming analysis, as the fan coils were turned off and on and caused disturbances to the flows around the system. The ceiling fan coil flow meter (meter 117 in Figure 3.23) showed flow of around 0.40-0.70 m^3/h even though these fan coils were not in use. Reasons for this can be leakage through the two-way valve which is supposed to be completely closed, sensor inaccuracy or a faulty calibration of the sensor. This occurred on all experiments and the issue has not been figured out, but is not considered to be of major importance as the ceiling fan coils are located on a different water loop, as seen in Figure 3.23.

The outputs of the simulation are room temperature and outlet water temperature. Important inputs are outside ambient temperature, inlet water temperature and flow. These five are thus measured carefully and used in the TRNSYS simulations as inputs and for comparison of the outputs. Other data to the simulation are considered as parameters and boundary conditions and are explained in section 3.3.2. The room air temperature was measured with two temperature loggers inside and two outside in case one should fail or have corrupted data. Inside the loggers were placed in the middle of the room at heights 1.5 and 2 meters and throughout the experiments showed very little discrepancy between them. The outside loggers were placed in the shade at a height of approximately 1 m and close to the windows, one on the south side and one on the east. Also here no significant discrepancy was present during experiments. The temperature loggers and DAS were synchronized immediately prior to experiment initialization and later cross-checked. Set-point temperature for the room was set high to 30 degrees to ensure continuous radiant floor

operation. Several experiments were conducted, but only one was chosen for the validation as this one had the most stable operating conditions. It was conducted December 8th from about 1 pm until about 11 am the next morning, comprising 22 hours of operation. The data is plotted in Figure 3.27.

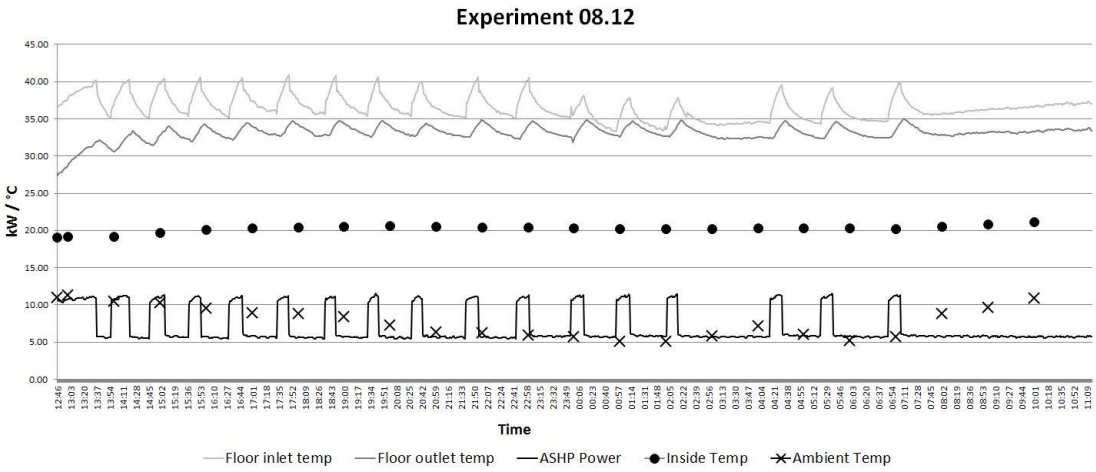

Figure 3.27: December 8th experiment. Operation from 12:46 to 11:09. Set-point for heat pump was 35 degrees. The water temperature undulates as the compressor changes between stage 1 and 2.

A stable operation can be seen with the ASHP switching between stage 1 and 2 with roughly constant indoor temperature and an outside temperature falling from about 12°C to 5°C at night. The room temperature set-point is at 30°C and the floor is thus always at full operation since room temperature does not even reach 21°C. The reason for this is the poor insulation of the lab room. Internal temperature sensors in the ASHP are used for the control of the heat pump and the values that are measured in the experiment might therefore deviate a bit from set-point 35°C. An analysis of the ASHP and the system as a whole is not a part of this work. The water flow to the floor during the experiment is plotted in Figure 3.28 and shows the nature of flow measurement, with highly rippling measurement values due to the turbulent flow of the water. According to Table 3-1 water flow meters are operating in a very narrow band of their range and this might cause some uncertainties as well.

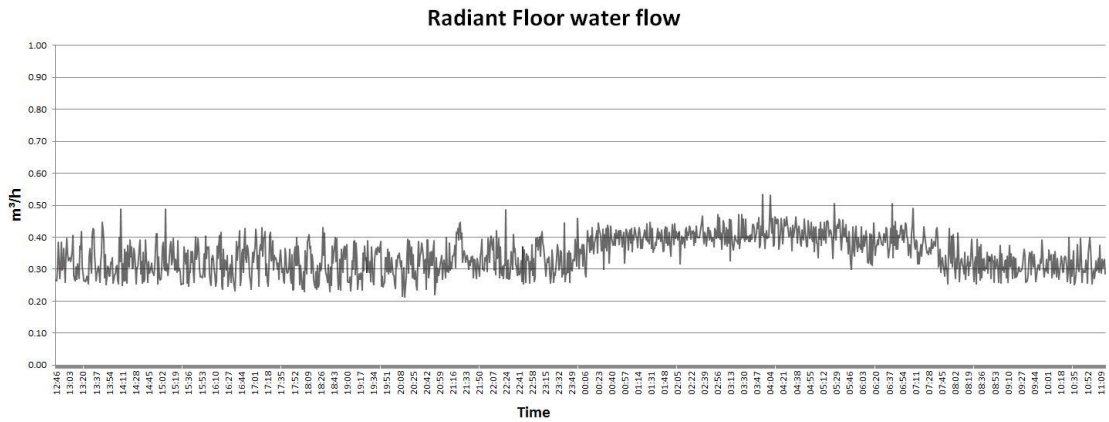

Figure 3.28: The flow through the radiant floor during the experiment December 8th.

The cause of the slight rise in flow during the night is not known, but it is assumed that other units have been turned off for the night, causing a higher total resistance to other water strings and thus more flow through the floor loop. Flow meter 122 did not show any changes in flow however. The water pump did not show any changes in power consumption. Supply temperature also decreases in the same time-span suggesting a higher flow through the heat pump, but this is not confirmed. For the simulation of the floor this will not cause problems however, as long as the measurements are correct.

To compare these values to the TRNSYS simulations, 12 minute averages are taken. The effect of this can be seen by comparing Figure 3.27 and Figure 3.28 to Figure 4.1. Values are evened out and the high fluctuations are not present. Top and bottom values are also cut. Radiant floors are not particularly fast reacting systems and this evening out of the experimental data is thus not considered to alter the results.

3.5 DATA PROCESSING AND ERROR ANALYSIS

Measuring flow and temperature is not an exact science and typically involve various errors. Limits on the precision of sensors, data acquisition error, human error, averaging error, etc. can all contribute to the uncertainty of the results. An example is solar irradiation through windows that when not considered can highly influence results. Accidents such as power outages and sensor failures can occur. Flow can be very unstable, with turbulent conditions in the vicinity of obstacles. Temperature can be highly influenced by air movement in a room, or by radiation from artificial lights or sunlight. The placement of the sensors is thus of crucial importance to reduce measurement error. In this work the temperature sensors are placed in the middle of the zone, not too close to the windows. Outside the sensors are placed in a height of approximately 1.5 meters, about 1 meter from the exterior wall and in the shade. Trees and the exterior shading device on the building blocks almost all incoming sunlight, and data for validation of the model are taken from times of no sunshine, e.g. during the night. Flow sensors are already installed in the system and their precision according to the manufacturer are given to the author as presented in Table 3-1. Entrained air bubbles and particle deposits in the pipes can highly alter their precision. Analysis of experimental measurements should contain error analysis to assess the uncertainty of the results. Here the measurements are not analyzed per se, but used as simulation inputs and output comparisons, and such an analysis is thus not required.

When using numerical models to simulate systems, truncation (rounding) and discretization errors occur. Detailed numerical modelling is not done in this work and these errors are therefore non-significant. Many systems are computationally expensive or even impossible to simulate, so approximations and simplifications must be made. The models used in this work are all approximations and simulation results should be analyzed with this in mind.

4 MODEL VALIDATION

In this chapter the measurements are compared to the simulation results to find the correlation between the simulation model and the experimental values. When the model does not correlate well to the measured data, the experiments and simulation model should be scrutinized for possible error before a calibration process is conducted. The initial results showed a significant discrepancy in the outlet water temperature of the floor between experiments and simulation. Outlet temperature from simulations was lower than that of the experiments by around 1-1.5°C. There are two main possible answers to why this occurs. Flow through the floor can be higher than the measurements show or the floor layer properties are incorrect in the simulation model. If the flow is higher, the outlet temperature will also be higher. If the conductivity of the floor top layers is higher than in reality, the floor will transfer more heat away from the fluid and thus decrease its outlet temperature. In the first case the performance of the radiant floor would be higher in reality than in the model, because of a higher flow while in the second case the performance would be higher in the model because of the increased conductivity. Radiant floor performance should be measureable by checking the room conditions during the experiments. The difference between measured air temperature and simulated was not bigger than around 1°C. The lab room infiltration number is unknown, but assumed significant because of poor window and door constructions. It is thus very hard to make a conclusion about the floor performance, because either the performance is good and the infiltration losses big or the performance is less good and the infiltration losses small, both creating the same heat balance and thus the same room temperature. The floor temperature could be measured to assess this, but this equipment is not available.

Possible flow measurement uncertainty is covered in section 3.4. Layer material properties of the laboratory system are unknown and thus uncertain. An improper installation of the tubes in the radiant floor might have led to a bad contact surface between the tubes and the concrete, and in this way causing a

high thermal resistance between them. Most probably it is a combination of these factors that contribute to the discrepancy experienced in the first results.

To calibrate the model to resemble the experimental results, an extra thermal resistance was put into the model by the means of lowered conductivity of the concrete slab that surrounds the tubes. The conductivity was changed from 1.8 to 1.0 kJ/hmK in TRNBuild. Density and capacity was slightly decreased to compensate for the thicker layer in the model, as explained in section 3.3.4. Flow through the tubes was increased in the model compared to the measurements, by 30 kg/h per loop, in total 90 kg/h for the whole floor. This adjustment is questionable, but a slight change in flow shows very good correlation to the measurements. In Figure 4.1 and Figure 4.2 the results of the calibration process is shown. As mentioned the air temperature difference was not very big in the first comparison and the infiltration number was calibrated slightly to 0.5 h^{-1}.

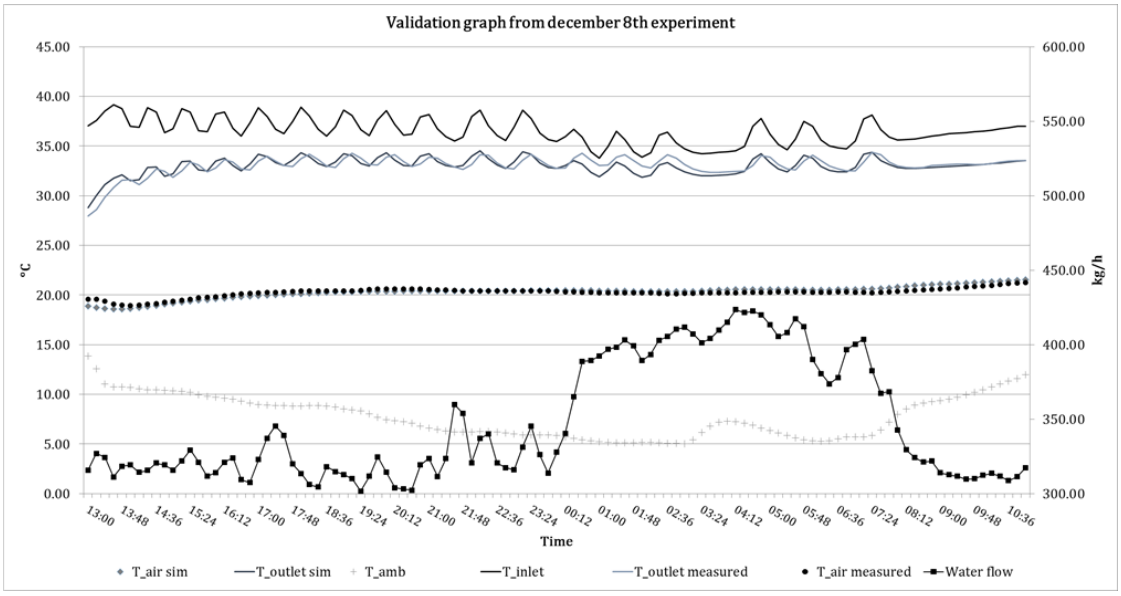

Figure 4.1: From measurements 08.12. Flows into the floor have been slightly increased for calibration. A good agreement between experimental data and simulation results can be seen.

In Figure 4.1 a change in water flow through the floor is seen during the day. The room conditions do not change during this time, and the change must come from influence by the system. This issue is addressed in section 3.4 and is not

considered to influence the results of the validation as the flow is implemented in the simulation as an input.

In both figures a very good correlation between experiment and simulation is shown. Biggest discrepancy in outlet temperature is about 1°C in Figure 4.1 and 0.4°C in Figure 4.2. For air temperature the maximum discrepancies are 0.5°C and 1°C, respectively. In the December 8th experiment (Figure 4.1) the supply temperature from the ASHP undulated, as in Figure 3.27. In the actual system a certain time lag exists between inlet and outlet water temperatures because the water needs time to pass through the system. The lag is not implemented into the simulation model and for this reason a certain "phase" difference can be seen in the figure. December 4th experiment did not have the same undulation and the discrepancy is thus smaller.

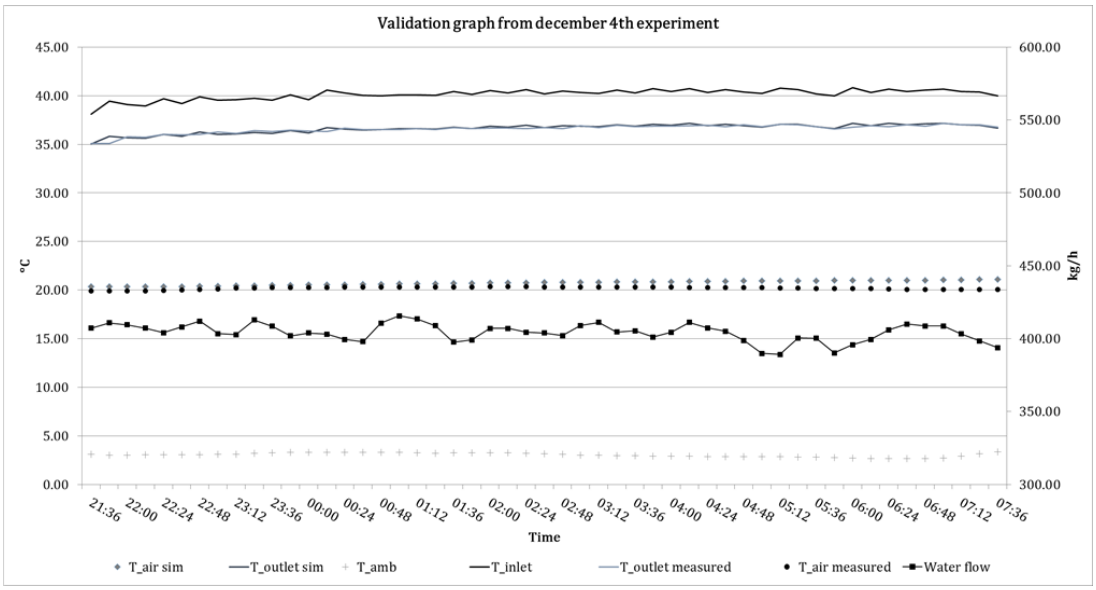

Figure 4.2: From measurements 04.12. Same flow adjustment as in Figure 4.1. Shows a good correlation between experimental data and simulation results. Stable operation on the heat pump ensures small undulation of the supply temperature.

A fictive layer is added to the top of the radiant floor model as an extra resistance to see if this could create equally good results. The outlet temperatures can be calibrated to the same values, but a discrepancy between air temperatures

arises, which cannot be calibrated by change the air infiltration rate, not even when it is set to zero. The air temperature of the simulations is off by about 2°C and this shows that the imposed change in water flow might be a good decision, because the floor is obviously performing worse in the simulations than in the experiments with this extra resistance.

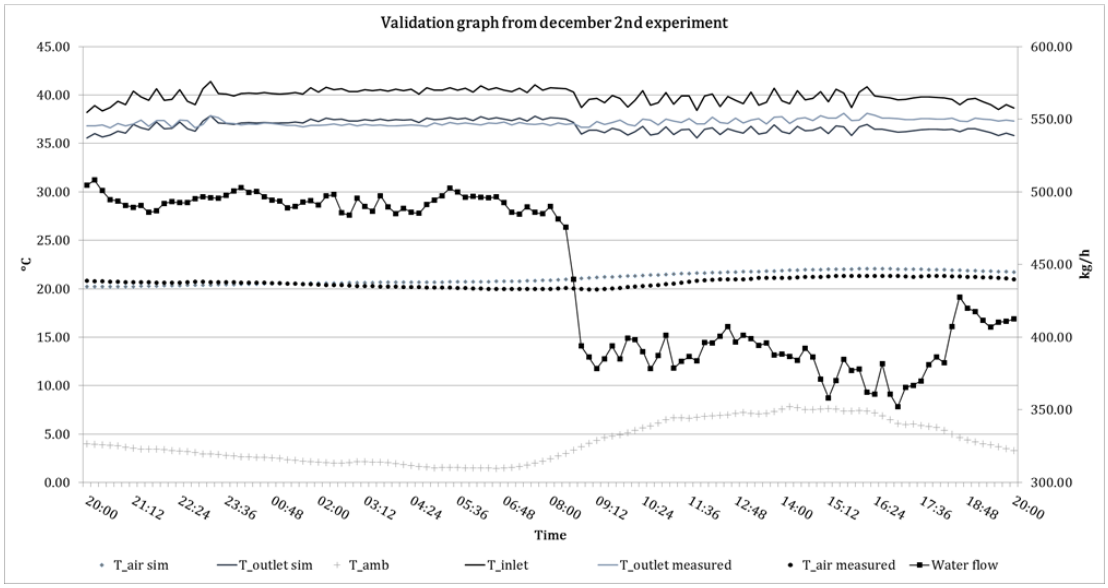

Figure 4.3: From measurements 02.12. Same flow adjustments as in Figure 4.1. Shows a good correlation during the night, but during the day of the 2nd there is a slight discrepancy and a decrease in flow.

A third comparison between simulation and experiment is shown in Figure 4.3 to further address the issue of the flow measurement previously mentioned. Simulation results correlates very well to experimental data during the night, but in the morning the radiant floor water flow drops about 100 kg/h, and a steady discrepancy between outlet temperatures is therefrom present. Air temperature shows no significant changes. Again, the reason for this change of flow is unknown. The outlet temperature measurement does not change even though the floor flow measurement changes. As the flow through a heat exchanger drops and given that the secondary side is the load, or cold side, the outlet temperature will drop. A radiant heating floor is a big heat exchanger with a cold side, and the outlet temperature should change with the flow through it. This issue is not

solved at time of writing and should be considered and figured out in future research of this system.

Distance between pipes was initially set to 15 cm based on pictures and measurements done in the lab, but is in the system information documented to 10 cm. TRNSYS will not accept 10 cm as explained in section 3.3.4. 12 cm was simulated and showed an inconsistency with the experimental data compared to 15 cm. Thus, based on simulations and experiments together with pictures from the time of construction, the distance between pipes is set to 15 cm in the model.

Final model layer properties can be found in Appendix C.

5 ANALYSIS OF THE RADIANT HEATING SYSTEM

An analysis of the installed system in the GEL is in this chapter conducted with the help of TRNSYS simulations of the validated radiant floor model. The purpose for the analysis is to evaluate the system for heating purposes in modern and future buildings where more and more of the heat is provided by renewable energy sources, heat pumps and district heating. The system is analyzed in Chinese (Shanghai) weather conditions. In the analysis, only the heating season is considered, which for Shanghai is regarded as November through April.

5.1 ASSESSMENT PARAMETERS AND INDICATORS

To be able to assess the system performance for different scenarios, the proper parameters for comparison must be elected. An end unit of a heating system is evaluated according to the thermal comfort provided to the occupants in the zones to which it provides heat and how much energy it utilizes for this purpose. Because renewable energy sources (RES) and heat pumps have better efficiency the lower the temperature they are providing, supply temperature is also of importance and can thus be seen as an indicator for the coefficient of performance (COP) of the entire heating system. Peak performance of the system is evaluated to assess if the system can deliver enough heat during maximum heat load conditions. In this work the energy use and thermal comfort are evaluated and their parameters are described more carefully in the following sections. Supply temperature and peak performance are handled more indirectly because they are a consequence of providing thermal comfort. If the system cannot provide during very cold periods it will naturally affect the thermal comfort negatively and it is then evident that the peak performance is unsatisfactory. Supply temperature is constrained by the thermal comfort requirements of the floor surface temperature and is optimized to provide sufficient heat.

5.1.1 Energy

To evaluate the energy use of the system between each simulation, the output parameter energy per square meter and year is selected. From the active layer model in type56 the Ntype59 output "energy input by fluid of active layer" is used for this purpose. The output gives the momentary heat delivered to each loop of the radiant floor as calculated by equation 18 in kJ/hr. A unit conversion to W/m^2 must be conducted before it can be integrated over the year to yield the final output in kWh/m^{2}a. How this is connected in TRNSYS is shown in Figure 5.1. The equation model labeled "UnitConversion" sums the output of the different loops, convert the units and divide by the total area of the zones.

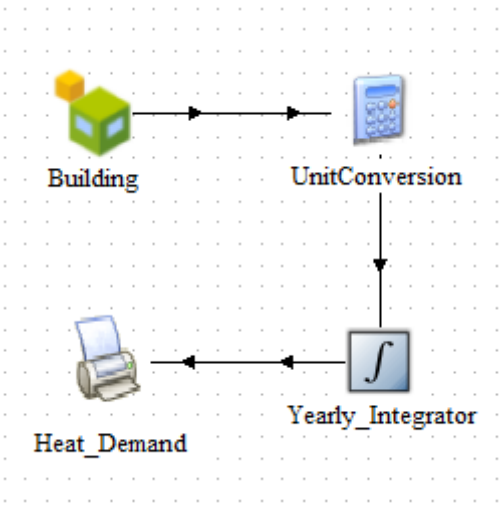

Figure 5.1: Simulation studio window of the heat demand handling.

This parameter only shows how much energy is put into the radiant floor from a source, such as a thermal storage tank, and does not directly give the heat input to the zone. The momentaneous heat input to the floor is equal to the heat delivered to the zones plus the heat stored in the floor plus the heat that is lost directly to the ambient. Over time the heat stored in the floor must either be transferred to the ambient or to the zone, so for long simulations the difference between supplied heat to the floor and delivered heat to the zone can be viewed as losses. For radiant systems this is expected to have a slightly higher value than for conventional systems because they intrinsically warm the surfaces in the

zone and thus indirectly causes higher transmission losses to the surroundings. A higher heat loss to zones/ground beneath the floor is also expected.

5.1.2 Thermal Comfort

To evaluate thermal comfort the Predicted Mean Vote (PMV) as explained in section 2.2 is used as the assessment parameter. Operative temperature would also be possible to use for this purpose, but is a rougher estimate. The detailed thermal comfort model is applied in the simulations wherein activity and clothing factors of the occupants are defined and PMV is thus considered more appropriate. Similar results would be expected with both parameters as the difference in activity and clothing factors between the zones are very small. PMV values are averaged over each month of the heating season in correspondence with equation 37 by a periodic integrator shown Figure 5.2. This integrator also calculates the maximum and minimum PMV averages every month as well as the time of these so that problematic conditions can be identified and studied. Occupancy is implemented into the simulation models, and it can be argued that PMV can only be evaluated when there are occupants present. Equation 36 is tried accordingly, and shows the same results as the easier to calculate monthly average. This is shown in Figure 5.3. Occupancy is here a number of either 0 or 1 in each time-step. Consequently, the simpler calculation method of equation 37 is used.

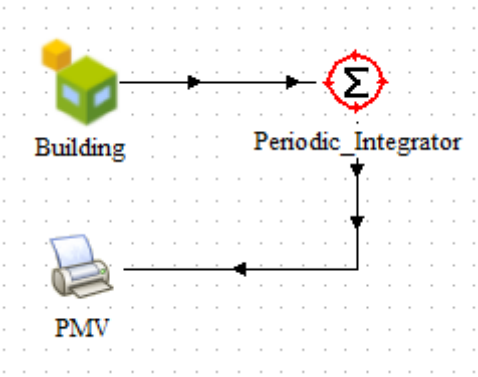

Figure 5.2: Simulation studio window of the PMV handling.

$$\mathrm{PMV}_{\mathrm{avg,occupancy}} = \frac{\int \mathrm{PMV} * \mathrm{Occupancy\,dt}}{\int \mathrm{Occupancy\,dt}} \tag{36}$$

$$\mathrm{PMV}_{\mathrm{avg,month}} = \frac{\int \mathrm{PMV\,dt}}{\int \mathrm{dt}} \tag{37}$$

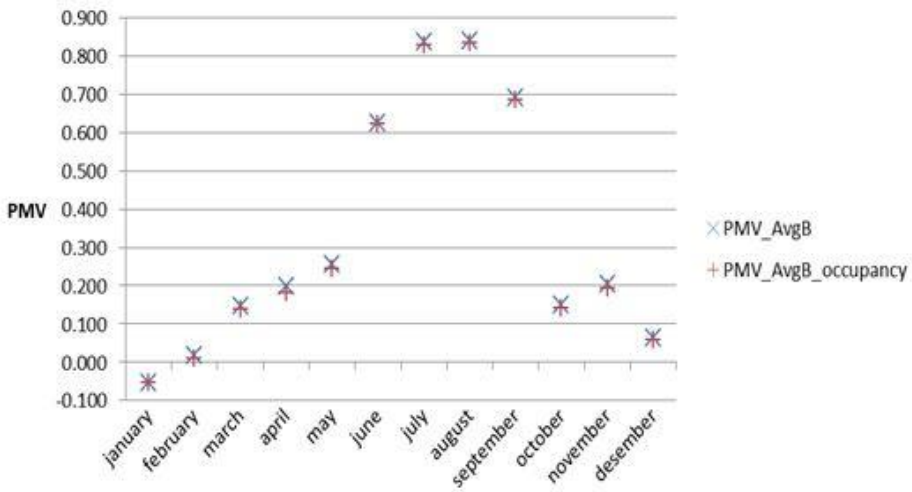

Figure 5.3: The difference between PMV month averages and PMV averages in occupancy hours per month for room B in the model.

Even though the average PMV can be zero, the momentaneous value will undulate around this average. To assess this difference from the average the sample standard deviation (SSD) as well as minimum and maximum PMV values is used. SSD is calculated according to equation 38. The closer the SSD is to zero, the closer the PMV is to the average value and the general comfort can be said to be better.

$$\mathrm{SSD_i} = \sqrt{\frac{\sum_{start_i}^{stop_i} (Value_i - Mean_i)^2}{N_i - 1}} \tag{38}$$

Maximum surface temperatures of the radiant floors are also monitored during simulations, as they are important to consider for thermal comfort. Surface temperatures over 27°C will be felt as too warm by occupants.

5.2 VALIDATED FLOOR MODEL IN A TYPICAL CHINESE APARTMENT

The radiant heating floor system implemented in GEL should be analyzed according to Chinese weather and building standard. First the model is simulated in a very basic way without controlling and compared to an ideal heating source model. Problems are highlighted and the system optimized looking at different control strategies: temperature control, flow control and other possible ways of optimization. A final assessment of the system with regard to performance is made in the end.

5.2.1 THE MODEL

A model of an apartment which is located in the 2nd floor of the GEL is given to the author by GEL students and used for the analysis. All the dimensions are given in the model, which is made in an older version of TRNSYS. The dimensions are taken into Trnsys3d, sketched and imported to TRNBuild so that the detailed long-wave radiation and comfort models can be utilized. Figure 5.4 shows the model in Trnsys3d. The left of Figure 5.5 shows the dimensions as seen from above, with north pointing upwards. It comprises three zones where the large one is considered as a living room and the two smaller ones as bedrooms. The northern bedroom is referred to as room A while the southern room B. One bedroom could possibly be considered a bath room, but this is not taken into account here. South, east, north and roof are exterior surfaces, while the west surface has adiabatic boundary conditions. The floor has a constant temperature boundary condition of 22°C. On the roof of the actual GEL building a large triangular structure, on which PV-modules and thermal collectors are installed, provides approximately full shading for the roof surface of the apartment. To model this shading the solar absorption α of the roof is changed from 0.6 to 0.1.

Wall layers are the same as for the model used in the validation simulations (see Appendix C) with exception from the ceiling, where an insulation layer is added to lower the u-value to 0.34 W/m²K. Windows are given to be of U-value 2.83 W/m²K as in the validation simulations, but this is changed to 0.86 W/m²K considering that the aim is to analyze a modern building. The roof has a U-value of 0.34 W/m²K.

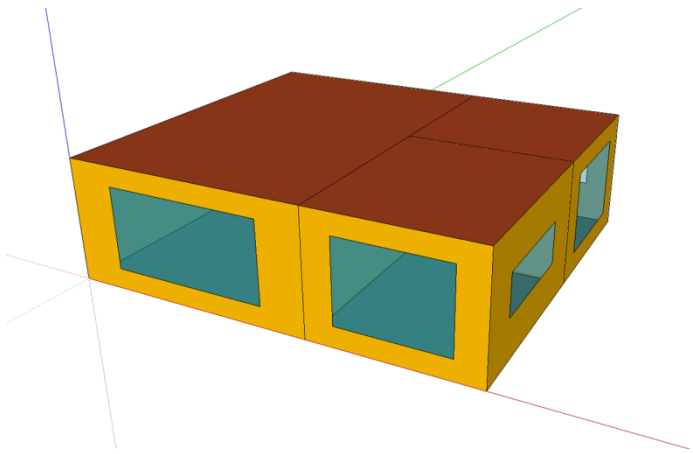

Figure 5.4: The model as made in the SketchUp plug-in Trnsys3d. 3 zones can be seen: One large living room and two smaller bedrooms to the east.

To capture a bit of real condition with possible solar irradiation effects the exterior shading on the eastern façade windows is set to 50%, while on all other windows 100%. Detailed shading and short-waved radiation analysis is not a part of the scope for this work and is thus omitted.

Detailed models of long-wave radiation and thermal comfort are utilized. The right of Figure 5.5 shows the positions used for thermal comfort. All are in a height of 1.5m. In the living room there are two positions used, but throughout the analysis these two did not show any difference in PMV between them. This is because of the shading of the windows of this zone and the homogenous floor temperature of the model. With a partitioned floor surface and no shading some difference would be expected. Also, the thermal comfort models do not consider short-wave radiation.

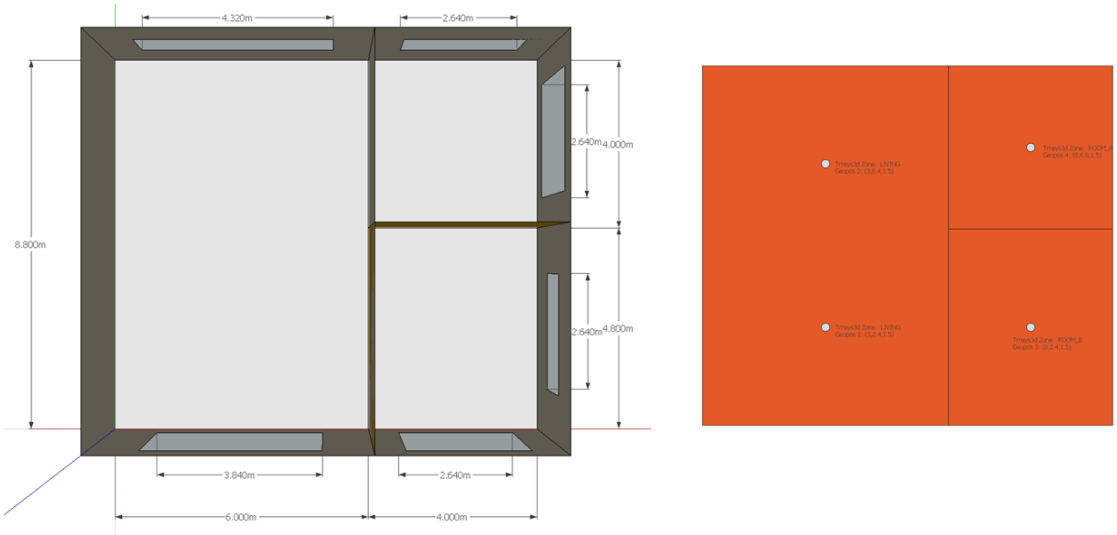

Figure 5.5: Room dimensions and geopositions used in the detailed thermal comfort model. White dots in the right figure are the location of the thermal comfort nodes.

Internal calculation of convection coefficients is used on internal surfaces. Infiltration is assumed constant and equal to 0.4 h^{-1}. Ventilation and internal gains are implemented according to schedules. In small bedroom there is one person present 23:00 – 07:00 on weekdays and 24:00 – 08:00 on weekends. In the larger bedroom 2 persons are present at the same times. For the living room all 3 persons are present 07:00 – 08:00 and 16:00 – 23:00 on weekdays and 08:00 – 11:00 and 17:00 – 24:00 on weekends. The activity of the persons in the living room is labeled "Seating, eating" in the standard ISO7730, while for the bedroom "Seated, at rest" in the same standard. In the living room there are also implemented internal gains from a computer of 140 W and 5 W/m^2 of artificial lighting heat gain which follows the occupancy schedule. The ventilation is demand controlled and follows the occupancy schedule for the entire model. The rate is set to 26 kg/h/person according to standards plus a constant air exchange rate of 0.15 h^{-1} for removal of pollutants from materials. Inlets are assumed in bedrooms, and outlet in living room. A type91 heat exchanger is used to model a constant 90% efficiency heat recovery unit.

Weather imposed is the typical meteorological year (.tm2) for Shanghai.

Each zone has one active surface on the floor and the model is the same as the one validated in chapter 4 with $d_x = 15$ cm. The floor surface of the living room is quite large and with only one loop the length of that loop would be long and the pressure drop significant. In real life this is normally tackled by splitting it into several, shorter loops. In the type56 model pressure drop is not accounted for, and for these simulations a partitioning of the surfaces in the living room is thus not necessary. This is not considered to have an influence on the results because the total flow and temperature drop would be the approximately the same for one loop as for several, in the simplified simulation model. For very detailed simulations a more realistic layout of the tubes should be considered, but for this model it is non-significant.

The heat curve for the model is shown in Figure 5.6. This is made with a simulation of an ideal heating using the TMY weather model, which do not capture worst case scenarios. Maximum heat load calculation is performed by TRNBuild and with a heating set-point of 22°C and design outdoor temperature of -4°C yields 41 W/m^2, which is depicted as a circle in the figure. It is thus not a super-insulated building, but as a typical Chinese apartment in which a radiant floor could be installed it is important to analyze.

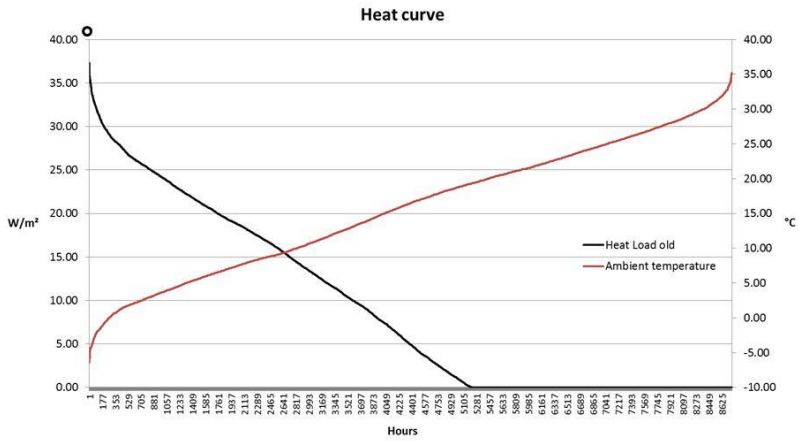

Figure 5.6: Heat curve of the Chinese model. Design outdoor temperature -4°C.

A summary of maximum heat load calculations is presented in Table 5-1. The heat load presented above can be recognized in the third row. Original windows are poorly insulated and cause a 10 W/m^2 increase in load compared to the proposed new windows. To see how this model would perform in a climate much colder than Shanghai, like the northern parts of China, a design outdoor temperature of -14°C was simulated. Even with the more insulated window this shows a maximum heating load of 57 W/m^{2}K, which is higher than the maximum heat rate from the floor (see Table 5-2). For the old window model in Shanghai conditions, the radiant floor can barely provide the maximum heat load of 51 W/m^{2}K. The model needs a better insulation level to be operated by a radiant floor and the proposed new window with a u-value of 0.86 W/m^{2}K is therefore used in this analysis. If a radiant floor is to be used in a cold climate, the level of insulation must be even better, and a focus on improving exterior wall insulation is recommended (In the GEL model the u-value for the exterior walls is 0.57 W/m^{2}K).

Table 5-1
Heat loads under different climates

Window U-value [W/m^{2}K]	Design outdoor temperature	Maximum heat load [W/m^2]
2.89	-4 °C	51
	-14 °C	72
0.86	-4 °C	41
	-14 °C	57

Maximum heat loads for the model with windows installed at GEL and proposed new windows. Two different climates are simulated: Shanghai climate with a design outdoor temperature of -4°C and a colder climate. Zone air temperature 22°C

5.2.2 Heating Floor vs Ideal Heating

The goal of the first simulations is to show why the system has to be controlled by comparing simulation results to that of an ideal heating model. Ideal heating is a question of definition. In this model the ideal heating is considered to be a heating source which can provide a room air temperature of 23°C for the living room and 22°C for the bedrooms. Cooling and latent heat consideration are omitted completely. In the simulations performed in this part the mass flow through the radiant floor is equal to an observed flow from the experiments of about 500 kg/hr, or 9 kg/hr/m². 3 different supply temperatures are simulated and the results can be viewed in Figure 5.7 and Figure 5.8.

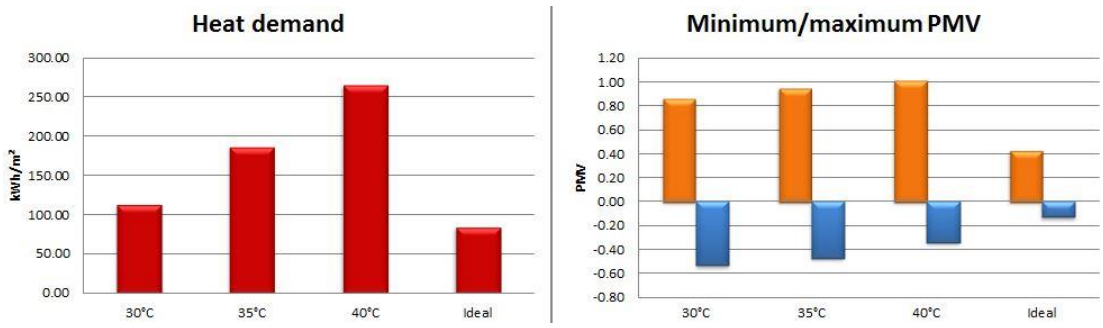

Figure 5.7: Heat demand and extreme values of PMV for constant flow and various constant supply temperatures. Min/max PMV values are for bedroom A.

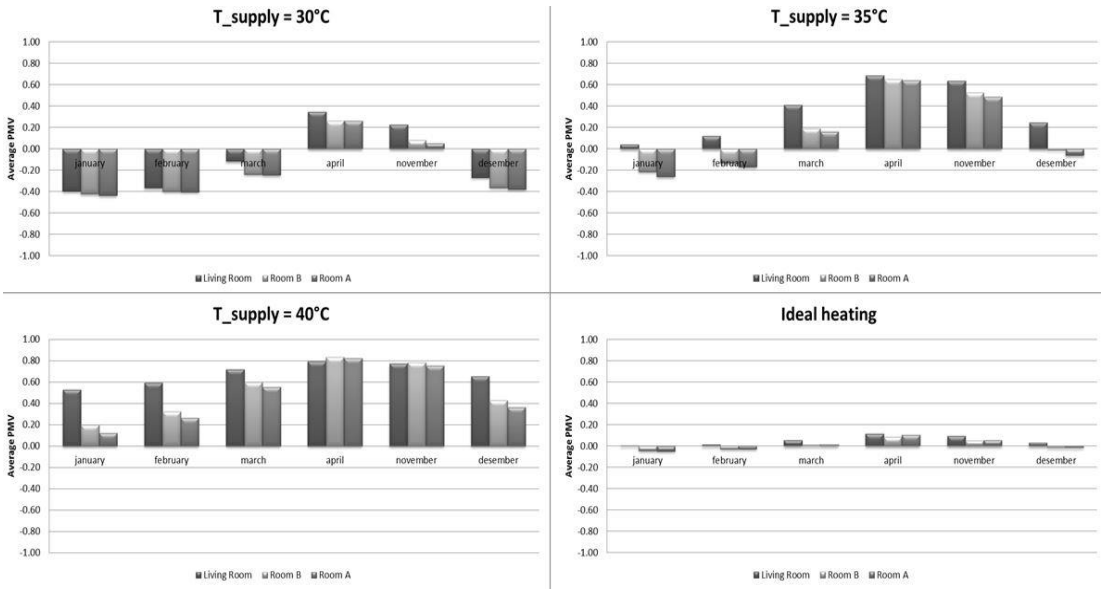

Figure 5.8: Average PMV for constant flow and constant supply temperatures.

It can be observed that the energy use increases with rising supply temperature, as expected. The ideal heating comprises a heating demand of 84 kWh/m²a, has very good thermal comfort because of almost zero average PMV values and a small minimum PMV value. Room A is the smallest and has a big east facing window. With 50% exterior shading solar irradiation will enter in the morning and this causes the maximum PMV value shown on the right of Figure 5.7. With a supply temperature of 30°C enough heat cannot be provided in the coldest months, and at the same time causes overheating in the mid-season months and especially in April which is the warmest. 35°C is way too hot in April and November, but still too cold in January. 40°C is better and the minimum PMV value is now -0.34, which is within thermal comfort limits. However, serious overheating occurs using this supply temperature and the heat demand is huge with 265 kWh/m²a. The surface temperatures of the floor also exceed thermal comfort criteria and reach over 30°C in April.

These results show that the system has the potential of providing enough heat and that different supply temperatures are suited to different heat loads. There is thus an urgent need for a control of the supply temperature to avoid overheating and will be simulated in the next section.

5.2.3 Supply Temperature

How to control the supply temperature of a radiant floor is covered in section 2.6. An outdoor reset line for supply temperature, depicted in Figure 5.9, is implemented into the model. Several different curves are tried and this is the one that gives the best results. A thorough optimization of the curve is not considered. The supply temperature is controlled by the momentaneous ambient temperature. Another option is to control for average ambient temperature, an option that is tried in the next section.

Two simulations are performed, with different mass flows. In the first simulation the same mass flow as before is kept and in the second a higher mass flow to the bedrooms is implemented to see if this can alleviate the low PMV values at peak

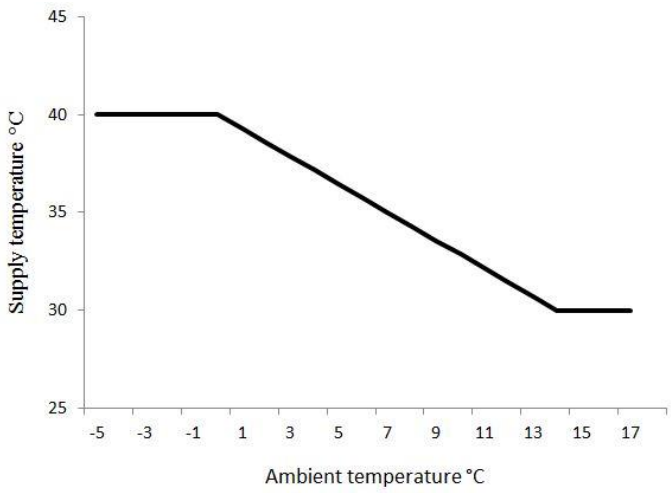

Figure 5.9: The outdoor reset line used in the simulations.

heat loads. Flow to living room floor is kept constant 9 kg/hr/m². The results of the simulation can be viewed in Figure 5.10 and Figure 5.11. Comparing the first simulation to the results in Figure 5.8, average PMV values are better and energy use is lower than both constant 35°C and 40°C. A minimum PMV value of -0.4 as well as a negative average PMV for the bedrooms in January does show that the system still does not provide enough heat during the cold periods of January.

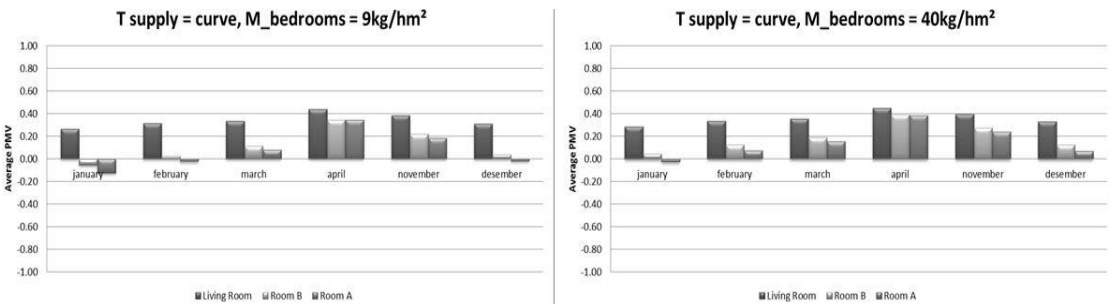

Figure 5.10: Average PMV for constant flow and ambient temperature compensated supply temperature. Living room has a constant flow 9 kg/hr/m².

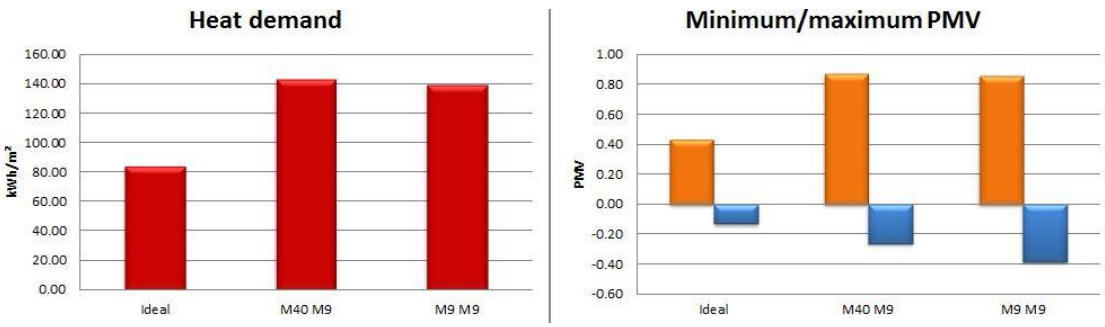

Figure 5.11: Heat demand and extreme values of PMV for constant flow and variable supply temperature, compared to the ideal heating. Min/max PMV are for bedroom A. M40 M9 denotes that bedrooms have a 40 kg/hr/m² flow, while living room has 9 kg/hr/m².

The maximum water velocity through the tubes is considered to be about 1 m/s due to turbulence noise and pressure drop considerations [32], and corresponds to about 40 kg/hr/m² in specific mass flow for this system. A pressure of approximately 813 Pa/m is calculated using the Moody diagram, see Appendix D. This mass flow is given to the bedrooms, which are experiencing the lowest temperatures, to see if the cold problem can be ameliorated this way. The results show that the average PMV as well as the minimum PMV for the bedrooms in January improves, but to the expense of overheating issues. Heat demand increases a little which is expected when average temperatures rise. Compared to the ideal heating there is still room for improvement and the overheating issue is grave. It is apparent that a flow control is necessary, and that each room should be controlled separately because they have different heat loads.

5.2.4 Flow Control

The ways to control flow are mentioned in section 2.6. In this section these will be simulated, together with some other ideas for optimization. Water flow to each active surface in the zones is controlled by one controller per loop. Set-point for the zones is 23°C and the controlled variable is operative temperature. Simple on/off controllers of type 22 in TRNSYS are simulated with a ±1°C hysteresis and the same flows as in the last section with a higher flow to the bedrooms. P-controllers and PI-controllers are simulated with a gain constant of

20 for both and an integral time of 8 for the PI. D-action is not considered. Time was spent on figuring out how to optimize the P and PI controllers, and in the end the values of 20 and 8 are chosen even though they are not optimized very well. With the time-step of these simulations of 1 hour an optimization of these values would be unrealistic due to the fast reacting nature of such controllers. The parameter values are thus not an optimization of the controllers, but merely values which work for the simulation model to show the main differences.

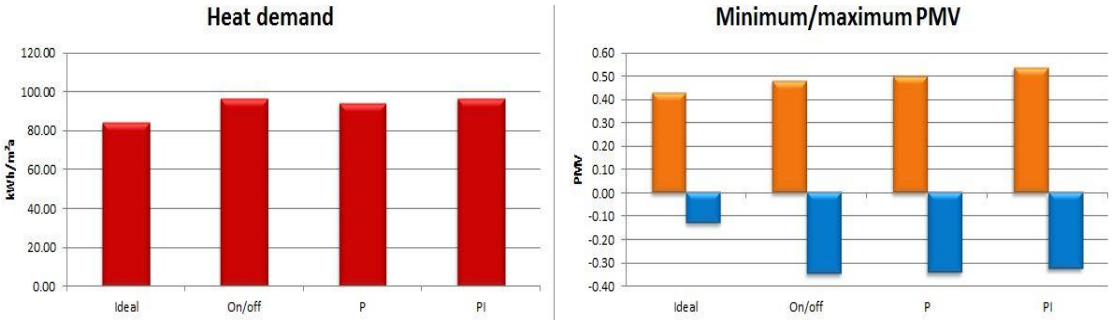

Figure 5.12: Heat demand and extreme values of PMV for variable flow and supply temperature, compared to the ideal heating. 3 different controllers are simulated. Min/max PMV are for bedroom A.

Results of the heat demand and thermal comfort are shown in Figure 5.12 and Figure 5.13 and it is clear that controlling the flow to the radiant floor is essential for energy saving and thermal comfort. Heat demand has dropped about 40 kWh/m^{2}a compared to constant flow, average PMV values have evened out and overheating has been reduced as the maximum PMV has dropped to about 0.5. The minimum PMV values have dropped however, especially in the bedrooms. The living room showed high minimum values for PMV throughout the simulations because the load there is not as big. That the minimum PMV values drop is natural as we put less energy into the system. The values are still over -0.4 which is satisfactory. These results reveal that there is not a big difference between the different controllers on neither thermal comfort nor heat demand.

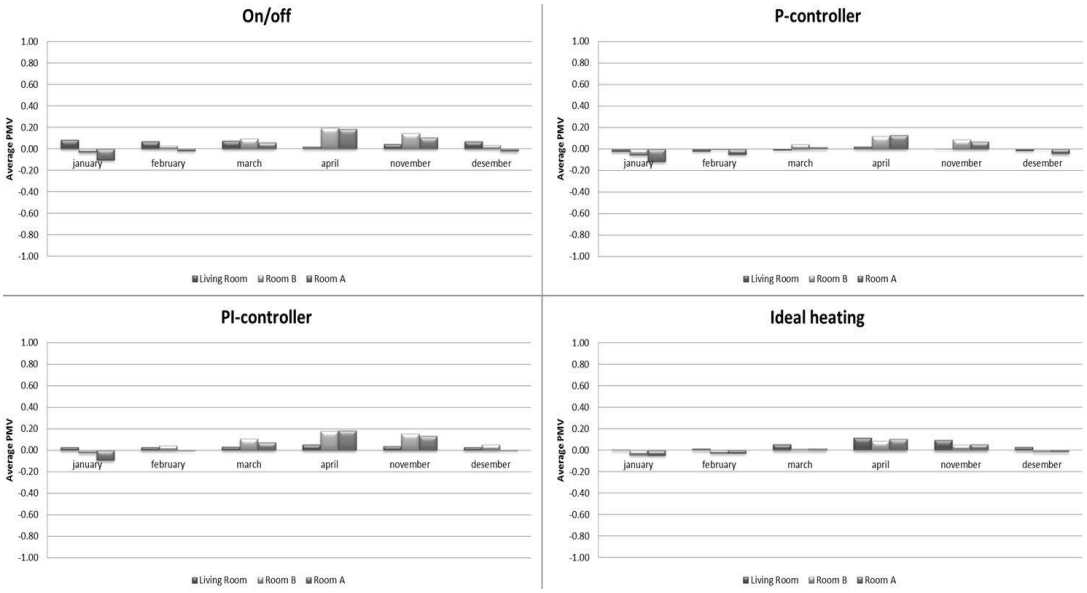

Figure 5.13: Average PMV for variable flow and supply temperature compared to the ideal heating. 3 different controllers are simulated.

In Figure 5.14 the sample standard deviation (SSD) is plotted for each month for on/off and PI controllers. It is evident from these graphs that the variation in temperature is smaller using a PI controller versus an on/off controller, which would also be expected. For bedrooms the controllability is insufficient to show this with d_x equal to 15 cm because the radiant floor can barely deliver enough heat to cover the heat load in these zones. With a smaller d_x the floor can handle the loads much more efficient (see section 5.2.5) and the controllability is thus much better.

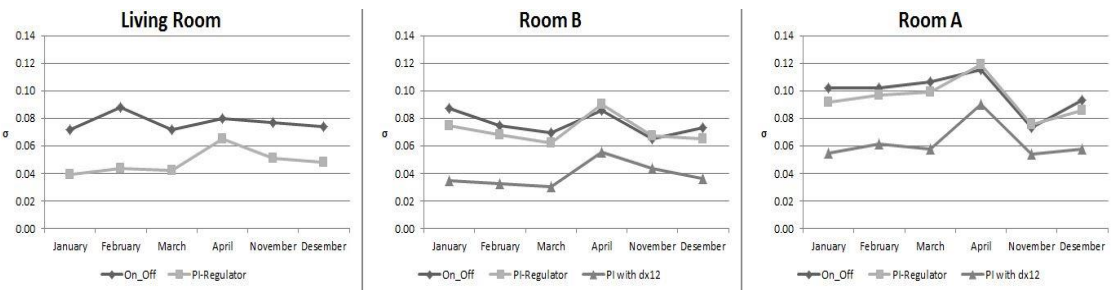

Figure 5.14: Standard deviation from average PMV values during heating season, per month. The significant increase in controllability is seen when the distance between tubes are decreased to $d_x = 12$cm.

The rise in SSD in April can be explained by the overheating periods also causing the maximum values in Figure 5.12 and the high average PMV values in April in Figure 5.13. April is a month where the temperatures undulate as much as 20°C between night and day and with limited shading on the bedroom eastern windows temperatures are high in the morning of these zones when the heating has been on all night. The floor does not cool fast enough and a small overheating occurs. This is not very serious as the operative temperatures do not reach higher values then about 24.5°.

The operative difference between the on/off and P control is depicted in Figure 5.15 for the first week of April, which shows the operative temperature and control signals from the controller of Room B with set-point temperature 22°C. The set-point temperature together with the differential of ± 0.5°C for the on/off controller is seen. The error associated with proportional control can be seen as the operative temperature hovers underneath the set-point for most of the time. This can be improved by tuning the controller by increasing the gain constant so that the valve opens more. The control signal curve would shift upwards and hence the operative temperature as well. Control signal equal to 1 corresponds to a mass flow of 40 kg/hr/m^2 which decreases linearly with the signal. A certain mass flow is required through the floor model because of the linearization mentioned in section 3.2.2 and the P controller turns off when the flow reaches a lower limit of 5.5 kg/hr/m^2. In real systems there are usually similar restrictions on mass flow to avoid a large $\Delta\theta$, which is associated with significant temperature differences on the floor surface depending on the tubing layout. This surface temperature gradient is not considered in the TRNSYS model as the entire surface is treated as one temperature node, and is thus not analyzed in this work. A small overshoot of the operative temperature can be seen when using on/off control, but this is not significant. The same configuration is simulated for a cold week in January and the results, depicted in Figure 5.16, show longer run time for the floor heating. The overshooting of zone temperature in April is replaced with a droop below the differential. Again, this is not a significant deviance, but it shows how the thermal capacity of the system creates a latency between control signal and heat output.

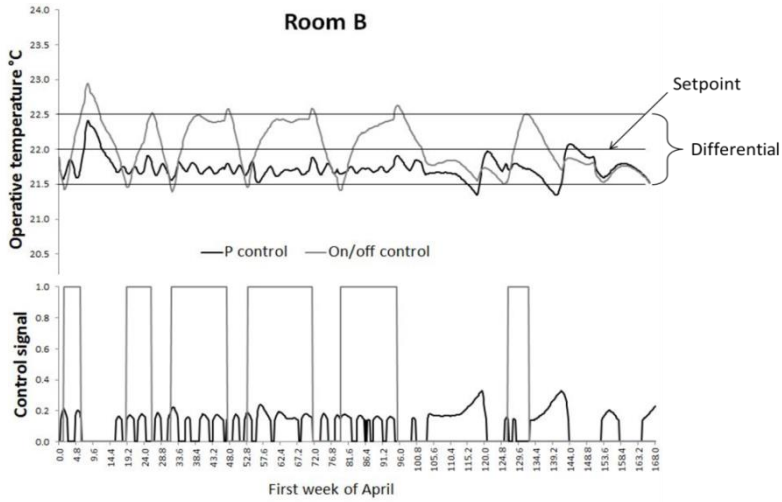

Figure 5.15: The difference between proportional and on/off control, April. The set-point temperature together with the differential of ±0.5 °C for the on/off controller is seen.

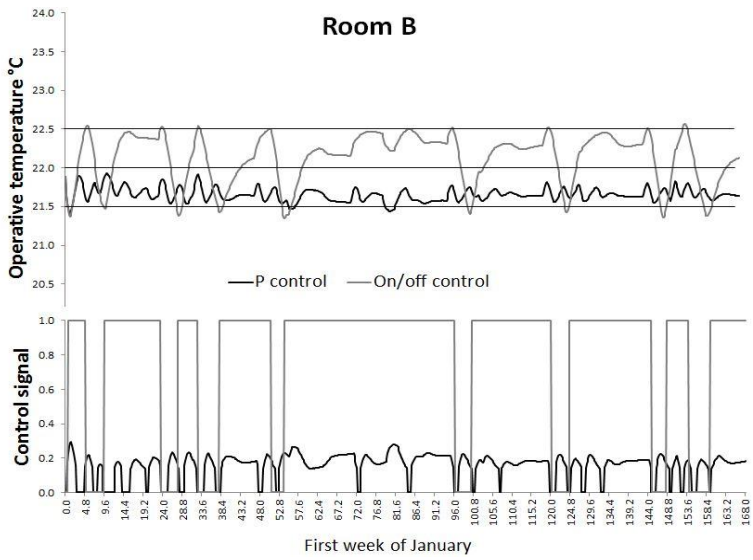

Figure 5.16: The difference between proportional and on/off control in January.

Figure 5.17 shows the operative temperature in each zone for the month of April using P or PI controllers as well as the averages. Set-point is still 23°C for all zones. P controllers are known to cause a certain constant error and this becomes evident in these graphs. The average operative temperature is closer to

set-point using the PI controller, which also explains that the maximum and average PMV values are higher for PI and that energy use is slightly higher compared with only P controller, simply because the average operative temperature is higher. The differences between the two controller types are small and for the living room it is virtually zero. Since the PI controller is showed to controlling the set-point better than the other two it is used in the further simulations. The designer of the system must make an evaluation according to the extra cost of a PI controller, but it is here shown that both P and on/off controllers work well enough.

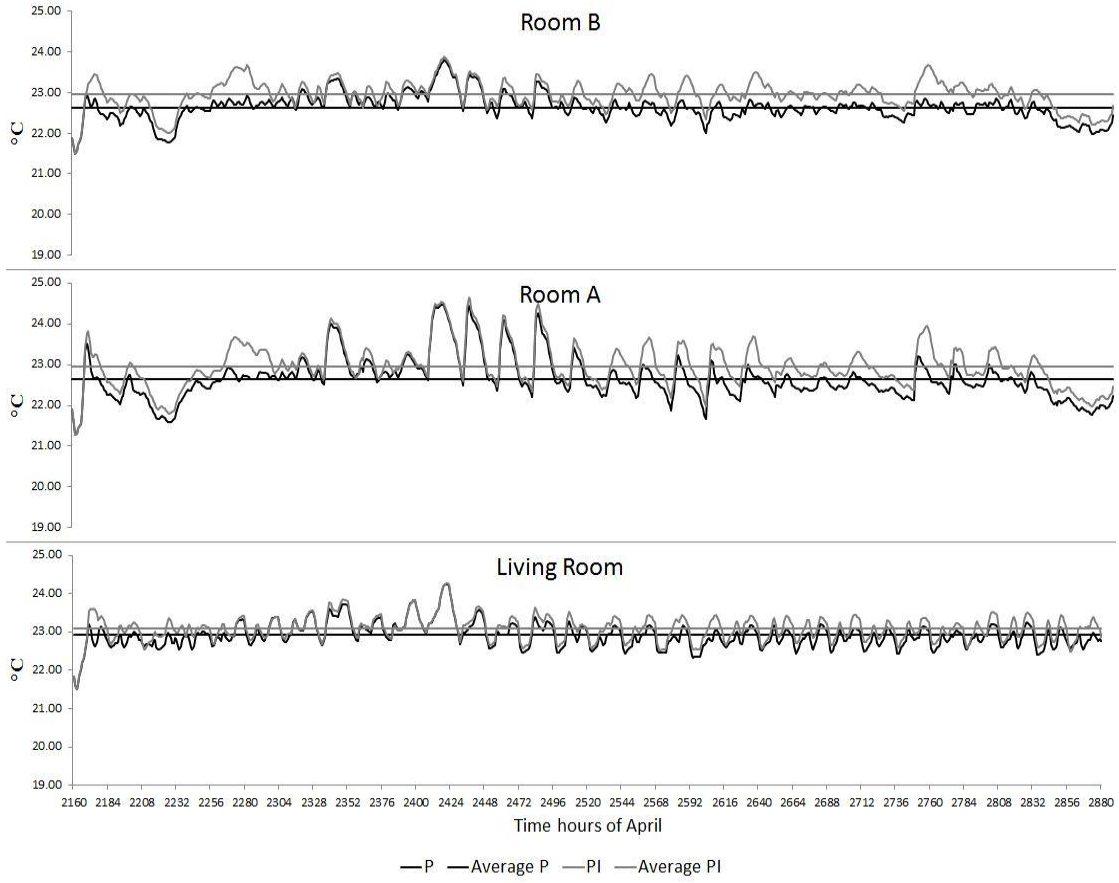

Figure 5.17: Operative temperature in the three zones. Common set-point 23°C. The constant error of the P-type controller can be seen. With integration action added the average value is closer to set-point.

To deal with the slightly high PMV averages and maximum values in April two different controlling approaches are tried. The first idea is to stop the heating system as the outside temperature increases to a given temperature, as active heating is obsolete when outside air temperatures are high enough. As the temperature undulates from under 5°C at night to 20°C during the day in April, heating runs all night with a relatively high supply temperature and results in overheating in the morning because of the slow-reacting radiant floor. The second idea is to control the supply temperature by an average of the ambient temperature instead of the momentaneous value to capture the trends of the outside climate. In this way the supply temperature will not be as high during the night in such conditions because the average of the ambient temperature will obviously be larger than its night value.

The results of these simulations are shown in figures on the next pages. T_{cut} refers to the temperature at which the heating system is shut off and 24h means that the supply temperature is controlled by a 24 hour average of the ambient air temperature. Comparing the results labeled "24h, PI" from Figure 5.18 to those of PI in Figure 5.12 shows that changing to a 24 hour average does not change much on system performance. The maximum PMV value drops from 0.54 to 0.50, so there is a minute improvement in this regard. Average values of PMV are not changed. This reaffirms the slow-reacting nature of the radiant floor. Small changes in supply temperatures to the floor do not significantly affect the total output.

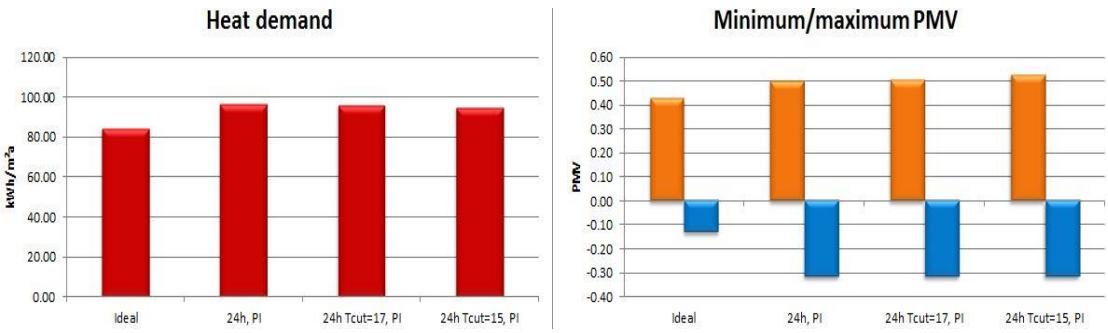

Figure 5.18: Compared the different strategies with ideal heating. Values on the right are from Room A. Very small differences observed.

Cut off temperatures 15°C and 17°C are simulated and results shown in the same figure. As cut off temperature drops heating demand also drops, as seen on the left of Figure 5.18. This is expected because the heating is turned off more frequently. Maximum PMV actually increases as cut off temperature is lowered. This only applies to room A however and as seen in Figure 5.19 the maximum PMV in the other rooms drop with falling cut off temperature. In room A it increases because with a lower cut off temperature the heating will switch on later at night, causing temperatures in room A to drop lower and thus flow and heat transfer to increase. More energy is thus stored in the floor in the morning as the sun starts to shine through its windows. This can be solved by effective shading of the large window in room A. Therefore the general trend is the maximum PMV falls with falling cut off temperature.

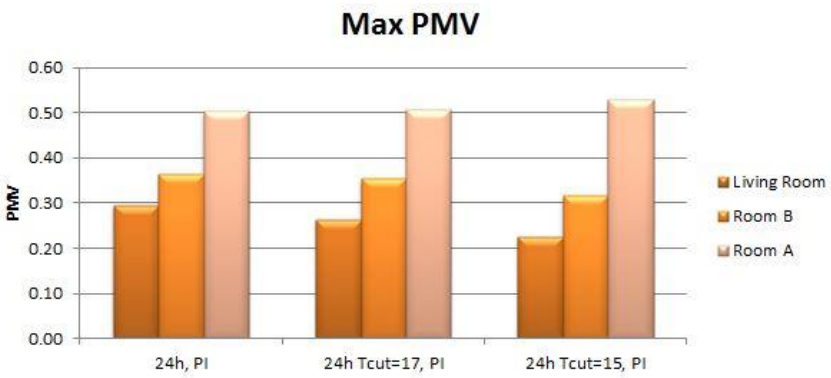

Figure 5.19: Shut-off temperature on the heating decreases overheating tops. Except for Room A, which is influenced by incoming solar radiation in the morning.

Figure 5.20 shows the operative temperature for room A and ambient instantaneous and average temperatures. If the supply temperature to the floor follows the average ambient temperature it is evened out, being cooler at night and higher during the day than it would otherwise be. The very tops of the operative temperature are cut, but very slightly. Cut-off temperature and 24h average control are shown not to be effective strategies for this RHS. The reason for this is that the system is slow-responsive, meaning that it in itself evens out much of the undulation in supply temperature.

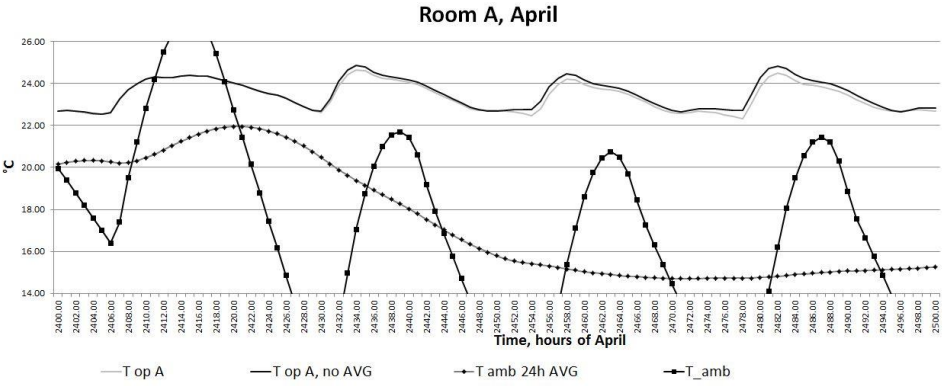

Figure 5.20: Operative temperatures for 24 hour average vs no average on the reset line temperature control. No big difference is observed. Supply temperature of the inlet water follows Figure 5.9.

In Figure 5.15 it can be seen that the flow through the floor is quite small when using P and PI controllers. A parametric study is performed to investigate how the flow through the floor affects heat transfer and outlet temperatures. The inlet temperature is set to constant 40°C and the zone air temperature to constant 21°C. The latter is achieved by setting a very high infiltration number and then setting an unbounded ideal heating source to control the air temperature to 21°C. Simulation results are shown in Figure 5.21. The total amount of energy supplied throughout the heating season is not plotted, but is found to be virtually constant, because the zone valves are open for a longer amount of time and thus delivers the same amount of heat even though the heat rate is smaller. Heat load and temperature difference between inlet and outlet (Δθ) are affected by the flow. The acceptable Δθ is dependent on the tube layout and must be decided by the designer of the system. A too high Δθ might lead to a significant temperature gradient along the floor and should be avoided for comfort reasons. When having decided the acceptable Δθ the water flow can be decided, and from water flow the necessary tube size can be determined to avoid high pressure drops. In this work the system parameters are already given and a detailed design procedure will hence not be necessary.

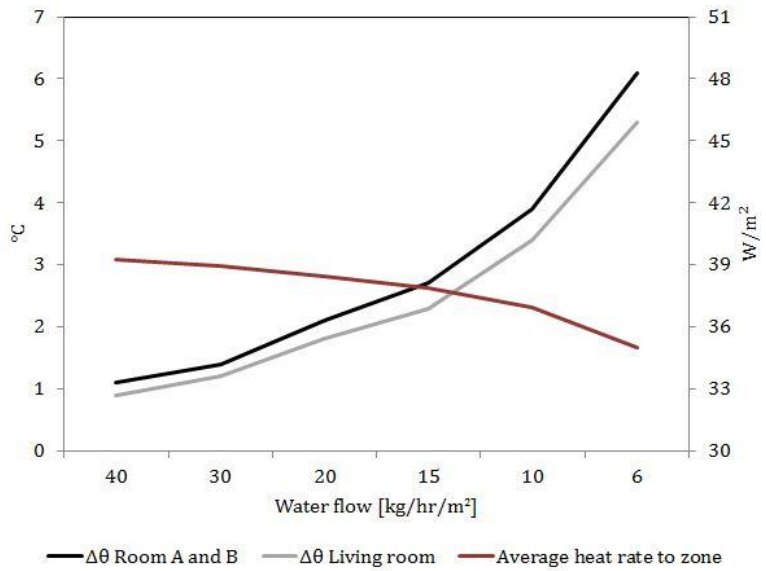

Figure 5.21: Heat rate to zone and temperature change of the heating water plotted against flow rate through the floor. Distance between tubes in the living room is 15 cm and in bedrooms 12 cm and therefore show different results. The heat rate is averaged for all zones.

5.2.5 Zones with Different Loads

The zones in buildings experience different load conditions, due to their different boundaries. In this model Room A is the smallest and has a biggest window surface, see Figure 5.4. In both bedrooms a larger portion of the boundaries is exterior and the heat load is thus higher for them than for the living room. Another factor to remember is that different rooms are used different and bedrooms should usually be a bit colder than the living room because cold air has higher perceived air quality and is preferred when sleeping. The thermal model for the bedrooms has a higher CLO value implemented to model bed sheets. In Figure 5.22 the effects of changing the set-point temperature of the zones are seen. By reducing it by 1°C in the bedrooms a far better thermal comfort is achieved in the transitional seasons because of reduced overheating, without aggravating the cold periods in January and December. The set-point should thus be a user-defined input depending of the individual utilization of each room.

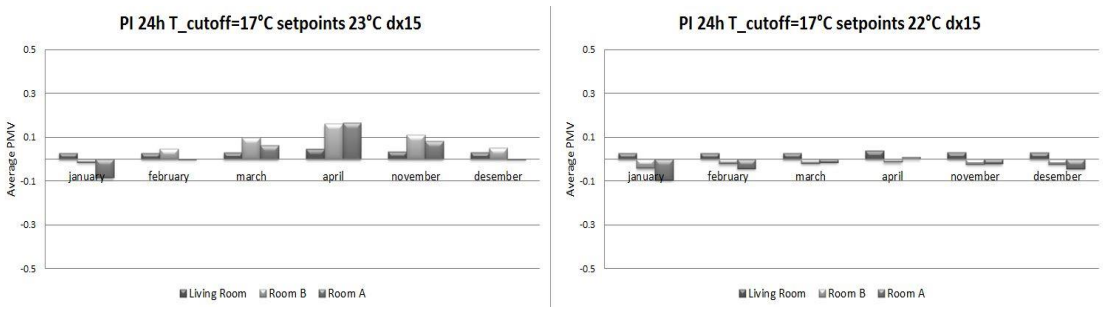

Figure 5.22: The effect of having different set-points in different rooms. Set-point for the living room 23°C in all simulations.

Figure 5.22 also shows that in January both bedrooms have a negative average PMV, which implies that for some periods the heating system cannot cover the load. This is especially true for room A because it is facing north-east, while room B is south-east facing and thus receives more solar gains. To increase the heating capacity of the floor the distance between the tubes in rooms A and B is changed to 12 cm. The results are shown in Figure 5.23 and show that the new tube layout in the bedrooms improves the thermal comfort compared to the right side

of Figure 5.22. Average PMV values are virtually zero throughout the heating season. The ideal model has some problems in the transitional months because it does not allow air temperatures below 23°C for living room and 22°C for bedrooms. In days where the ambient air temperature outside during the day is very high, this leads to overheating. The radiant floor is controlled by operative temperature and the air temperature can thus be quite low without heating being called. Heat demand of the system is now 94 kWh/m²a, and the ideal at about 84 kWh/m²a, as seen in Figure 5.24.

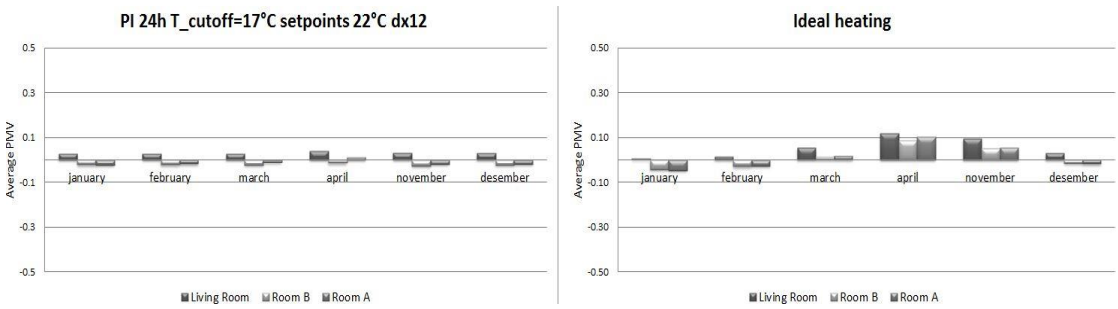

Figure 5.23: Comparison of average PMV between the final design, with a distance between tubes of 12 cm for the bedrooms and 15 cm for the living room, and the modelled ideal heating.

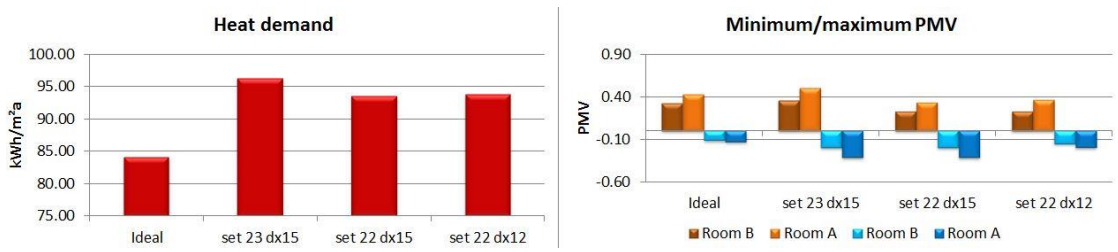

Figure 5.24: Comparison of total heat demand and extreme thermal comfort values for different designs and set-points. dx12 and dx15 denotes the distance between tubes in the bedrooms, and set 22/23 the set-point temperature in the bedrooms. For living room d_x is always 15 cm and set-point always 23°C.

The final result in Figure 5.23 has a PI controller, a cut-off temperature of 17°C, a 24 hour average ambient temperature controlled supply temperature, with varying set-points and a closer tubing distance in the bedrooms. As showed in the previous section the 24 hour average and cut-off temperature controls are obsolete and can be omitted. The PI controller can also be replaced by a simple on/off zone valve without compromising on energy use or comfort.

Figure 5.25 shows the effect on surface temperatures of changing the distance between the tubes d_x for rooms A and B in January. The surface temperature of the floors increases with decreasing d_x. From the extra dips for $d_x = 12$ cm it can be noted that more on/off cycles for the system occurs. This would be more apparent if using on/off type controllers. With an even smaller d_x it is expected that the maximum surface temperature would exceed the thermal comfort criteria of 27°C. Limitations of the simulation model impede this to be simulated.

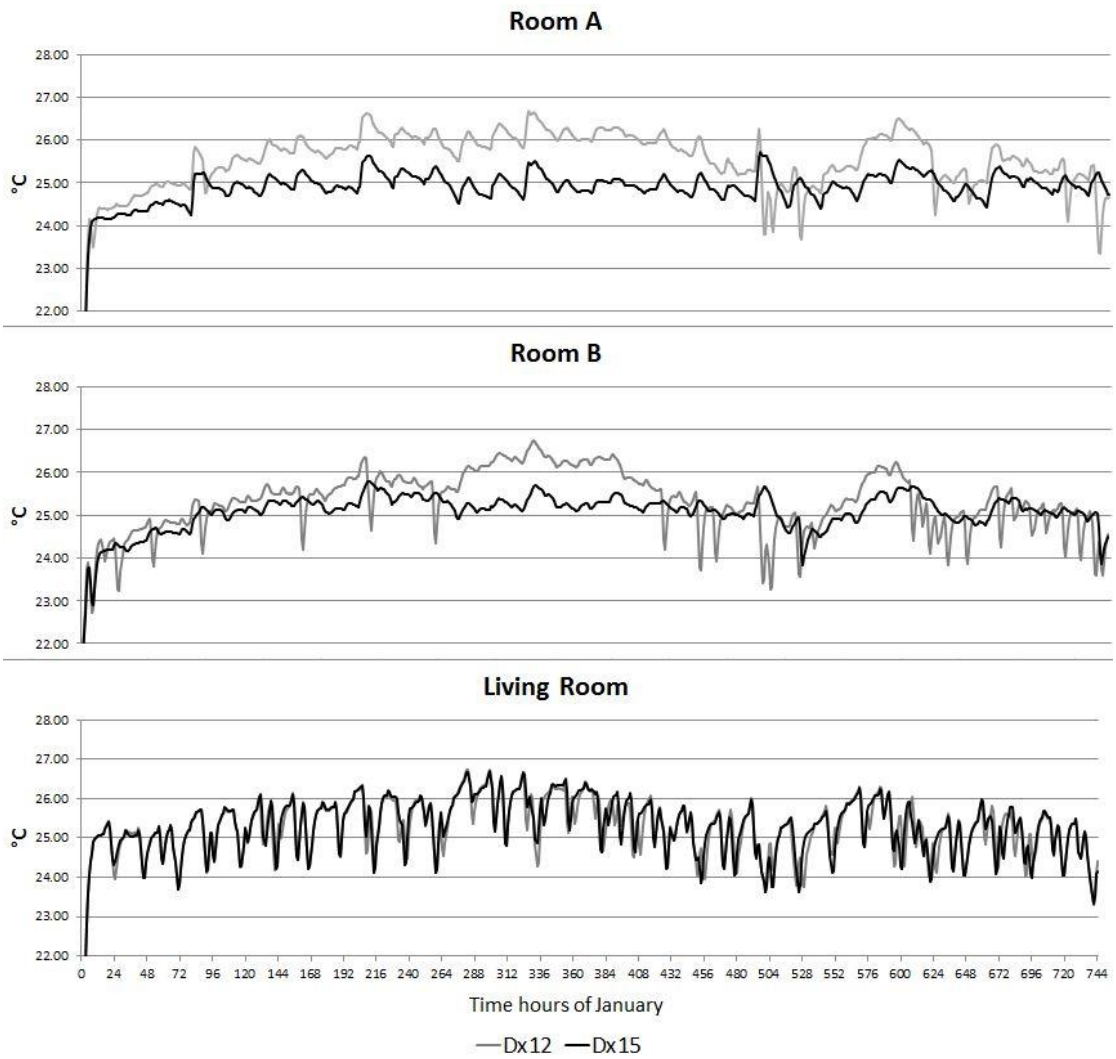

Figure 5.25: Floor surface temperature in the three zones for January with different distance between tubes. It is seen how a smaller d_x increases floor temperature and thus heat transfer. PI-controllers used in the simulation.

5.2.6 Night Setback

A frequently used control strategy for heating systems to conserve energy is to lower the temperature of the zones at night, when the occupants are either absent or sleeping. A four hour setback from 24:00 to 04:00, with water supply temperature lowered to 30°C is simulated and the results are displayed in Figure 5.26 and Figure 5.27. It is clear that the energy saving is virtually zero and that the setback causes some cold periods in January. Different schedules and supply temperatures are simulated and show the same results. The reason is that the heat which is not put into the thermally heavy floor during the night has to be put into it in the morning to reach the operative core temperature, and the energy primarily saved is thus subsequently spent.

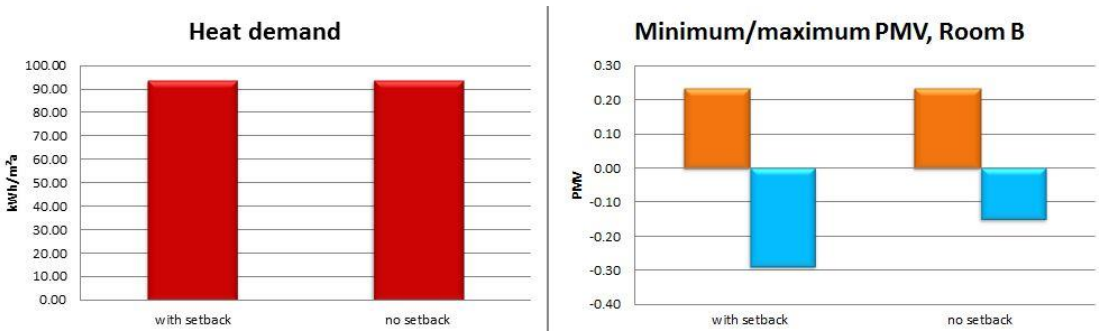

Figure 5.26: Comparison of total heat demand and extreme thermal comfort values for room B between setback and no setback. No energy is saved using setback. Cold period occur with setback.

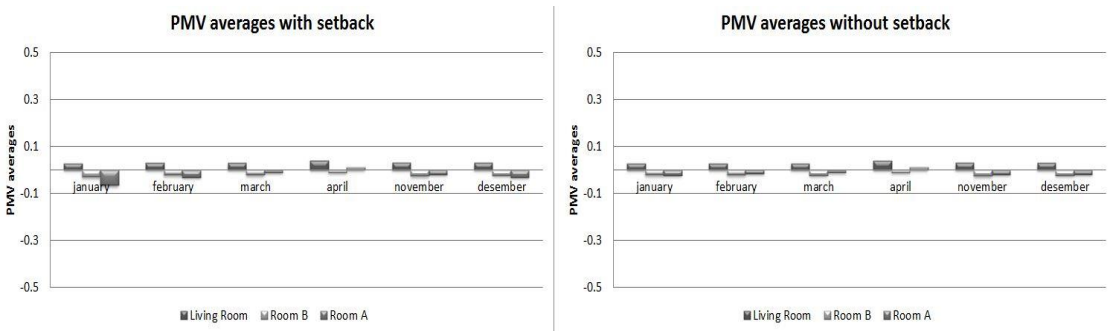

Figure 5.27: Comparison of average PMV between setback and no setback. The setback causes some cold periods in January.

5.2.7 Heat Transfer and Surface Temperatures

The heat rate performance of the floor is analyzed in this section. The heat transferred to the zone is not equal to the heat input to the radiant floor because of the heat storage. To assess the heat transfer to the zone, the output NTYPE 19 of Type 56 Multi-zone Building Model is used, which gives the total energy from the surface of the floor to the zone including radiant and convectional heat transfer. Heat transfer results are presented in Table 5-2 for d_x equal to 12 cm and 15 cm. The air exchange rate is set to a high number so that the air temperature can be controlled by an ideal heating model with set-point 21°C. With colder zone air temperature the heat transfer would be higher, but 21°C is here assumed as a minimum requirement for thermal comfort. The supply water is controlled as before with outdoor temperature control for temperature and zone set-point for flow in each loop. Supply water flow is kept constant at its maximum of 40 kg/hr/m^2, while the supply temperature is constant at 40, 42 and 45°C. Exterior shading for all windows is 100 %.

Table 5-2
Heat transfer rates and corresponding surface temperatures.

Distance between tubes 12 cm in all zones						
Supply temperature	Heat transfer to zone [W/m^2]			Surface temperatures [°C]		
	Liv	A	B	Liv	A	B
45 °C	55.0	57.4	57.2	27.8	27.1	27.3
42 °C	48.3	50.5	50.3	27.0	26.3	26.4
40 °C	43.8	46.0	45.8	26.3	25.7	25.8
Distance between tubes 15 cm in all zones						
45 °C	49.0	51.0	50.9	27.0	26.4	26.5
42 °C	43.0	45.0	44.8	26.3	25.6	25.7
40 °C	39.1	41.0	40.8	25.7	25.1	25.2

The air temperature of the room in these simulations is set to constant 21°C. Flow is at its maximum of 40 kg/hr/m^2. Mean radiant temperature changes as the surface temperatures are dependent on outdoor conditions. Heat transfer is at its maximum in the morning after a cold night. The radiant floor at GEL has a distance of 15 cm between tubes.

It is evident that the short distance between tubes yields a higher heat transfer and surface temperatures, as expected. A linear relationship between heat transfer and supply temperature can also be noted. For $d_x = 15$ cm heat transfer increases with 2 W/m^2 for each unit increase in supply temperature. For $d_x = 12$ cm the same relationship is 2.25 W/m^2. Heat output and surface temperatures are 5-6 W/m^2 and 0.6-0.8°C higher with the same supply temperature for $d_x = 12$. If an upper limit for surface temperature of 27°C due to thermal comfort requirements is presumed it can be seen that with $d_x = 12$ the upper limit of supply temperature is 42°C while for $d_x = 15$ it is 45°C. They both supply approximately 50 W/m^2 to the zone at these supply temperatures. With shorter distance between the tubes the supply temperature can thus be lowered, which increases performance of heat pumps and RES. The extra pressure drop as well as the extra material costs due to the extra length of the loops must be considered and an evaluation conducted to see which solution is the best overall. Table 5-2 also shows that the heat output in the bedrooms is higher than in the living room even though the surface temperature is lower. Both bedrooms have a bigger part of their surfaces as exterior surfaces. Accordingly, mean radiant temperature is lower there than in the living room. Therefore, in the peripheral zones of a building the distance between tubes can be lowered or the supply temperature increased compared with other zones, without exceeding the requirement for maximum surface temperatures. The extra heat load is handled through radiant heat transfer between the floor and the inside of the exterior walls and windows. Nevertheless, to ensure a good performance of the floor for the different conditions a good heat load assessment must be conducted.

In a radiant heating floor one part of the heat will go into the zone above it, one part will be stored in the thermal mass and the last part will flow into the zone underneath. This is the $\dot{Q}_2$ in Figure 3.9 and should be assessed for a comprehensive thermal evaluation of the radiant floor. NTYPE 20 of Type 56 Multi-zone Building Model gives the same output as NTYPE 19, but for the opposite surface, i.e. the surface facing the zone beneath the radiant floor. This boundary zone is assumed to have a constant air temperature of 22°C. Figure 5.28 shows the different heat flows. Total heat input is the total heat input to the

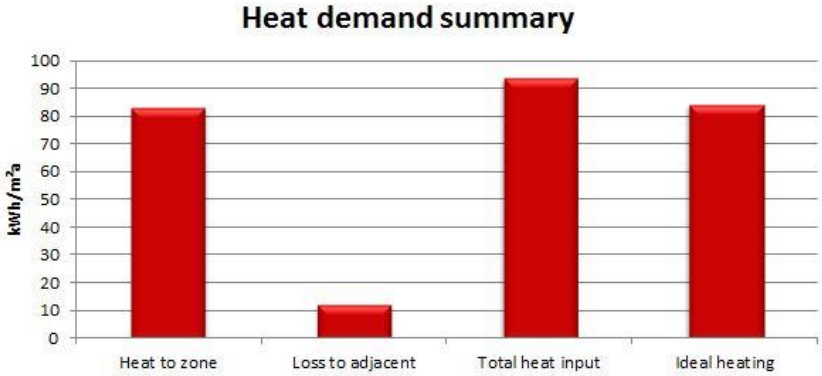

Figure 5.28: Heat summary compared with ideal heating for final design. Heat to zone corresponds with the heat delivered by ideal heating.

radiant floor calculated based on water flow and Δϑ, cf. equation 18. Heat to zone is the yearly integration of NTYPE 19, loss to adjacent is the yearly integration of NTYPE 20 and ideal heating is the heat demand for the ideal heating model used in the simulations. About 13% of the heat is transferred to a different zone.

The total heat input approximately equals the sum of the heat to the zone and the loss to adjacent. The reason why they do not match perfectly is that there is some influence of the sun, and that during the summer some heat will flow through the floor because the boundary is kept at 22°C throughout the year. The effects of this are not considered to be significant. It can now be noted that a major part of the extra heat that is needed to heat the zones with a radiant floor compared to the ideal heating is lost through the floor to the zone(s) beneath. If there are several zones on top of each other where all are heated with such a radiant floor this extra gain from the zone above should be taken into consideration. If needed, extra insulation should be installed to avoid this heat loss.

Based on the analysis of the radiant floor above, a model is selected to use for the analysis of the heat source in the next section: On/off thermostats with a differential of ±0.5°C. Flow is 9 and 40 kg/hr/m² to living and bed rooms, respectively. d_x = 12 cm for bedrooms and 15 cm for living room. Reset line controlled supply temperature based on the instantaneous outdoor temperature, and no setback or cut-off for the heat control.

5.3 TOTAL SYSTEM SIMULATION

The radiant floor model developed in the previous section is coupled with a heat pump to see how it performs together with a heat source. The heat pump is modelled with type 401, presented in section 3.2.4, utilizing of the performance curves (see Figure 5.29) of the ASHP installed at GEL. Since this heat pump is very large, a scaling factor is employed on the curves to model smaller heat pumps. Another approach would be to scale up the heat load of the building model to simulate an array of apartments being supplied by a common heat pump. The approaches are regarded equivalent and the former is applied for simplicity. The heat pump is single-staged.

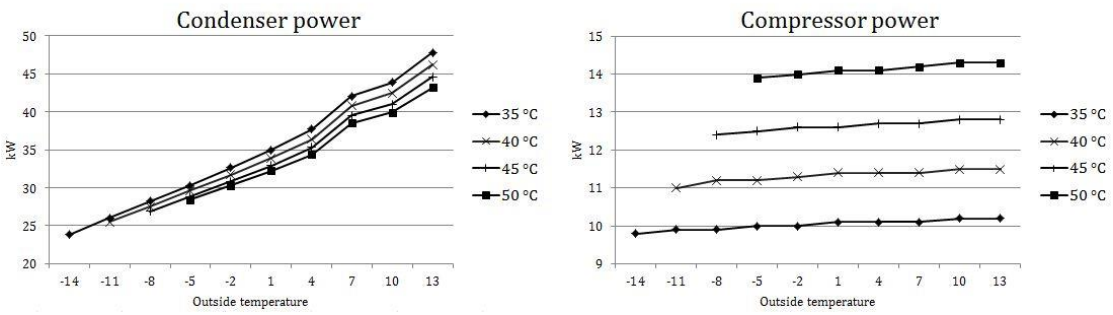

Figure 5.29: Performance curves of the ASHP installed at GEL, for different condenser outlet temperatures. Data from product sheet is included in Appendix E.

Two connection options are analyzed: A connection where the heat pump is directly connected to the load and another where they are hydraulically separated by a water buffer tank. The model given to the author by GEL researchers that was used in the previous analysis is revised to passive house standard to assess the system for a modern super-insulated apartment.

5.3.1 Revised Building Model

Table 5-3 shows the new values for the exterior surfaces of the model. This is achieved by implementing a simple thermal resistance in the wall construction of type 56 in TRNBuild. The resistance is chosen so that the u-values of the walls are within the requirements of the passive house standard [33].

Table 5-3

U-values of exterior surfaces used in the revised model.

Construction	Old U-value (W/m^2K)	New U-value (W/m^2K)	Requirement (W/m^2K)
Exterior wall	0.574	0.216	0.22
Roof	0.342	0.172	0.18
Windows	0.860	0.680	0.80

The boundary wall and floor are considered adjacent surfaces and their constructions from section 5.2 are thus kept.

The following values are in the revised building model:

Geometry — Same as in section 5.2. Thermal resistance is added to the exterior surfaces to correspond to passive house standard requirements. See Table 5-3 and Appendix C.

Heating — Same as in section 5.2. 3 loops of hydronic radiant floor with distance between tubes 12 cm for bedrooms and 15 cm for living room. Tube outside diameter 20 mm and tube wall thickness 2 mm. Plastic tubes.

Cooling — Cooling conditions not considered.

Ventilation — Turned off to ease simulation time. Was demand controlled and did not account for a significant part of heat loss.

Shading — Full shading assumed. Exterior shading coefficient equal to 1.0 for all windows in the model.

Windows	Triple-glazed window with krypton filling. U-value 0.68. G-value 0.407. Window ID 4001 of the TRNSYS window library. Shading coefficient 0.3.
Gains	Same as in section 5.2.
Infiltration	Set to be 0.3 h^{-1} and constant.
Boundary conditions	Same as in section 5.2.
Set-point Temperatures	Operative temperature 23°C for the living room and 22°C for the bed rooms.

Because the heat load and demand decrease as the building is better insulated a new heat curve will develop, and is shown in Figure 5.30. The difference is quite substantial due to the more insulated walls and in parts because the ventilation is shut off. The flow through the loops is thus decreased to 10 kg/hr/m^2 and is still being controlled by on/off type controllers. Maximum heat load calculation yields 2.05 kW (23.3W/m^2), with room set-point temperature 22°C.

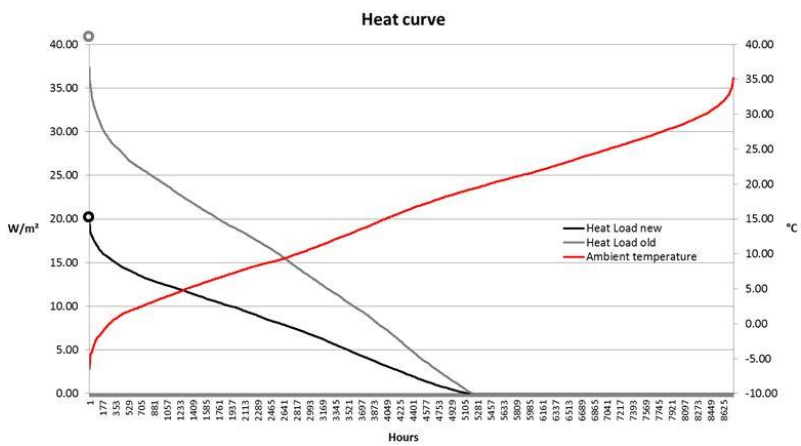

Figure 5.30: Heat curve of the old vs the revised model. Design outdoor temperature is -4°C.

The heat demand for the revised model is 46 kWh/m^{2}a using a radiant floor. A simulation done with an ideal heating source and set-points the same as for the

radiant floor shows a heat demand of 41 kWh/m²a. The radiant floor uses more energy because of losses to zones underneath and losses due to higher interior surface temperature of exterior walls.

It is also expected that a downward shift in the outdoor reset line can be implemented without impairing the thermal comfort. A lower average supply temperature should increase the performance of the heat pump. As a result, three different reset lines will be simulated to see the effects on the heat source performance and zone thermal comfort. These are shown in Figure 5.31.

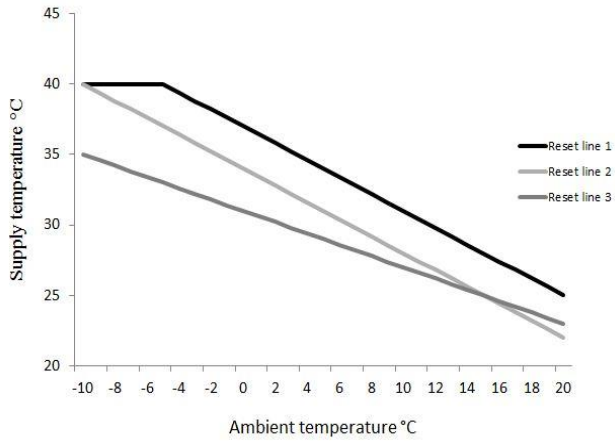

Figure 5.31: The revised outdoor reset lines used in the simulations. Line 1 is the old reset line used in the previous simulations.

5.3.2 Direct connection

With a direct connection between the heat pump and the radiant floor, the heat source can be controlled directly by the outdoor reset line. Heat losses of the storage and distribution of the heating water are reduced. Condenser outlet temperature is thus minimized and the performance (COP) of the heat pump maximized. The heat pump modelled in this work is single stage controlled, meaning that it is either on or off. The inlet temperature to the floor will oscillate around the set-point temperature by a differential set by the heat pump thermostat, which should not be too small to avoid frequent on/off cycles. If there is a high demand on supply temperature accuracy, a mixing assembly must be installed and the heat pump set-point increased to always deliver at least the set-point temperature. For a radiant floor there is usually no such requirement, as the thermal mass evens out the temperature variance. A direct connection as sketched in Figure 5.32 can be used.

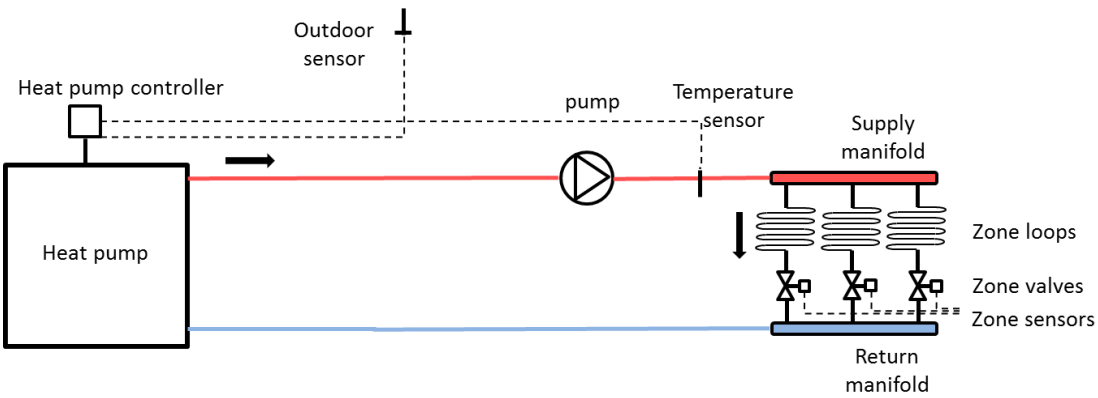

Figure 5.32: Schematic diagram of the simulated indirect connection principle. Heat pump controlled supply temperature.

The drawback of this connection principle is that the volume and hence thermal mass of the water in the system is quite small. This can lead to frequent on/off cycles for the heat pump, especially when the heat pump is oversized compared to the load. Energy delivered to the water is much higher than the energy emitted by the water, the heat balance is offset and set-point temperature will be reached quickly. Sizing the heat pump according to maximum heat load

condition will lead to high cycle numbers and it is therefore normal to install a secondary heat source to aid the heat pump on very cold days.

A direct connection model is built as depicted in Figure 5.33. Zone valves control the flow *into* the zone and are thus modelled on the supply manifold even though they usually are placed on the return manifold in real systems. The heat pump is controlled by an on/off controller with the reset line 1 as set-point and a differential of ±5°C. Zone valve controllers have a differential of ±1°C and send their signal to the heat pump controller so that it shuts off whenever all the zone valves are shut. If one zone valve opens, the heat pump starts. Set-point temperatures are 23°C for the living room and 22°C for bedrooms. A small storage tank on the return pipe models the volume of the heating water flowing in the system, which is approximated to 50 liters. Heat losses in the distribution system are not considered and the tank heat loss coefficient is hence set to zero. Weather data is the TMY2 file for Shanghai.

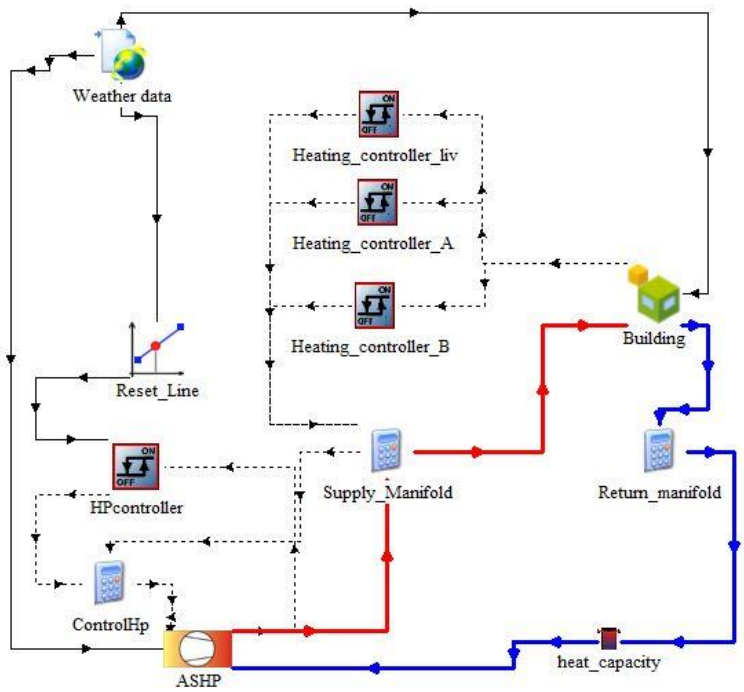

Figure 5.33: Simulation studio screenshot simplified to show how the direct connection model is built.

The model is first simulated without the heat capacity of the system heating water in mind and the simulation is very unstable, and often crashes due to divergence. With a sufficiently small heat pump and the heat capacity modelled, as a simple one-node storage tank model, the simulations run realistically. The heat-up- and cool-down constants of the heat pump are 3 and 5 minutes, respectively. A time-step of 0.1 hour (6 minutes) is chosen to capture the relatively short on/off cycles. The wall transfer function model (see section 3.2.1) employed in the building model has limits on the time-base used in its calculations, which for this model is about 0.4 hour. This means that the outputs from the active layer model come in steps rather than continuously, but this is not regarded as a problem for the final results. An even shorter time-step is not considered because these output steps become more and more severe the shorter the time-step, and long simulation times. The defrosting calculation of the heat pump model causes the simulation to crash for an unknown reason and is thus omitted. The COP reduction caused by icing and defrosting should be quite similar for the different simulations so this problem is considered non-significant, but it should be taken into account when reading COP results.

Table 5-4
Performance of ASHP of different sizes.

Scaling factor	Capacity [kW]	Load coverage	On/off cycles	Seasonal COP	Demand coverage	Total COP	Total energy kWh/m²a
0.03	0.9	45 %	364	4.77	93 %	3.77	12.2
0.04	1.2	60 %	992	4.26	98 %	4.04	11.4
0.05	1.5	75 %	1931	3.95	99 %	3.86	11.9
0.06	1.8	90 %	2793	3.66	99 %	3.60	12.8
0.07	2.1	105 %	3260	3.45	100 %	3.40	13.5

Maximum heat load at 2 kW, total heat demand 46 kWh/m²a. Scaling factor is the factor multiplied by the original performance curves of the ASHP. Capacity is the condenser power at design conditions, which are -4°C ambient temperature and 40°C condenser outlet temperature. COP not including icing and defrosting losses. Total COP assumes direct electrical heating as secondary heat source and is equal to heat demand divided by total electrical energy used by compressor and electric heater. Set-point temperature for heat pumps is reset line 1.

Table 5-4 shows results from simulation of heat pumps of different sizes. The number of on/off cycles should be viewed as a reference and not absolute because this number is highly sensitive to uncertainties of many parameters, like

water volume of the system, COP reduction of defrosting, etc. As noted before, the simulation models are simplifications and approximations and uncertainties are present and at times significant. Changing one parameter in the simulation while keeping all other parameters equal, does however allow for a comparison of cycle number between the runs.

From the table it is evident that even with a small heat pump a large proportion of the heat demand can be covered. The capacity listed is from design outdoor condition and is thus at its minimum, as heat pump performance worsens with lower source temperature. Because temperatures are rarely very low in Shanghai, 93 % of the demand is covered with a heat pump that delivers only 45 % at design conditions. Already at 3-4°C this heat pump will cover 100 % of the heat load. It can also be seen that a big heat pump that can cover 100 % of the heat load delivers marginally more energy throughout the year than a smaller heat pump. The COP and number of cycles are plotted in Figure 5.34 and shows how the COP falls with the size of the heat pump as the number of on/off cycles increase because of the oversizing. COP in these results is seasonal.

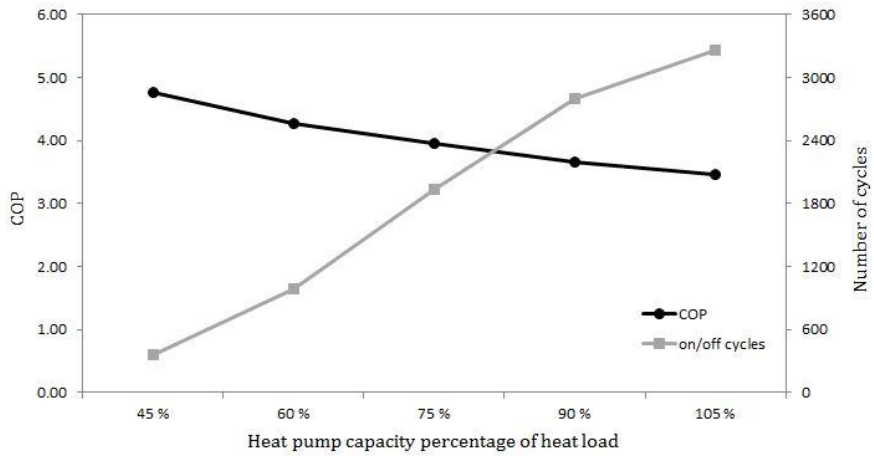

Figure 5.34: Graphical representation of seasonal COP and number of cycles from Table 5-4, for different heat pump sizes.

The designer has to consider heat demand coverage, number of on/off cycles and seasonal COP when sizing the heat pump. The second heat pump from the top of

Table 5-4, with heat load coverage of 60 % at design conditions, is chosen for remaining simulations with this type of connection. It covers 98% of the seasonal heat demand, and lacks 850 W to cover the calculated maximum heat load. For this reason, an electrical heating element should be installed internally in the heat pump or on the pipes to supply extra heat during extreme conditions. The choice is a compromise between demand coverage and start/stop cycles. A heat pump running fully monovalent and covering 100% of the heat demand will have a very high number of cycles compared to the one chosen. With a smaller one, the increase in COP is countered by the need for direct electrical heating, which has a COP of just 1, and overall COP will thus be smaller. The rightmost column in Table 5-4 shows that with this heat pump the highest total COP is achieved.

Figures 5.35 and 5.36 show one week of operation in April, using reset lines 1 and 2 (see Figure 5.31) respectively. Reset line 3 is simulated, but found to be too low, not providing adequate heat for thermal comfort. The upper graph of both figures shows the heat supplied by the heat pump (condenser power) and condenser water flow. The flow is governed by the zone valves to each floor loop, and it can be seen how the flow changes step-wise as the zone valves open and close. Start/stop cycles are more frequent when the flow, and hence load, is low. The first figure also shows the operative temperature in the zones for the same time-span, from where the condenser flow can be linked to the set-point for the zones, which are 22°C for room A and B and 23°C for the living room. When a zone valve is shut, the temperature of the zone naturally drops, before rising again when the valve opens. COP is also plotted to show how the COP is lower at small loads because the heat pump turns off and on at each time-step (6 min) and cycle losses are significant. It is a weakness of the direct connection to radiant floors that the zone valves opens and closes totally. This causes a big difference in load and therefore unstable operating conditions for the heat pump, and is especially true for small systems with few floor loops and low system water volume, like the one simulated in this work. A big enough differential on the room thermostats are therefore important to avoid a frequent opening and closing of the zone valves, without causing thermal discomfort, and is the reason why the differential is changed from ±0.5°C of the simulations in section 5.2 to

±1° here. Condenser power as high as 2 kW is seen, which is as high as the maximum heat load, and is caused by the high outside temperature, on which the condenser power is highly dependent (see Figure 5.29). During design conditions the temperature and thus condenser power are much lower.

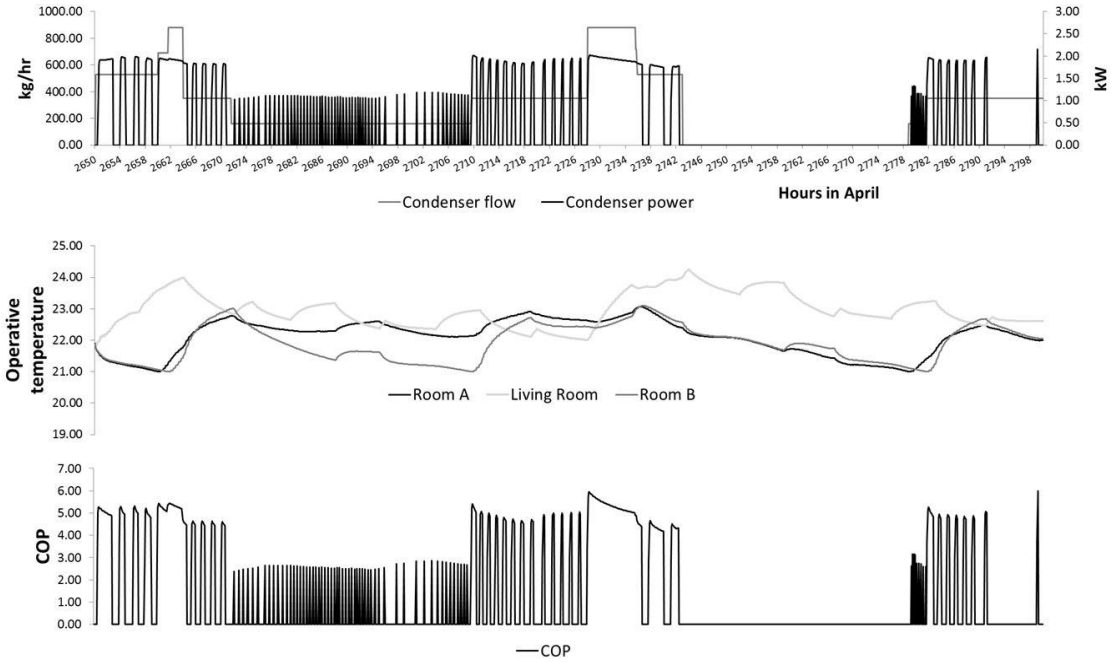

Figure 5.35: 1 week of operation with the selected heat pump and set-point temperature for condenser outlet following the reset line 1. Heat pump cycle length at low load is 12 minutes.

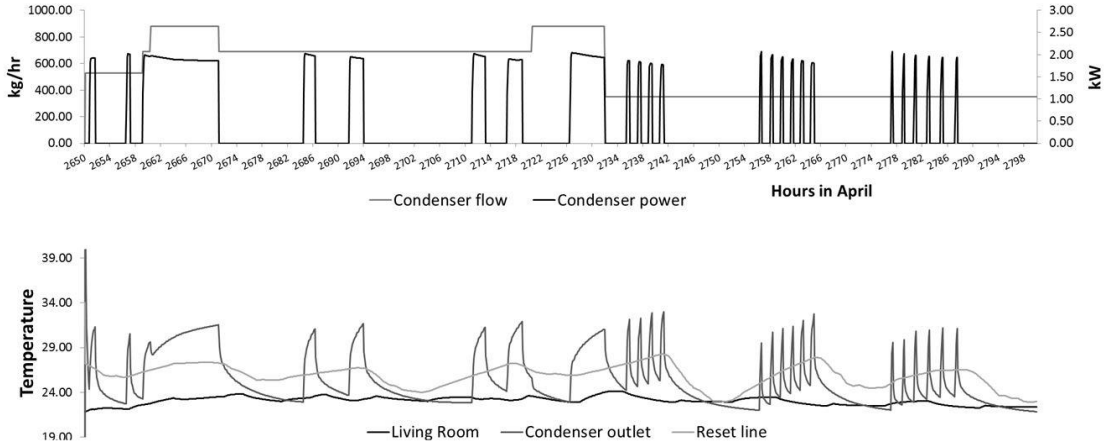

Figure 5.36: 1 week of operation with the selected heat pump and set-point temperature for condenser outlet following the reset line 2. Heat pump cycle length at low load is 18-30 minutes.

In Figure 5.36 the same week is simulated with heat pump set-point temperature following reset line 2. The lower graph shows this reset line set-point temperature together with the condenser outlet temperature and living room operative temperature. Set-point temperature for reset line 2 is lower than that of reset line 1, and the effects of this on heat pump on/off cycles are evident.

Table 5-5 shows the simulation summary using the chosen heat pump for the three reset lines. Even though the seasonal COP is better with reset line 2, due to the lower average condenser temperature, it also provides a bit less energy for the same reason. This energy has to be replaced by an alternative source, and if this is direct electric heating, the total COP will be the same for the two lines. Results for reset line 3 are included and show the same pattern. No difference in thermal comfort observed between lines 1 and 2.

Table 5-5
Performance of the ASHP for reset line 1 and 2.

Reset Line	Capacity [kW]	Load coverage	On/off cycles	Seasonal COP	Demand coverage	Total COP	Total energy kWh/m²a
1	1.2	60 %	992	4.26	98 %	4.04	11.4
2	1.2	60 %	289	4.43	97 %	4.05	11.4
3	1.2	60 %	172	4.50	94 %	3.75	12.3

Same simulation properties as in Table 5-4.

With a differential of ±5°C on the heat pump control there will be a problem whenever the supply set-point temperature is lower than 26-27°C. The return temperature from the floor loops are rarely lower than 1-2 degrees below room set-points, and will therefore be within the differential of the heat pump controller. There might be a call for heat with a supply temperature of 25°C without the heat pump starting. There should be some control mechanism that can start the heat pump even though the return temperature is within the ±5°C differential. A smaller differential can also be implemented to avoid this, but would lead to a higher cycle frequency. Table 5-6 shows the results of a simulation with the heat pump differential at ±3°C and room differential at ±0.5°C, for control with reset lines 1 and 2. Compared to the value in Table 5-4 the effects on cycle number can be seen. Demand coverage is a little higher at the expense of seasonal COP and total COP. COP is improved due to a lower average set-point temperature. Heat source control is not a part of the scope for this work, and this will not be addressed further here.

Table 5-6
Performance of the ASHP with new differentials on controllers for the two reset lines.

Reset Line	Capacity [kW]	Load coverage	On/off cycles	Seasonal COP	Demand coverage	Total COP
1	1.2	60 %	3512	4.12	98 %	3.88
2	1.2	60 %	1856	4.33	97 %	3.98

Except for the differential, same simulation properties as in Table 5-4.

5.3.3 Indirect Connection

The main reason to separate the heat source from the heat emitter is that the heat capacity of the water in the tank causes a latency of the temperature change and in this way eases the operation and control of the system. A storage/buffer tank can also be connected to different heat sources, letting the user choose the cheapest source available. A solar collector system might be connected to the tank, especially if the tank also serves to supply domestic hot water to the building. In bigger heating systems there will always be storage tanks installed. With a more stable heat pump operation, a bigger heat pump can be chosen and a monovalent operation might be viable. A big buffer tank can be connected to a big heat pump and in this way cover 100 % of the heat demand, but it is a question of investment cost. It will usually not be economically sensible to choose the big heat pump with a correspondingly big tank, but rather a smaller one with an extra electric heater in the tank. Figure 5.37 shows the simple heat storage system simulated in this section. A mixing assembly is required as the temperature in the tank usually exceeds the set-point temperature of the heating system. The valve mixes supply and return water to reach the set-point temperature given by the reset line. The heat pump is controlled by a thermostat in the tank. Two separate hydraulic systems are installed, which also contributes to a higher investment cost. Heat pump control and zone valves no longer have an operative connection between them and the system will be more stable and hence easier to control properly.

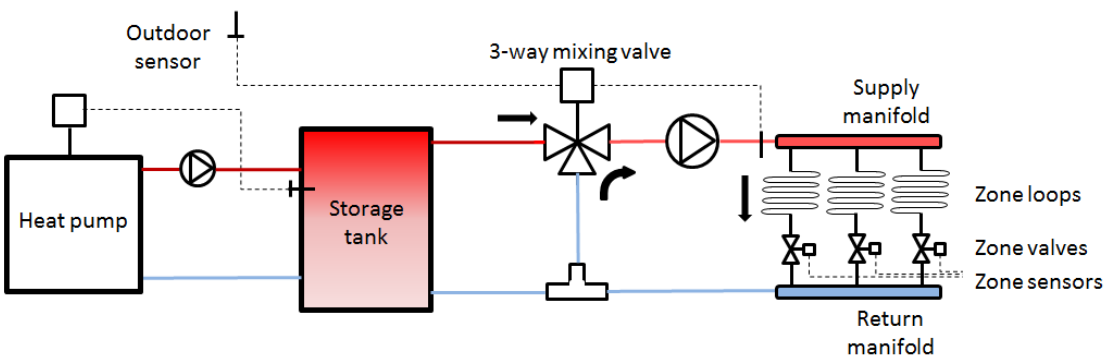

Figure 5.37: Schematic diagram of the simulated indirect connection principle. Mixing valve controlled supply temperature.

An indirect connection model is built as depicted in Figure 5.38. The building and radiant floor model is the same as the one in section 5.3.2, except that the differential on the radiant floor loop controls are changed to ±0.5°C. This ensures a more even indoor temperature without causing operative issues for the heat pump, because they are now hydraulically separated. Diverter and tee-piece models are connected to simulate a 3-way mixing valve. Even though they are on opposite sides compared to Figure 5.37, it is computationally equivalent and is done in this way in TRNSYS due to convergence problems when connecting them the other way. The diverter reads the tank temperature and the return temperature and calculates the flows necessary to reach a supply temperature equal to the set-point. Energy for pumps and heat losses from storage and distribution is neglected. An on/off controller reads the tank outlet temperature and signals the heat pump to switch on if it is below the lower differential from the set-point. The differential is set to ±3°C and the set-point for the heat pump should therefore be supply water set-point plus 3°C. Condenser flow rate set to 500 kg/hr when the heat pump is running. Various tank set-points temperatures, heat pump sizes and tank sizes are simulated.

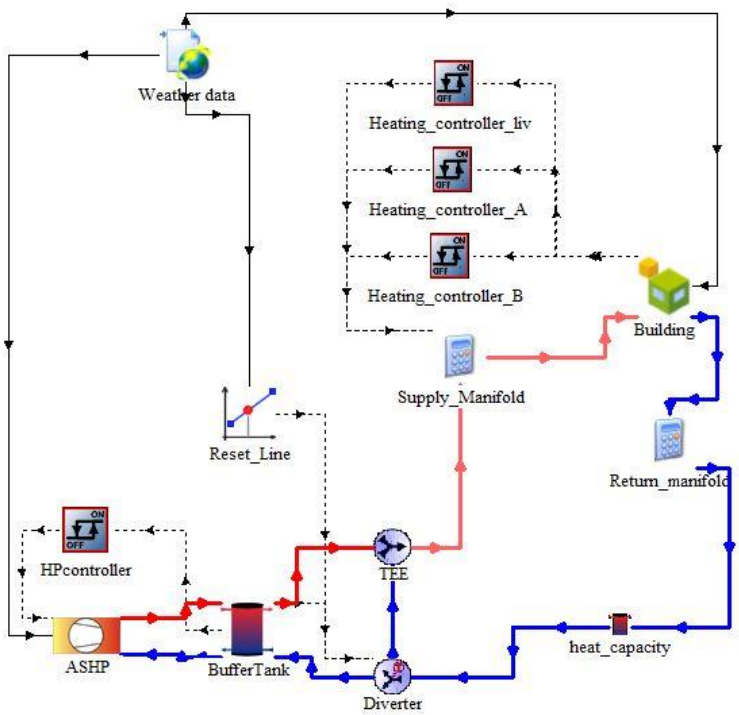

Figure 5.38: Simulation studio screenshot simplified to show how the indirect connection model is built.

Figure 5.39 shows a parametric study of the volume of the buffer tank on cycle numbers and performance. COP remains almost unaffected by the tank size, and the same is observed for the condenser heat output. The tank only causes a latency of the temperature change of the water, cf. equation 26, and does not affect performance. COP should increase as numbers of start/stop cycles decrease, but the cycle numbers are small and their influence of COP is hence negligible. In real systems energy use of a second circulator and heat losses from the tank as the tank size increases would lower COP slightly, but this is not accounted for here. It is evident that the storage tank serves the purpose of stable system operation, as the number of cycles drops significantly with tank size. In the remaining simulations a tank volume of 300 L will be used. A smaller tank would probably be sufficient, but this is not assessed as it is not considered to be important for the analysis.

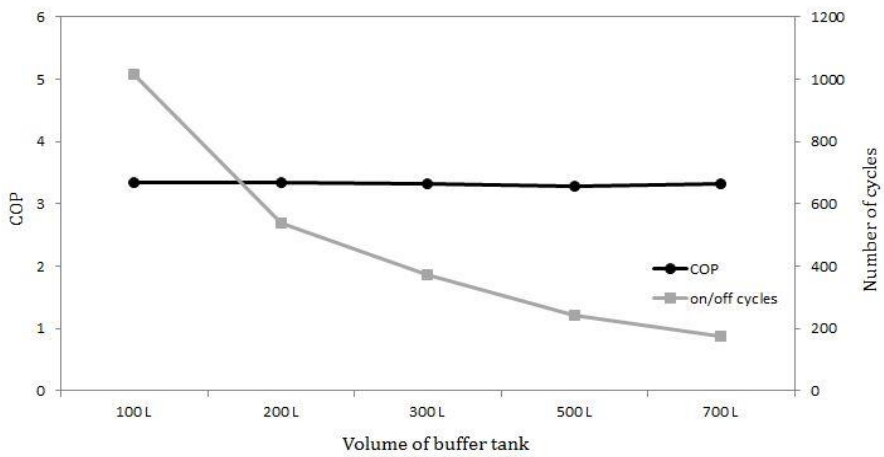

Figure 5.39: Seasonal COP and number of cycles for different sizes of storage tanks. The 1.2 kW heat pump from Table 5-4 is used in the simulation. Tank set-point temperature 40°C.

Table 5-7 shows results from simulation runs of the presented indirect connection principle for different sizes of heat pumps. Compared to the runs of section 5.3.2 it can be seen that the total energy use is a bit higher, and that start/stop cycle numbers are much lower. As the rooms are controlled by a

smaller differential, and the heat pump is controlled so that there is always at least supply water set-point temperature in the tank, the thermal comfort is more adequately regulated. COP is reduced due to the higher average set-point temperature for the heat pump. With a heat pump which delivers 90 % of the maximum heat load, total heat demand coverage is achieved. This seems paradoxical, but is due to the average nature of the weather model, which does not incorporate worst case scenarios. In a normal year this heat pump will provide all the demanded heat, but a backup heating source must be installed nonetheless, to aid the heat pump during extreme conditions.

Table 5-7
Performance of ASHP of different sizes with an indirect connection.

Capacity [kW]	Load coverage	On/off cycles	Seasonal COP	Demand coverage	Total COP	Total energy kWh/m²a
0.9	45 %	201	4.46	92.0 %	3.50	13.1
1.2	60 %	360	4.02	98.1 %	3.80	12.1
1.5	75 %	503	3.74	99.5 %	3.69	12.5
1.8	90 %	626	3.56	100 %	3.55	13.0

Maximum heat load at 2 kW, total heat demand 46 kWh/m²a. Tank volume for all simulations 300 L. Set-point temperature for heat pump condenser outlet equal to reset line 2 + 3°C. Capacity is the condenser power at design conditions, which are -4°C ambient temperature and 40°C condenser outlet temperature. COP not including icing and defrosting losses. Total COP assumes direct electrical heating as secondary heat source and is equal to heat demand divided by total electrical energy used by compressor and electric heater.

For both direct and indirect conditions both average PMV and minimum PMV values are very small as long as the heat pump is big enough and supply temperature high enough. This is as expected, since the radiant floor model is already verified for thermal comfort in the previous sections.

6 ALTERNATIVE HEAT EMITTER: FAN COIL UNIT

An alternative heat emitting system to the radiant floor is fan coil units (FCU). Modern FCUs have enhanced heat transfer and energy efficient fans and can be operated with a quite low temperature on the supply water. Low temperature FCUs are installed in GEL, and it is important to analyze these two low temperature heat emitters and compare them to make an assessment of which is the most appropriate for a modern building project. The FCUs analyzed here are small and placed on the floor in the zones. They are flow controlled by a proportional controller which measures the zone temperature, calculates the difference between this and the set-point temperature and sends a continuous signal to the actuator on the flow control valve that is proportional to this difference/error. To compare the FCU with the radiant floor, both connection principles are simulated, as shown in Figure 6.1.

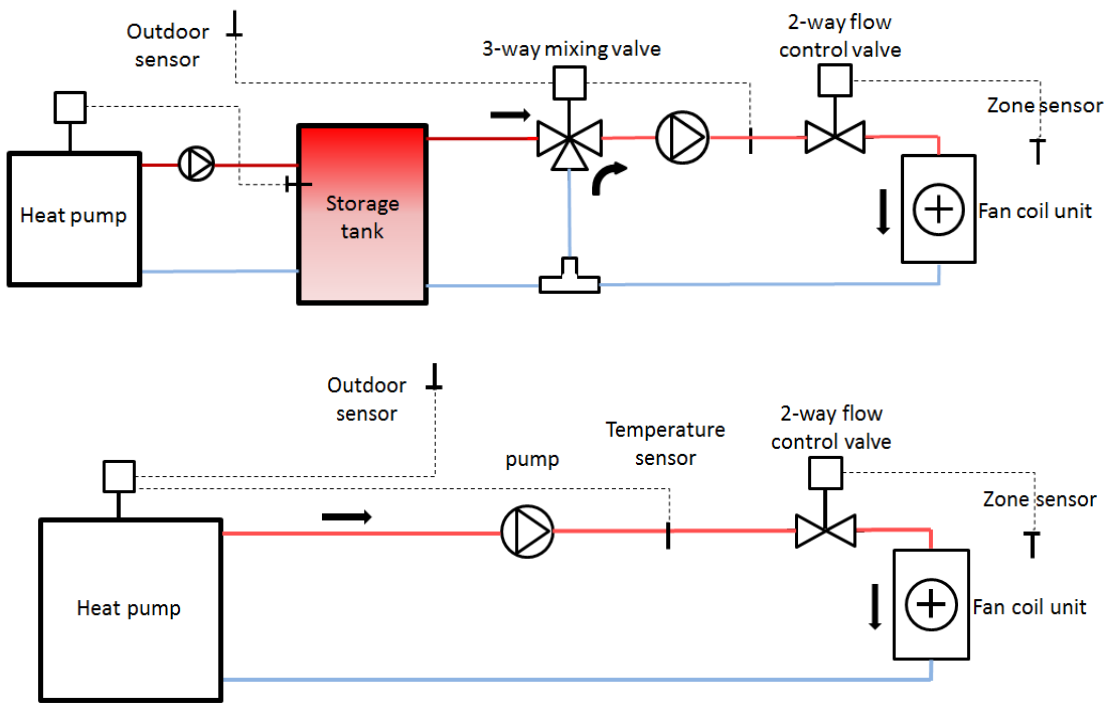

Figure 6.1: Schematic diagram of simulations of fan coil units as heat emitting system. Flow control to each fan coil. In the model, 4 fan coils in parallel are simulated.

6.1 FAN COIL UNIT MODELLING

As information about the FCUs installed at the GEL is not available, an FCU from the supplier Sabiana S.p.A. [34] is modelled as a simple heat exchanger. The simulation model is calibrated using measurements for the FCU "Carisma CRC13", as given in the reference by the supplier. A tube and shell heat exchanger model, type 5g in TRNSYS, with a constant overall heat transfer coefficient of 83.3 W/K and one shell pass is found to be closest to the measured values. Table 6-1 shows the results from the calibration procedure. The FCU is controlled in 6 different stages in reality, but is modelled to operate continuously within its operative range. The heat transfer coefficient is dependent on both flow velocities and temperatures, but is modelled constant, which causes some discrepancy between simulation and measurements. This error is maximum 10 %, at the very low end of the operative range. Measurements are done with a supply water temperature of 50°C, whereas in the simulations temperatures between 25 and 40°C are used, which could also contribute to inaccuracy of the model. At 40°C supply water temperature and 21°C room air temperature this FCU model supplies minimum 0.5 kW and maximum 0.9 kW. 4 FCUs will therefore deliver 41 W/m^2. The radiant floor delivers on average about 42 W/m^2 (39 W/m^2 for living room loop and 46 W/m^2 for bedroom loops) under the same conditions. Their nominal powers are thus almost exactly the same.

Table 6-1
Accuracy of the simulated fan coil compared to measurements from supplier.

Stage	Air flow kg/hr	Water flow kg/hr	Measured kW	Simulated kW	Error
1	105	101	0.76	0.83	10 %
2	125	117	0.90	0.95	5 %
3	150	132	1.02	1.07	5 %
4	175	147	1.15	1.17	2 %
5	195	161	1.26	1.25	-1 %
6	220	177	1.39	1.33	-5 %

The modelled FCU is the Sabiana Carisma CRC13. Air flow, water flow and measured heat transfer are all given in the product data sheet [34]. TRNSYS type 5g shell and tube heat exchanger model with 1 shell pass and an overall heat transfer coefficient equal to 83.3 W/K.

Two FCUs are put in the living room zone and one in each bed room, which will cause some discrepancies in the nominal powers as the floor areas of the zones are not proportional, but this must be viewed as a realistic approach. Figure 6.2 shows how the two models are built in the simulation studio. Heat storage (300 L) and distribution systems are equivalent to the ones simulated in the previous sections. The active layer in each zone of the building model is removed and replaced with a purely convective gain which is given as an input to the building model. Outputs from the living room fan coil model are multiplied by 2. The FCUs are controlled by a P-controller with a gain constant of 1. To avoid the constant error associated with P-controllers, a hysteresis is modelled with on/off controllers connected in series with the P-controllers. When the P-controller reaches the minimum of the operative range of the FCU it usually turn the FCU off, but with this approach it keeps the FCU running at its minimum until the zone temperature reaches an upper differential of +0.3°C. In this way the zone air temperature will oscillate around the set-point temperature instead of always be under it. The air flow and water flow of the fan coils are interpolated between the stages from Table 6-1 according to the output signal from the controller. Reset line 2 is simulated, but is not found to be adequate for the FCUs as they do not supply enough heat. With reset line 1 the supply temperature is high enough and this is thus used in the simulations.

Fan coil units cause stratification of the zone air because of the high temperature of the coil outlet temperature. Stratification causes reduced local thermal comfort because of air temperature gradients. Air warmer than the set-point is trapped in the upper part of a room, which is usually not within the occupancy zone, causing higher average temperatures and hence increased transmission losses. These stratification effects are not captured in the TRNSYS model because the room air is calculated as a single node.

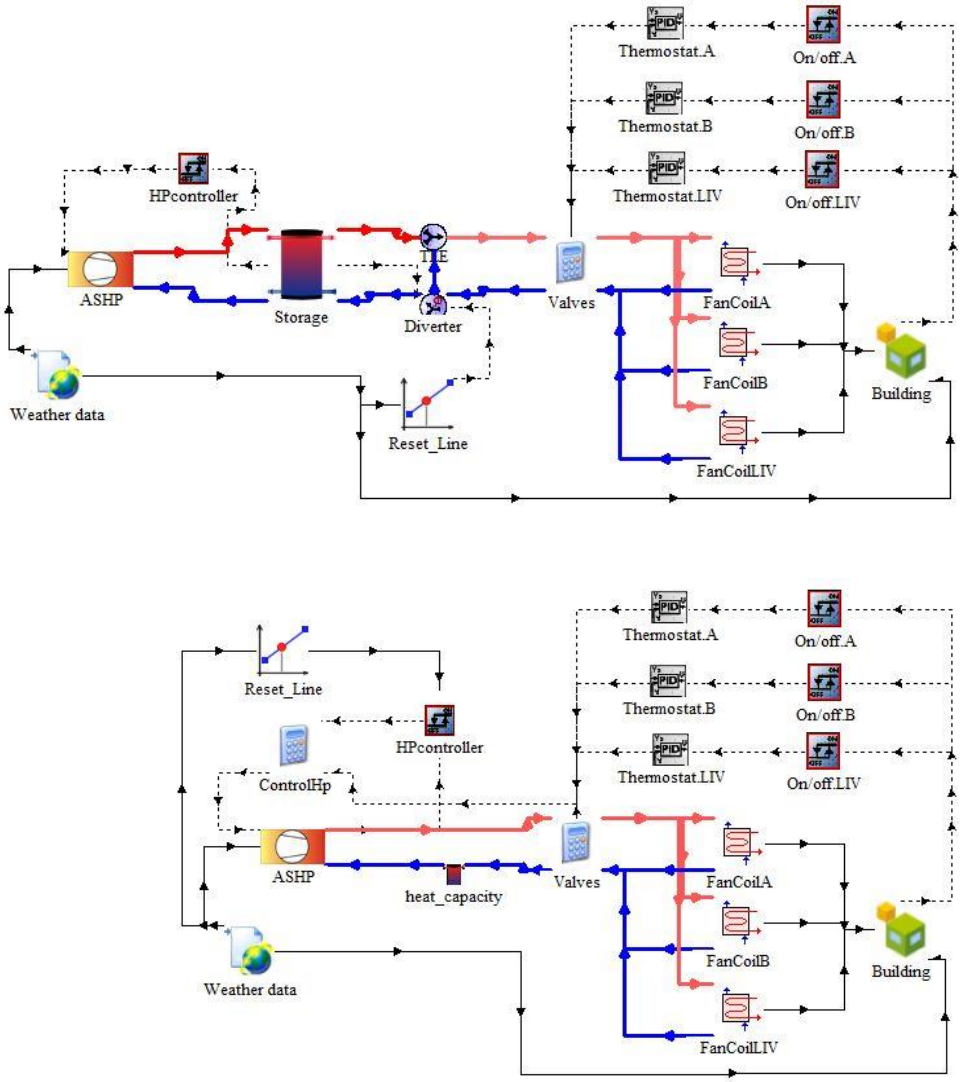

Figure 6.2: Simulation studio screenshot simplified to show how the model is built. Top show the indirect connection and the bottom the direct connection, with fan coil units as heat emitting system.

6.2 SIMULATION RESULTS

A detailed presentation of the operation of the system is not considered necessary, as it is similar to the simulations done in section 5.3. To notice is that the zone operative temperature is very stable using the FCU model and that the outlet air temperature of the FCU can be over 40°C. Temperature effectiveness of the FCU is 70-80 %. Table 6-2 contains the most important results of the simulations. The heat demand using the fan coil units is the same as for an ideal heating source and is 41 kWh/m²a, 11 % less than for the radiant floor. In section 5.2.7 the heat loss to underlying zones when using a radiant floor is discussed. The radiation also heats the inside surfaces of exterior walls, which increases the transmission heat losses. FCUs supply a purely convective heat transfer to the zone and these losses are therefore not present. However, because the FCUs have a smaller overall heat transfer coefficient than the radiant floor a higher supply temperature is required to supply enough heat, which leads to a deterioration of the heat pump COP. Energy use for electricity to the system is raised, and the total energy use is 12-13 kWh/m²a, slightly higher than for the radiant floor (see section 5.3). The direct connection with the FCU causes a reduction in demand coverage, because of the big differential on the heat pump controller. A smaller differential would lead to very large start/stop cycle numbers. It is seen that the cycle numbers are higher than for the radiant floor, and is due to the thermal mass and thus temperature change latency inherent with radiant floors.

Table 6-2
Performance of ASHP of different sizes using FCU as heat emitter.

Capacity [kW]	Load coverage	Connection Principle	On/off cycles	Seasonal COP	Demand coverage	Total Energy kWh/m²a
1.2	60 %	Direct	4194	3.7	97 %	12.6
		Indirect	445	3.5	99 %	12.1
1.5	75 %	Direct	5072	3.4	97 %	13.6
		Indirect	612	3.3	100 %	12.5

Maximum heat load at 2 kW, total heat demand 41 kWh/m²a. COP not including icing and defrosting losses. Set-point temperature for heat pumps is reset line 1. Total energy assumes that direct electrical heating supplies the remaining heat demand.

6.3 COMPARISON

A comparison of the simulation results of sections 5.3 and 6.2 is presented in Table 6-3. For the radiant floor the direct connection performs better because the set-point temperature for the heat pump is lower. When using a buffer tank this set-point temperature must be higher to ensure the same supply temperature to the floor, thus decreasing the COP. The stabilizing effect of using a buffer tank is seen, as cycle numbers are significantly lower. The indirect connection is found better for fan coil units, because of unstable operation with a direct connection. The radiant floor has a much bigger thermal mass than the fan coils and therefore evens out and slows down temperature change of the heating water flowing through it. It should be noticed that the total energy used by the different systems are similar and that practical considerations might alter the decision on which system is appropriate for a building project.

Table 6-3
Result summary from simulations in sections 5.3 and 6.

Heat emitter	Connection principle	On/off cycles	Seasonal COP	Demand coverage	Total COP	Total energy kWh/m²a
RF	Direct	1856	4.3	97 %	4.0	11.6
RF	Indirect	360	4.0	98 %	3.8	12.1
FCU	Direct	4194	3.7	97 %	3.3	12.6
FCU	Indirect	445	3.5	99 %	3.4	12.1

Maximum heat load at 2 kW, total heat demand 46 kWh/m²a with radiant floor and 41 kWh/m²a with fan coil units. Tank volume for all simulations 300 L. Supply water set-point temperature according to reset line 2 for RF and line 1 for FCU. Results for RF direct are with small differentials on the thermostats for comparison. Heat pump capacity is 1.2 kW for the condenser power at design conditions, which are -4°C ambient temperature and 40°C condenser outlet temperature. COP not including icing and defrosting losses. Total COP assumes direct electrical heating as secondary heat source and is equal to heat demand divided by total electrical energy used by compressor and electric heater.

As mentioned, operative temperature is very stable using the FCUs and the average PMV values, which were used as a thermal comfort indicator in chapter 5, are virtually zero for the entire heating season. Minimum PMV values are around -0.2 and hence negligible. Operative temperature consists of two temperatures: Air temperature and mean radiant temperature, see section 2.2. For the radiant floor the air temperature is lower, while the mean radiant temperature is higher. For FCU this is reversed, and temperature of the air must be increased, as surfaces are colder. Perceived air quality is a function of air temperature and is decreasing with increasing temperature. The high outlet air temperature that occurs using the FCU can cause significant thermal stratification, which is not modelled in this work. There is also the chance of draft in the vicinity of the FCU, and the air movement will transport dust more efficiently. The air flows in the zone are hard to predict and a computational fluid dynamics (CFD) simulation should be conducted to further assess the thermal comfort for both heat emitting systems. Experience and previous work show that radiant floors are very comfortable, and it is highly expected that the results from the CFD analysis would prefer this system with regards to comfort.

Radiant floors are more difficult to install and when installed it is expensive to make changes to the layout. Emphasis on the radiant floor design procedure is thus more important than for FCUs. A radiant floor will have a higher investment cost, which must also be taken into account. Especially for retrofitting of buildings can FCUs be the best option for this reason.

7 RADIANT FLOOR SYSTEM DESIGN PROPOSAL

This chapter proposes a design for the hydronic radiant heating system for the typical Chinese building model from section 5.2. The radiant floor is simulated using the validated simulation model from chapter 4. It is assumed that the climate is Shanghai. Detailed flow analysis and circulator sizing is not considered.

Tubes

The layout of the tubes is assumed to follow the same pattern as the installed system in GEL, see Figure 3.20. In the living room a d_x of 15 cm (center to center distance between tubes) is prescribed. The tubes should be slightly closer to each other at the external periphery of the zone, and slight further apart in the middle of the zone, but with 15 cm as an average. To avoid too large loop lengths three different loops should be placed in the living room floor. For the bedrooms the same applies, but with a d_x of 12 cm and just one loop per zone. If this is technically difficult because of the rigidity of the tubes, smaller tubes can be used. In that case, pressure drop calculations must consider the smaller diameter and thus higher flow resistance of the loops.

Control

Each zone is flow controlled by a zone valve which is governed by a zone thermostat. Even though a zone might have more loops, like in the living room, the loops should be simultaneously controlled by one single zone thermostat. The zone valves are on/off controlled with a differential of $\pm$0.5°C. If there are very high requirements on the set-point temperature, PI controllers together with motorized flow control valves should be used instead.

Flow

The flow through each loop is designed so that the temperature drop through that loop is smaller than a decided value. This $\Delta\theta$ is usually 2-5°C [35]. A $\Delta\theta$ of 3°C is prescribed and, using the graph of Figure 5.21, the flow through the floor should be 12 and 14 kg/hr/m^2 for the living room and bedrooms, respectively.

The total flow will therefore be about 1130 kg/hr. The following rough estimate on pressure drop is calculated, based on tube lengths, utilizing the moody chart in Appendix D:

Zone	Flow velocity [m/s]	Tube length [m]	Pressure drop [kPa]
Living Room	0.29	117	11.4
Room A	0.37	133	19.4
Room B	0.37	160	23.3

The pressure drop over the loops of the bedrooms is much higher than the one for the living room loops, and an evaluation must be made on whether these values are acceptable. If not, the solution is to divide each bedroom loop into two loops.

Supply temperature

The supply temperature should be controlled by the outdoor reset line in Figure 5.9. An optimization of this line is not conducted in this work. A 3-way mixing valve provides the desired supply temperature.

Heat source and storage

The 1.2 kW heat pump used in the simulations is chosen as a heat source, with a direct electrical heater as a backup. The direct connection has shown best energy performance, but a storage tank is prescribed for system stability and future heat source flexibility. The volume is initially set to 300 L, but should be chosen based on technical considerations such as available space, as system performance is shown be insensitive to tank volume. The sizing must take into consideration that additional heat sources such as solar collectors might be installed later. If the heat source is provided centrally in e.g. an apartment complex, the source and storage systems will be placed there and sized according to total load.

8 CONCLUSION

The aim of this work has been to analyze the hydronic radiant floor installed at the Green Energy Laboratory for modern buildings in a Chinese environment, with a special focus on the Shanghai climate. The preferred simulation tool has been TRNSYS, with the active layer model within the Type56 Multi-zone building model.

Chapter 1 was the introduction to this work and included the background information and motivation for the study.

Chapter 2 provided the underlying theory of the heat transfer processes inherent with hydronic radiant floors, and the main differences between a radiant and an all air heating system. A general introduction to occupant thermal comfort, the heat balance of a building, control theory and heat pump theory was also included.

Chapter 3 explained why and how to model the theory into computer simulation programs. The simplifications and approximations involved were highlighted, before the simulation tool TRNSYS was introduced. The radiant heating system installed in GEL and the modelling in TRNSYS of this system was presented. Information on the experiments and data acquisition was included.

Chapter 4 presented the results from the validation of the simulation model against the experimental data, and showed a good correlation between the calibrated model and the measurements.

Chapter 5 explained how the validated model was put into a simulation model of a typical Chinese apartment. Results from the simulation done on this model was presented and discussed. Focus was to show, using a logical sequence, why and how to control a hydronic radiant floor. It was found that the floor can provide a typical Chinese apartment in Shanghai with sufficient energy and comfort. Then

the heat emitting system was coupled with a source and thermal storage in a super-insulated building model to perform a comprehensive system analysis.

Chapter 6 contained the simulation results from a different heat emitting system, using fan coils instead of radiant floors. It was shown that the two heat emitting systems uses about the same amount of electrical energy.

Chapter 7 was a presentation of a design proposal for the radiant floor in the typical Chinese building model used in the first part of Chapter 5.

The following states the main findings of this work:

- The radiant floor installed at the Green Energy Laboratory can provide the entire heating for a typical Chinese apartment and at the same time ensure good thermal comfort, for Shanghai weather conditions. In colder climates the insulation of this apartment model is insufficient and must be improved if a radiant floor is to be considered. The radiant floor has a heating power of 50-57 W/m^2, depending on the ratio of external surfaces of the zone. The heating power is constrained by thermal comfort requirements on floor surface temperatures.

- The cheapest and thus usual way of controlling a radiant floor is to use simple on/off thermostat controllers. This work affirms that this strategy can be utilized in each zone without compromising the thermal comfort. P or PI control can be employed if there are high requirements on accurate temperature control.

- Based on the simulation results in Chapter 5, alternative heat saving control techniques such as heating cut-off and night setback are not effective because of the high thermal mass of the floor.

- Together with an air source heat pump, the seasonal COP of the system was shown to be as high as 4.0 for a direct connection without heat storage tank. Cycling time for the heat pump was 12-30 minutes at low loads. With a tank the operation of the heat pump is much more stable with cycle times of several hours, which prolongs the technical lifetime of the unit.

- Based on the system simulation of the two different heat emitting systems, the total heat demand is 11 % lower when using FCUs. The reason is the extra transmission losses inherent with radiant floors. However, the FCU requires higher supply temperature, which decreases the performance of the heat pump. It was shown that the total use of electricity for the heat pump is about the same for the two systems. The extra losses from the stratification of the zone air occurring when using FCUs is not considered.

This work has shown that the hydronic radiant heating system installed at the GEL is a promising technology for the future buildings of China. Focus on insulation must be high when considering radiant heating systems in the much colder northern climates, as a normal level of insulation was found unsuited for the utilization of a radiant floor. Both fan coil units and radiant floors have been shown to use about the same amount of electricity with an ASHP as heat source.

9 FURTHER WORK

The active layer model in TRNSYS is constrained by its internal mathematical approximations. A more comprehensive simulation model could be developed to simulate a wider array of different radiant heating floors. With a better model, more detailed parametric studies on concrete layer thickness, tube layout, etc., could be performed to evaluate their impact on seasonal system COP.

Some problems of flow measurement occurred during the experiments and are explained in Chapter 4. This uncertainty should be looked into in future experiments on the system.

The choice for heat source becomes more open with a storage tank installed in the heating system. Here, only a single heat pump together with an electrical heater is simulated. An investigation should be performed on how good seasonal COP could be achieved with solar collectors supplying heat to the tank. A TRNSYS solar collector simulation model could be connected to the tank model and simulation runs conducted in both Shanghai and colder climates of China. Solar photovoltaic panels supplying the system with electricity should also be simulated and compared to the solar thermal collectors.

The simulated heat pump is single-staged. Modern heat pumps with modulating control should be simulated.

Investment and operational costs are very important to the builder of a project. To make a conclusion about whether the fan coil units or the radiant floor is the best option a comprehensive cost analysis should be considered.

The thermal comfort model of type 56 in TRNSYS is limited and does not consider local parameters such as air movement, stratification and short-waved solar irradiation. A detailed computer fluid dynamics (CFD) analysis on both heat emitting systems would be interesting, to make a thorough thermal comfort assessment of each system.

BIBLIOGRAPHY

1. IEA. *https://www.iea.org/topics/sustainablebuildings/*. 2014.
2. Connolly, D., et al., *Heat Roadmap Europe: Combining district heating with heat savings to decarbonise the EU energy system.* Energy Policy, 2014. **65**(0): p. 475-489.
3. Bean, R., B. Olesen, and K.W. Kim, *History of Radiant Heating and Cooling Systems Part 1.* ASHRAE Journal, 2010.
4. Bean, R., B. Olesen, and K.W. Kim, *History of Radiant Heating and Cooling Systems Part 2.* ASHRAE Journal, 2010.
5. Hu, R. and J.L. Niu, *A review of the application of radiant cooling & heating systems in Mainland China.* Energy and Buildings, 2012. **52**: p. 11-19.
6. Cengel, Y.A., *Heat and mass transfer. A practical approach*. 3rd ed. 2006: McGraw-Hill Education.
7. Siegenthaler, j., *Modern Hydronic Heating*. 3 ed. 2012, Clifton park, NY: Cengage Learning.
8. www.hlk.co.at. *150.000 m2 Flächenkühlung*. 2007; Available from: http://www.hlk.co.at/upload/pdf/fachartikel/uponor_107.pdf.
9. Kosonen, R., *A flexibility chilled beam system in hot and humid climate*. 2014. p. 227-233.
10. Olesen, B.W. and G.S. Brager, *A better way to predict comfort.* ASHRAE Journal, 2004. **46**(8): p. 20-28.
11. Tye-Gingras, M. and L. Gosselin, *Comfort and energy consumption of hydronic heating radiant ceilings and walls based on CFD analysis.* Building and Environment, 2012. **54**: p. 1-13.
12. Ole Fanger, P., *What is IAQ?* Indoor Air, 2006. **16**(5): p. 328-334.
13. Feng, J., S. Schiavon, and F. Bauman, *Cooling load differences between radiant and air systems.* Energy and Buildings, 2013. **65**: p. 310-321.
14. Wang, H., H. Shu, and L. Duanmu, *A review on radiant cooling system in buildings of China*. 2014. p. 101-108.
15. Regjeringen.no, *Strategi for utbygging av vannbåren varme.* 2002.
16. Olesen, B.W., *Using building mass to heat and cool.* ASHRAE Journal, 2012. **54**(2): p. 44-52.
17. Cholewa, T., et al., *On the heat transfer coefficients between heated/cooled radiant floor and room.* Energy and Buildings, 2013. **66**(0): p. 599-606.
18. Pfafferott, D.J. and D. Kalz, *Thermo-Active Buildings Systems*. 2007, FIZ Karlsruhe GmbH.

19. Park, S.H., et al., *Evaluation of the thermal performance of a Thermally Activated Building System (TABS) according to the thermal load in a residential building.* Energy and Buildings, 2014. **73**: p. 69-82.

20. Nesbakken Haugen, E., *Lecture TEP14: Fuktproblematikk i bygg og anlegg. Mikrober – venn eller fiende? Hva er mikrobiell forurensning – og hva er normalt?*, S.E.A. NTNU, Editor. 2013.

21. Dokka, T.H., et al., *A zero emission concept analysis of an office building.* SINTEF academic press, 2013: p. 84.

22. U.S.DoE. *Building Energy Software Tools Directory*. 2011.

23. Behrendt, B.M., et al. *A system for the comparison of tools for the simulation of water-based radiant heating and cooling systems*. 2011.

24. Le Dréau, J., et al., *Thermal Mass & Dynamic effects. Danish Building Regulation*. 2013, Indoor Environmental Engineering Research Groupd: Aalborg University

25. University of Wisconsin-Madison, S.E.L., *TRNSYS 17 Manual*. 2012.

26. Delcroix, B., et al., *Conduction transfer function in TRNSYS multizone building model: Current implementation, limitations and possible improvements.* Fifth National Conference of IBPSA-USA, 2012.

27. L.M. Hensen, J. and R. Lamberts, *Building performance simulation for design and operation*. 2011, New York, USA: Spon Press.

28. Peeters, L., et al., *Internal convection coefficients for building simulation.* 12th Conference of IBPSA, Sydney, 14-16 November, 2011.

29. Afjei, T. and M. Wetter, *TNRSYS type: Compressor heat pump including frost and cycle losses*. 1997, Zentralschweizerisches Technikum Luzern.

30. Chuan, Z., X. Zhai, and R. Wang, *Experimental study of an air source heat pump space cooling system with different kinds of indoor terminals.* 2014.

31. Uponor.no. *Gulvvarmesystem*. Available from: https://www.uponor.no/vvs/system/gulvvarme.aspx.

32. Byggdetaljer_552.122, *Vannbåret lavtemperatur golvvarmeanlegg med stor energifleksibilitet.* Byggforskserien, 2001.

33. Byggdetaljer_473.015, *Dokumentasjon av passivhus og lavenergibygninger i henhold til NS 3700 og NS 3701.* Byggforskserien, 2013.

34. *Variant VVS: Carisma viftekonvektorer, produktblad*. 2011, file:///C:/Users/owner/Downloads/pb%203.f.2%20carisma.pdf.

35. Byggdetaljer_552.111, *Vannbåret golvvarme.* Byggforskserien, 1991.

36. Li, S. and P. Karava. *Modeling and predictive control of buildings with distributed energy generation and storage*. in *eWork and eBusiness in*

Architecture, Engineering and Construction - Proceedings of the 10th European Conference on Product and Process Modelling, ECPPM 2014. 2015.

37. Yin, W. and Q. Zhang, *The experimental analysis of GSHP-RF heating system in controlled operation*, in *Lecture Notes in Electrical Engineering*. 2014. p. 665-673.

38. Park, S.J., et al., *An evaluation of apartment heating system for Energy-saving.* Journal of Asian Architecture and Building Engineering, 2014. **13**(2): p. 453-458.

APPENDIX A: ACTIVE LAYER CALCULATIONS

The thermal resistances derived to describe the thermo-active layer in a building structure are here presented (see Figure 3.12). The equations in this appendix are all from the TRNSYS 17 manual [25]. For symbols, see Figure 3.9.

Figure A-1 shows the calculation of the resistance R_x as done in TRNSYS.

	Resistance in x-direction	Criteria
Radiant heating or cooling system (ceiling or wall)	$R_x \approx \frac{d_x \cdot \ln\left(\frac{d_x}{\pi \cdot \delta}\right)}{2 \cdot \pi \cdot \lambda_b}$	$d_x \geq 5.8 * \delta$ $\frac{d_i}{d_x} > 0.3$ $\frac{\delta}{d_x} < 0.2$
Capillary tube system	$R_x \approx \frac{d_x \cdot \frac{1}{3} \cdot \left(\frac{d_x}{\pi \cdot \delta}\right)}{2 \cdot \pi \cdot \lambda_b}$	$dx < 5.8 * \delta$ $\frac{d_i}{d_x} > 0.3$ $\frac{\delta}{d_x} < 0.2$
Floor heating systems	$R_x = \frac{d_x \cdot \left(\ln\left(\frac{d_x}{\pi \cdot \delta}\right) + \sum_{s=1}^{100} \frac{g_1(s)}{s}\right)}{2 \cdot \pi \cdot \lambda_b}$ $g_1(s) = -\frac{\frac{\alpha_2}{\lambda_b} \cdot d_x - 2 \cdot \pi \cdot s}{\frac{\alpha_2}{\lambda_b} \cdot d_x + 2 \cdot \pi \cdot s} \cdot e^{\frac{-4 \cdot \pi \cdot s}{d_x} \cdot d_2}$	$d_x \geq 5.8 * \delta$ $\alpha_2 = \frac{\lambda_{Insulation}}{d_{Insulation}} < 1.212 \frac{W}{m^2 K}$ $\frac{\delta}{2} \leq d_2;$ $\frac{d_1}{d_x} \leq 0.3$

Figure A-1: Calculation of the thermal resistance R_x according to type of thermo-active building element. The criteria are present due to simplifications of more complicated equations that require and inefficient amount of computing time.

R_z is found by the equation

$$R_z = \frac{1}{2 * \dot{m}_{sp} * n * c} \tag{A-1}$$

where $\dot{m}_{sp}$ is the specific mass flow rate, n is the number of sections the element is split into and c is the specific heat capacity. This is a linearization of the exponential behavior of the temperature change along the pipes, which is especially non-linear for low specific mass flow rates. If the boundary condition

$$\dot{m}_{sp} * c * n * (R_{cond} + R_{conv} + R_x) \geq \frac{1}{2}$$

does not hold it could lead to a significant loss of precision of the linearization and thus of the model. TRNSYS has a built in security and will not run if this is violated. The actual precision of the model with respect to this inequality and the ones associated with Figure A-1 is an interesting area of scrutiny.

R_{cond} is found by the equation

$$R_{cond} = \frac{d_x * ln\left(\frac{\delta}{\delta - 2 * d_r}\right)}{2 * \lambda_r * \pi} \tag{A-2}$$

where λ_r is the pipe conductivity. It is derived from a standard 1D conduction equation for cylinders.

R_{conv} is found by the equation

$$R_{conv} = \frac{d_x^{0.13}}{8.0 * \pi}\left(\frac{\delta - 2 * d_r}{\dot{m}_{sp} * l}\right)^{0.87} \tag{A-3}$$

where l is the length of the pipe. It is a correlation for internal forced convection for a turbulent flow in a tube. According to the TRNSYS documentation it has a "sufficient level of precision".

The total resistance R_{total} thus becomes

$$R_{total} = \frac{1}{2 * \dot{m}_{sp} * n * c} + \frac{d_x^{0.13}}{8.0 * \pi}\left(\frac{\delta - 2 * d_r}{\dot{m}_{sp} * l}\right)^{0.87} + \frac{d_x * ln\left(\frac{\delta}{\delta - 2 * d_r}\right)}{2 * \lambda_r * \pi} + R_x \tag{A-4}$$

where R_x can be found in Figure A-1, according to situation.

APPENDIX B: WALL TRANSFER FUNCTION

A brief introduction to the wall transfer function method employed in TRNSYS for calculation of heat transfer through walls. Figure B-1 shows a wall element and the heat flows to and from it as calculated by TRNSYS. The subscripts $_{S,O}$ and $_{S,I}$ stand for external and internal surface, respectively. S is the solar gains of the wall. $\dot{q}_r$ and $\dot{q}_c$ are the net radiative and net conductive surface heat flow. T is the associated temperatures. Equations B-1 and B-2 shows the calculation of the heat flows into the two surfaces. These are summations of the previous values for the surface temperatures and heat flows over a time interval, the time-base. The time-base is long for heavy walls and short for less heavy walls. The coefficients *a*, *b*, *c*, and *d* are computed as a matrix of the time-base. For more details on this model see TRNSYS17 manual 05-Multizone building.

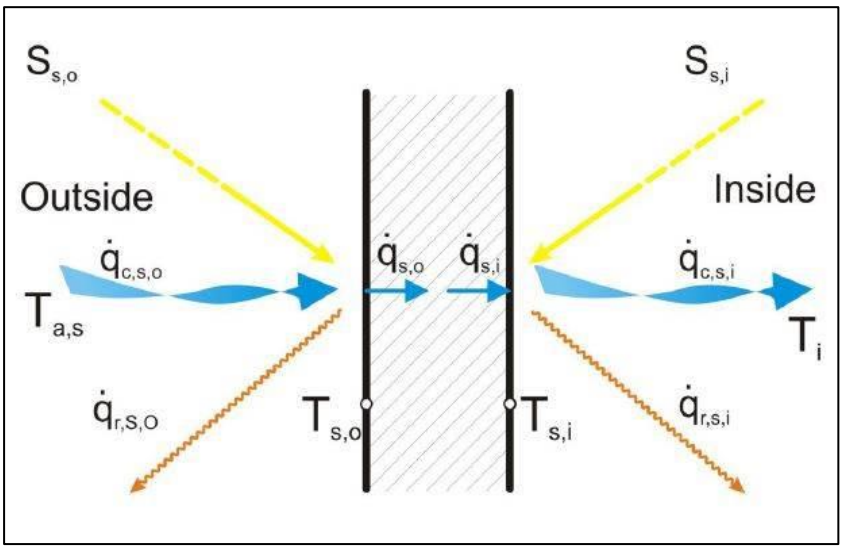

Figure B-1: Heat flows through a building structure for TRNSYS simulation. Source: TRNSYS17 manual.

$$\dot{q}_{s,i} = \sum_{k=0}^{n_{b_s}} b_s^k T_{s,o}^k - \sum_{k=0}^{n_{c_s}} c_s^k T_{s,i}^k - \sum_{k=1}^{n_{d_s}} d_s^k \dot{q}_{s,i}^k \tag{B-1}$$

$$\dot{q}_{s,o} = \sum_{k=0}^{n_{a_s}} a_s^k T_{s,o}^k - \sum_{k=0}^{n_{b_s}} b_s^k T_{s,i}^k - \sum_{k=1}^{n_{d_s}} d_s^k \dot{q}_{s,i}^k \tag{B-2}$$

APPENDIX C: BUILDING MODEL INFORMATION

Data used in the simulations of the laboratory.

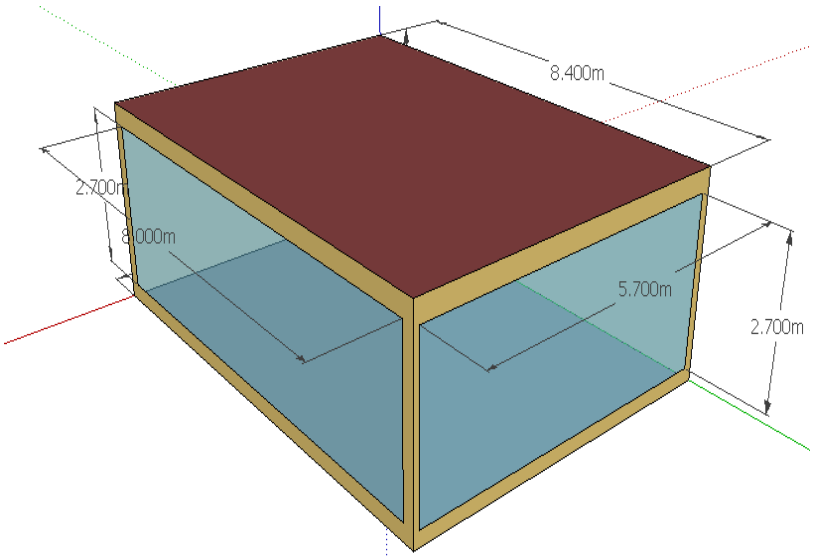

Figure C-1: Dimensions of the simulated room. Larger window faces south. Height 3 m.

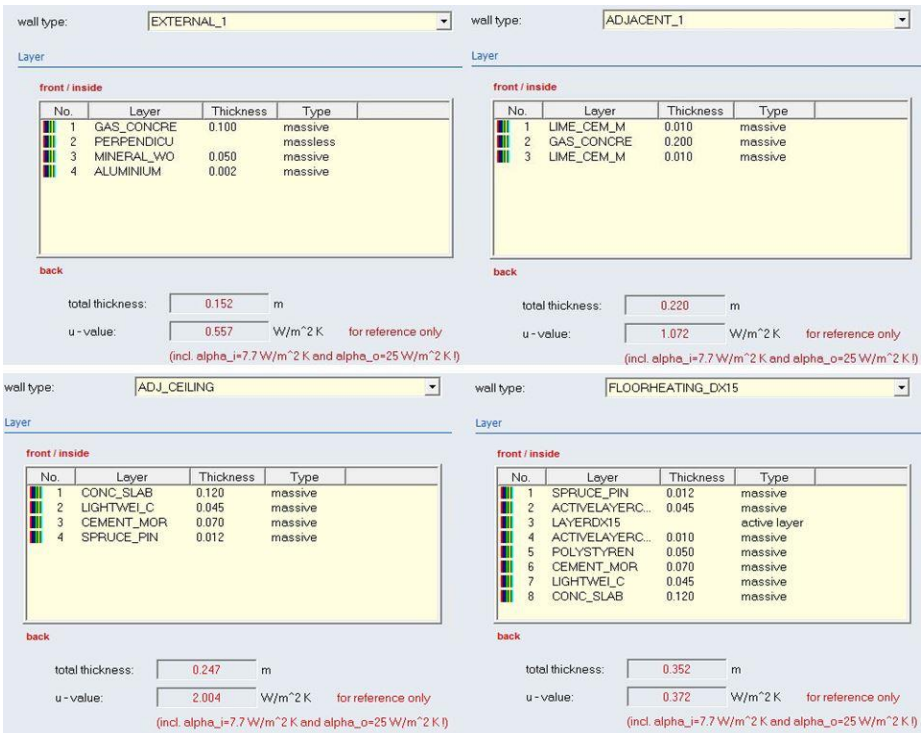

wall type: EXTERNAL_1

Layer

front / inside

No.	Layer	Thickness	Type
1	GAS_CONCRE	0.100	massive
2	PERPENDICU		massless
3	MINERAL_WO	0.050	massive
4	ALUMINIUM	0.002	massive

back

total thickness: 0.152 m

u-value: 0.557 W/m^2 K for reference only

(incl. alpha_i=7.7 W/m^2 K and alpha_o=25 W/m^2 K !)

wall type: ADJACENT_1

Layer

front / inside

No.	Layer	Thickness	Type
1	LIME_CEM_M	0.010	massive
2	GAS_CONCRE	0.200	massive
3	LIME_CEM_M	0.010	massive

back

total thickness: 0.220 m

u-value: 1.072 W/m^2 K for reference only

(incl. alpha_i=7.7 W/m^2 K and alpha_o=25 W/m^2 K !)

wall type: ADJ_CEILING

Layer

front / inside

No.	Layer	Thickness	Type
1	CONC_SLAB	0.120	massive
2	LIGHTWEI_C	0.045	massive
3	CEMENT_MOR	0.070	massive
4	SPRUCE_PIN	0.012	massive

back

total thickness: 0.247 m

u-value: 2.004 W/m^2 K for reference only

(incl. alpha_i=7.7 W/m^2 K and alpha_o=25 W/m^2 K !)

wall type: FLOORHEATING_DX15

Layer

front / inside

No.	Layer	Thickness	Type
1	SPRUCE_PIN	0.012	massive
2	ACTIVELAYERC...	0.045	massive
3	LAYERDX15		active layer
4	ACTIVELAYERC...	0.010	massive
5	POLYSTYREN	0.050	massive
6	CEMENT_MOR	0.070	massive
7	LIGHTWEI_C	0.045	massive
8	CONC_SLAB	0.120	massive

back

total thickness: 0.352 m

u-value: 0.372 W/m^2 K for reference only

(incl. alpha_i=7.7 W/m^2 K and alpha_o=25 W/m^2 K !)

Figure C-2: The wall and floor layers of the room. "External 1" is the exterior walls. "Adjacent 1" are the adjacent and boundary walls, and "Adj ceiling" is given for the ceiling. The ceiling boundary condition is equal to that of the boundary walls. "Floorheating dx15" is the radiant floor. Same properties are used in the typical apartment model. In the revised model, thermal resistances are added in the wall constructions to lower the U-value.

WinID	Description	Design	U-Val...	g-Val...	T-sol	Rf-sol	T-vis
1002	InsulatingGlass, 2.8	4/16/4	2.83	0.755	0.693	0.126	0.817
4001	Insulating, 0.7, Krypton	4/8/4/8/4	0.68	0.407	0.268	0.231	0.625
2003	Insulating,Kr, 1.1 71/60	4/16/4	0.86	0.598	0.426	0.266	0.706

Figure C-3: The given data for the windows. 1002 are the windows installed at the GEL. 2003 is used for the typical Chinese building model. 4001 is used in the revised building model.

Wall	Layer	Thickness [m]	Conductivity [W/mK]	Thermal Capacity [kJ/kgK]	Density [kg/m³]	Thermal resistance [m²K/W]
Ext	GAS_CONCRE	0.1	0.28	1	700	0.36
	PERPENDICU	x	x	x	x	0.13
	MINERAL_WO	0.05	0.04	0.9	80	1.13
	ALUMINUM	0.002	200	0.86	2700	0.00
Adj	LIME_CEM_M	0.02	0.97	1	1800	0.02
	GAS_CONCRE	0.2	0.28	1	700	0.72
Ceil/floor	CONC_SLAB	0.12	1.14	1	1400	0.11
	LIGHTWEI_C	0.045	0.56	1	1000	0.08
	CEMENT_MOR	0.07	1.39	1	2000	0.05
	SPRUCE_PIN	0.012	0.14	2	600	0.09
Act	ACTIVELAYERC	0.055	0.28	0.7	1200	0.20
	LAYERDX15*	x	x	x	x	x
	POLYSTYREN	0.05	0.03	1.25	25	2.00

Figure C-4: Layer properties of the layers in Figure C-2.

*Pipe wall thickness 0.002 m. Pipes spacing cc 0.15 m. Pipe outside diameter 0.02 m. Pipe wall conductivity 1.26 kJ/hmK. Specific heat coefficient of water 4.18 kJ/kgK.

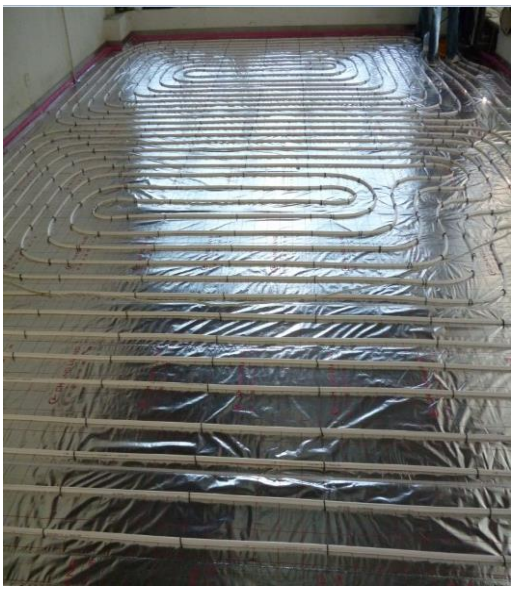

Figure C-5: The layout of the radiant underfloor heating in the room.

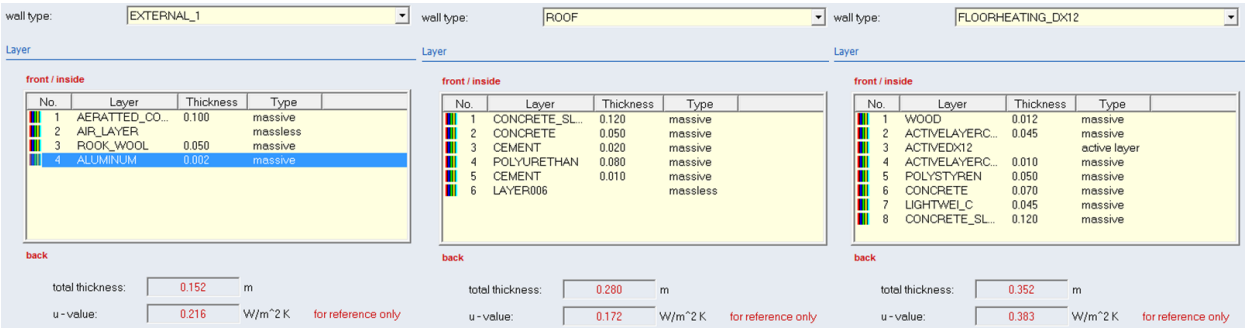

Figure C-6: Exterior wall, roof and floor heating construction used in the revised model of section 5.3.1. For the living room an equivalent floor heating construction is used with the only difference that the distance d_x between the tubes are changed to 15 cm. Boundary condition for the floor is 22°C.

APPENDIX D: PRESSURE DROP CALCULATIONS

Calculation of the pressure drop ΔP due to friction of a fluid moving through a pipe is done by the Darcy-Weisbach equation:

$$\Delta P = f * \frac{L}{d} * \frac{\rho * \dot{u}^2}{2} \tag{D-1}$$

L is tube length, d is internal diameter, ρ is fluid density, $\dot{u}$ is the mean velocity of the fluid and f is the Darcy friction factor. This factor is found with the help of empirical equations or from a chart called Moody diagram, see Figure D-1. With the material roughness of 0.0025 mm for plastic tubes and an internal diameter of 16 mm the relative pipe roughness is equal to $1.56*10^{-4}$ for the tubes used in this work. Assuming a kinematic viscosity of $0.658*10^{-6}$ m^2/s, a density of 1000 kg/m^3 and average flow velocity of 1 m/s for the heating water, the Reynolds number equals 22857. Using the diagram, the friction factor is found to be about 0.026. Using equation D - 1, without the tube length L, the pressure drop per meter tube is found to be 813 Pa/m.

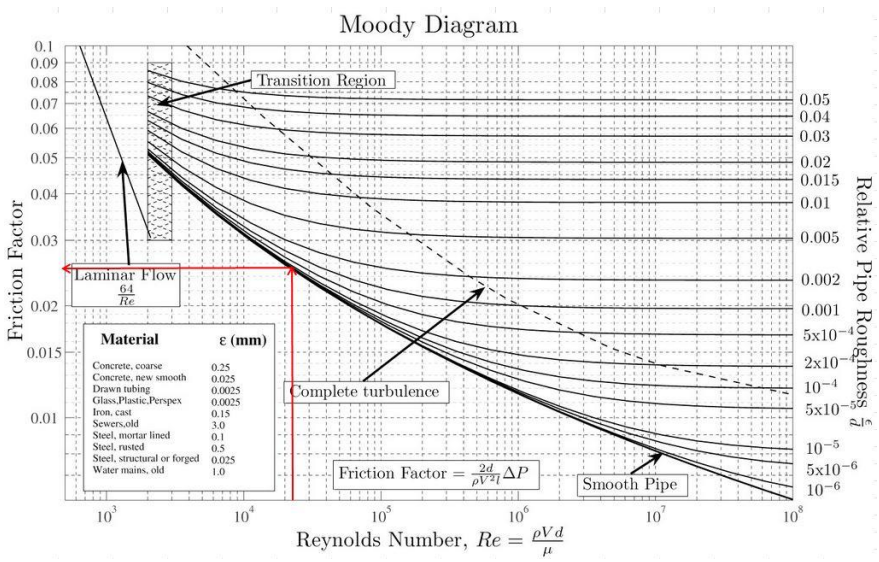

Figure D-1: The Moody diagram used to decide the friction factor f.

APPENDIX E: HEAT PUMP PERFORMANCE CURVES

		Outlet water temp							
		35				40			
T_out(DB)	T_out(WB)	Capacity(kW)	POW (kW)	COP	Flow(l/min)	Capacity(kW)	POW (kW)	COP	Flow(l/min)
-14	-	23.8	9.8	2.4	68.6				
-11	-11.8	26	9.9	2.6	75	25.5	11	2.3	73.5
-8	-	28.2	9.9	2.8	81.3	27.5	11.2	2.5	79.4
-5	-6.2	30.3	10	3.0	87.5	29.6	11.2	2.6	85.3
-2	-3.4	32.6	10	3.3	94	31.7	11.3	2.8	91.5
1	-0.7	35	10.1	3.5	101	33.9	11.4	3.0	98
4	2	37.7	10.1	3.7	108.6	36.4	11.4	3.2	105.3
7	6	42.1	10.1	4.2	121.4	40.8	11.4	3.6	117.8
10	7.4	43.9	10.2	4.3	126.8	42.5	11.5	3.7	122.8
13	10.2	47.8	10.2	4.7	137.7	46.2	11.5	4.0	133.4
		45				50			
T_out(DB)	T_out(WB)	Capacity(kW)	POW (kW)	COP	Flow(l/min)	Capacity(kW)	POW (kW)	COP	Flow(l/min)
-14	-								
-11	-11.8								
-8	-	26.9	12.4	2.2	78				
-5	-6.2	28.8	12.5	2.3	83.5	28.4	13.9	2.0	82.5
-2	-3.4	30.8	12.6	2.4	89.2	30.3	14	2.2	87.7
1	-0.7	32.9	12.6	2.6	95.4	32.2	14.1	2.3	93.5
4	2	35.3	12.7	2.8	102.3	34.4	14.1	2.4	99.9
7	6	39.5	12.7	3.1	114.4	38.5	14.2	2.7	111.6
10	7.4	41	12.8	3.2	119	39.9	14.3	2.8	115.7
13	10.2	44.6	12.8	3.5	129.2	43.2	14.3	3.0	125.5

Figure E-1: Performance data as provided by Carrier for the air source heat pump installed at GEL

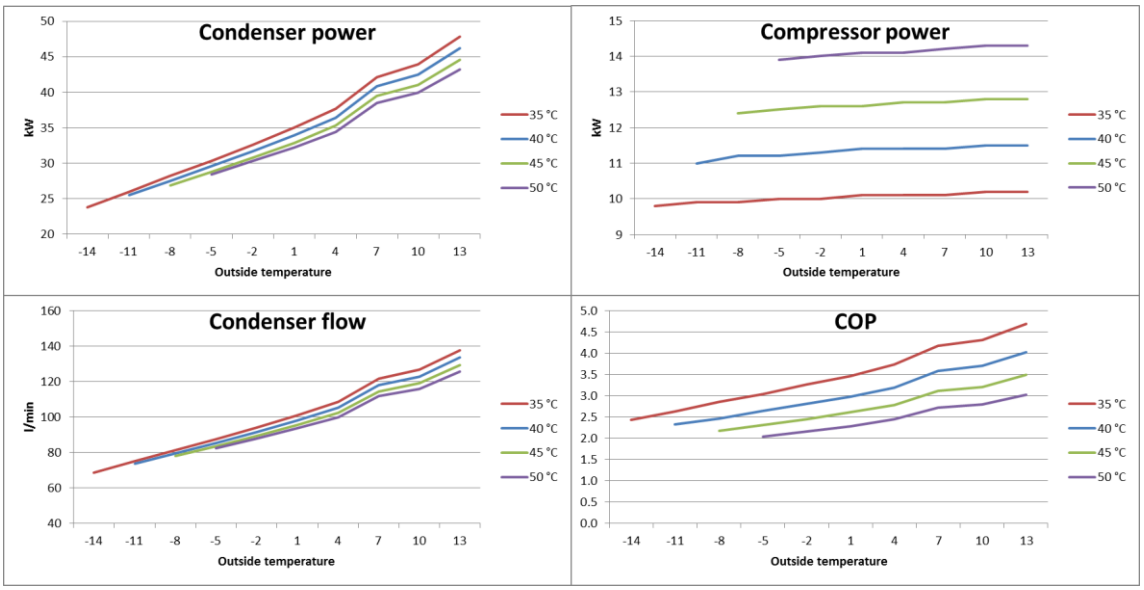

Figure E-2: Curves corresponding to the data of Figure E-1.

APPENDIX F: SCIENTIFIC PAPER DRAFT PROPOSAL

Radiant heating floors in a Chinese context: A total system performance analysis based on detailed building simulation.

Ludvig Nielsen[a], Laurent Georges[a], Yanjun Dai[b], Vojislav Novakovic[a]

[a] *Department of Energy and Process Engineering, Norwegian University of Science and Technology (NTNU), Kolbjørn Hejes vei 1B, 7491 Trondheim, Norway*

[b] *Institute of Refrigeration and Cryogenics, Shanghai Jiao Tong University (SJTU), Shanghai 200240, China*

Abstract

Contemporary and future standards on energy efficiency of buildings impose new requirements on space heating technologies. One promising technology is hydronic radiant heating systems (RHS). However, complexity in design and operation often makes RHS less competitive to traditional heating systems. Proper design procedures and control strategies should be developed to make RHS an economic solution for the future. In this study a RHS installed at the Green Energy Laboratory (GEL) at the Shanghai Jiao Tong University (SJTU) is analyzed with the use of the simulation tool TRNSYS. A simulation model is built and validated against measurements. The goal is to analyze the performance of the installed RHS for Chinese apartments in a Shanghai climate, with a focus on energy efficiency. Results show that the installed RHS can supply the entire heat load for a typical building in Shanghai. It is shown that for colder climates, a certain level of insulation is required, as the floor has a maximum heat output of about 50 W/m^2 at a supply temperature of 45°C. On/off thermostat control of the flow to each zone is confirmed to be sufficient. A stable heat pump operation is achieved with a storage tank, as cycling time is increased. Simulations of fan coil units (FCU) as an alternative heat emitting system (HES) show that total heat demand is reduced by 11 %. However, the heat pump performance is reduced due to higher supply temperatures, and the total electricity consumptions for the two systems are similar. RHS is affirmed as a good solution for Chinese residential buildings, but a more detailed analysis of thermal comfort and costs should be conducted to further assess its market competitiveness.

Keywords

Radiant underfloor heating, low temperature heating, TRNSYS, building performance simulation, Shanghai, China, passive house, low temperature fan coil units, thermal comfort.

1. Introduction

Climate change and energy scarcity put higher requirements on the use of energy in the society today. China is the biggest energy consuming and CO_2-emitting country in the world. About 40% of current worldwide primary energy use is consumed by buildings [1]. Coal boilers mainly supply space heating in China [2]. Problems of local pollution in the cities, together with a rapidly growing economy and urbanization, result in major incentives for a shift towards low-grade renewable energy sources (RES). RES for heating perform better when supplying a lower temperature. In new buildings, heat demand is reduced, which makes low temperature heat emitting systems viable. At the same time, focus on occupant thermal comfort is increasing, as research shows the correlation between thermal comfort and productivity [9].

Hydronic radiant heating systems utilize low water temperatures and are known for their inherent thermal comfort. In Nordic countries, RHS are widely in use in residential buildings. China has a long history of using "Kang", an ancient radiant heating technology. After a strong economic revolution, Chinese buildings have improved considerably, and today radiant heating is a preferred technology in many Chinese building projects [3].

Nevertheless, problems of design and operation of RHS in China are experienced. Hu et al. [5] investigated some RHS building projects in China, and concluded that there is a need for better design procedures and total system energy performance research on the topic. Even though RHS have a big energy saving potential, this is not always achieved. Economic barriers often cause other heat emitting systems to be chosen over RHS. One example from Norway is found in ref. [21], where Dokka et al. chose an all air heating system, due to simplicity and "a potential cost reduction", for his zero emission building concept. With better design procedures and operational strategies, the cost of RHS will decrease and thermal comfort increase, from which RHS is expected to gain popularity, especially in China.

Building performance simulation (BPS) tools are well equipped to perform total system energy and operational strategies analyses. Using BPS, Li et al. [36] showed that significant energy savings can be achieved with predictive control strategies on a RHS coupled with a storage tank, a ground source heat pump (GSHP) and solar collectors. Yin and Zhang [37] did an experimental analysis of two control strategies with a RF and a GSHP, and found that the heat pump is best controlled by an zone air thermostat. Park et al. [38] simulated several heat emitting systems and found that an electrical air to air heat pump system perform better than a radiant floor (RF). However, the source used for the floor was a conventional boiler, which does not benefit from the lower supply temperature inherent with RF.

A radiant floor model has been developed in TRNSYS and validated to experimental data from GEL. At GEL, an air source heat pump (ASHP) provides the heat for the lab. No previous studies on a radiant floor coupled with an ASHP for Chinese climates were found. Total system simulations were thus performed with an ASHP as source. Two different connection principles are studied: One with a direct hydraulic

connection between source and load, and one with a buffer tank between them. To evaluate the RF against an air heat emitting system, a fan coil unit (FCU) model was simulated together with the same heat pump.

As TRNSYS does not incorporate local thermal comfort effects like radiant asymmetry, short-waved radiation and air movement, the main focus in this study is energy efficiency. A rough thermal comfort assessment is done with the detailed thermal comfort model employed in TRNSYS.

2. Methodology

The laboratory building and installed system are first presented, before the selected TRNSYS radiant floor model is explained. Experimental setup for validation data is described. Building and system models for the analysis of the RF and FCU are presented.

2.1. Green Energy Laboratory

GEL was constructed by SJTU in cooperation with the Italian Ministry for Environment, Land and Sea, at the Minhang campus in 2012. It is a 1500 m^2 research center for energy-efficient solutions in buildings and contains many laboratories with state of the art HVAC technologies. For its low-energy technologies it has been rewarded the LEED Gold certification. Amongst these is the radiant underfloor heating system which is analyzed in this study.

2.1.1. Lab room model

The room is located in the south-east corner on the ground floor in the GEL building. Fig. 1 shows the lab as drawn in Google SketchUp. It is an empty room with different heating and cooling systems installed. An air-water heat pump supplies heat and cool to the system. The fan coil units (FCU) were tested by Chuan, et al. [30] for cooling conditions. The whole building has an exterior shading façade, which blocks direct solar irradiation. West and north walls and ceiling are adjacent to other zones, with a boundary temperature of 22°C. Yearly average temperature in Shanghai is assumed for the ground and is 17.2°C. Wall parameters are found in Fig. 4.

2.1.2. Radiant floor model

The hydronic radiant floor installed in the lab room is sketched in Fig. 2. Three loops are laid in a counter flow pattern. The system is installed on top of the original concrete floor of the GEL.

The thermo-active layer model in the TRNSYS Type 56 Multi-zone building model was selected appropriate to simulate the RF. Thermal resistances are modelled in a resistance network (Fig. 3) between the inlet temperature and the zone temperature. The linearization of the exponential water temperature drop causes restrictions on the model, in regards to water flow, layer thickness and distance between tubes.

Another model (Type 653) exists in the TESS library, but as it was not available to the author it has not been considered.

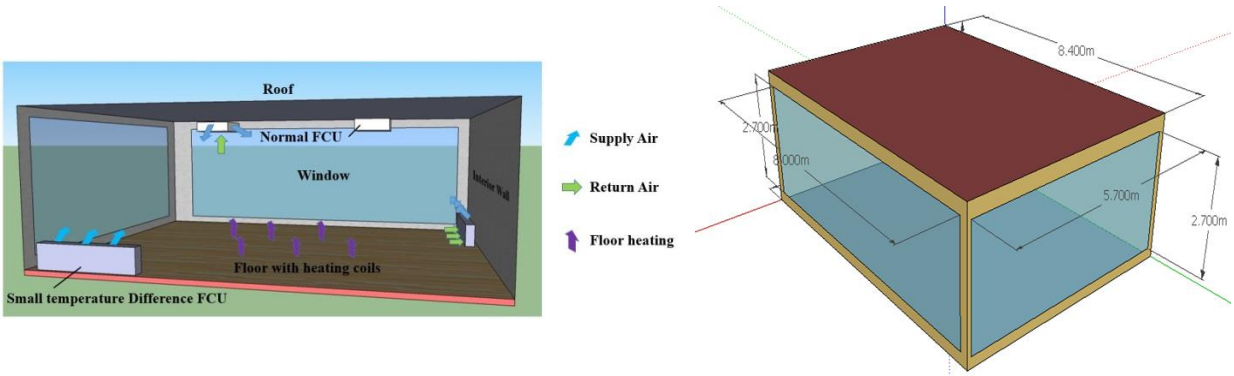

Fig. 1. The office lab room. "Roof" is an adjacent room in the first floor. The fan coil units (FCU) provide both heating and cooling, while the floor is only used for heating. The large window faces south, the small to the east. Height of room is 3 m. Windows have a U-value of 2.89. Source: Chuan, Z. [30].

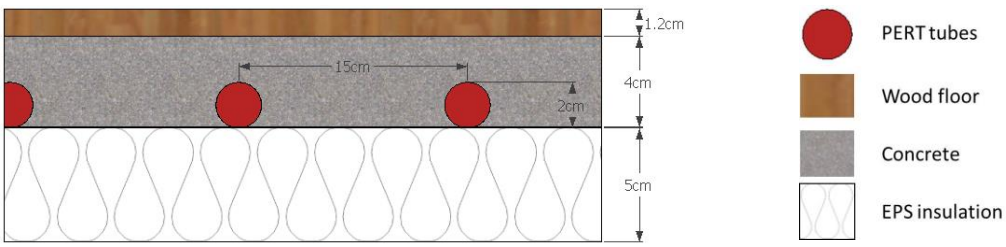

Fig. 2. The RHS installed at GEL. Tube wall thickness 0.002 m. Pipe wall conductivity 1.26 kJ/hmK. Specific heat coefficient of water 4.18 kJ/kgK.

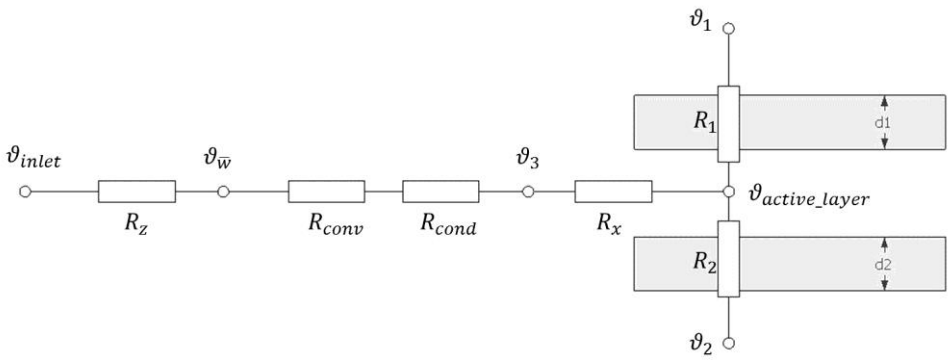

Fig. 3. The total resistance network of the thermo-active construction element between inlet temperature and zone temperatures.

2.2. Experiment (and validation)

Measurements were taken in the lab for validation of the simulation model. Flow and temperature sensors send signals to a data acquisition system (DAS). The DAS

digitalizes the signals and send them to a computer, where the measurements are recorded in an excel worksheet. Two air temperature loggers were set in a height of 1 m and 1.5 m in the middle of the lab room. Two more were set outside to measure the outdoor air temperature. Water inlet and outlet temperature to the RF were measured, together with the flow.

The measured inlet temperature, ambient temperature and water flow were used as inputs to the simulation model. Outlet water temperature and zone air temperature from the simulations were compared to the measured values. After a calibration process, the radiant floor model was validated.

2.3. Typical apartment building model

A model of an apartment which is located in the 2nd floor of the GEL was given to the author by GEL students. The aim was to find out if the installed RF could be used as a HES for this apartment. Model dimensions and properties are given in Fig. 4. WinID 2003 windows are used. Three different zones are modelled. An occupancy schedule for 3 persons is modelled, see Table 1.The activity of the persons in the living room is labeled "Seating, eating" in the standard ISO7730, while for the bedroom "Seated, at rest". In the living room there are also implemented internal gains from a computer of 140 W and 5 W/m^2 of artificial lighting heat gain which follows the occupancy schedule. The ventilation is demand controlled and follows the occupancy schedule for the entire model. The rate is set to 26 kg/h/person, plus a constant air exchange rate of 0.15 h^{-1} for removal of pollutants from materials. Inlets are assumed in bedrooms, and outlet in living room. A type91 heat exchanger is used to model a constant 90 % efficiency heat recovery unit. An infiltration of 0.4 h^{-1} is assumed. Water flow to bed rooms is 40 kg/hr/m^2, and to living room 9 kg/hr/m^2, as the living room has a smaller heat load.

The validated radiant floor model was implemented. The living room has three loops with a distance between the tubes of 15 cm. Bedrooms have one loop per zone, but also have a higher heat load. Consequently, the distance between the tubes is set to 12 cm.

Weather imposed is the typical meteorological year (.tm2) for Shanghai. Design outdoor temperature is - 4°C. Only the heating season (November-April) is considered.

Table 1
Occupancy schedule used in the typical apartment model.

	Persons	Weekdays	weekends
Living room	3	07:00 - 08:00 and 16:00-23:00	08:00 - 11:00 and 17:00-24:00
Room A	1	23:00 - 07:00	24:00 - 08:00
Room B	2	23:00 - 07:00	24:00 - 08:00

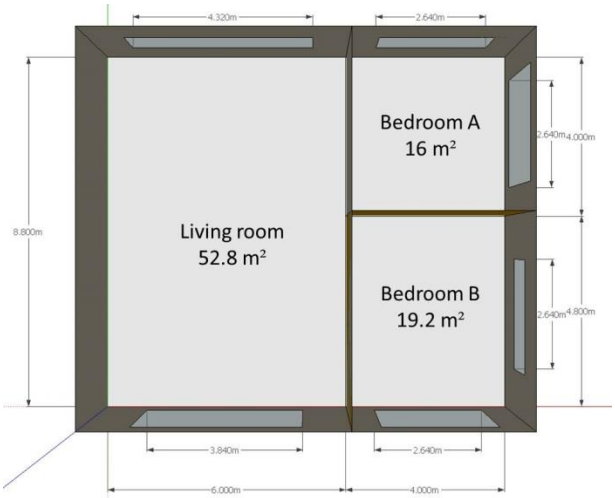

Wall	Layer	Thickness [m]	Conductivity [W/mK]	Thermal Capacity [kJ/kgK]	Density [kg/m³]	Thermal resistance [m²K/W]
Ext	GAS_CONCRE	0.1	0.28	1	700	0.36
	PERPENDICU	x	x	x	x	0.13
	MINERAL_WO	0.05	0.04	0.9	80	1.13
	ALUMINUM	0.002	200	0.86	2700	0.00
Adj	LIME_CEM_M	0.02	0.97	1	1800	0.02
	GAS_CONCRE	0.2	0.28	1	700	0.72
Ceil/floor	CONC_SLAB	0.12	1.14	1	1400	0.11
	LIGHTWEI_C	0.045	0.56	1	1000	0.08
	CEMENT_MOR	0.07	1.39	1	2000	0.05
	SPRUCE_PIN	0.012	0.14	2	600	0.09
Act	ACTIVELAYERC	0.055	0.28	0.7	1200	0.20
	LAYERDX15*	x	x	x	x	x
	POLYSTYREN	0.05	0.03	1.25	25	2.00

WinID	Description	Design	U-Val...	g-Val...	T-sol	Rf-sol	T-vis
1002	InsulatingGlass, 2.8	4/16/4	2.83	0.755	0.693	0.126	0.817
4001	Insulating, 0.7, Krypton	4/8/4/8/4	0.68	0.407	0.268	0.231	0.625
2003	Insulating,Kr, 1.1 71/60	4/16/4	0.86	0.598	0.426	0.266	0.706

Fig. 4. Building model. Height of zones is 3 m. North is upwards. Boundary condition for the west wall and floor is 22°C. Ceiling is an exterior surface. The roof of the building has a large shading construction. To model this, the solar absorptance was set to 0.1. Layer properties to the right. The SPRUCE_PIN is the wood floor covering. "Act" is the RF with concrete and insulation layer properties. Values are from the calibrated model.

2.4. System simulation models

A total system simulation was conducted in a revised building model to analyze the system in a modern super-insulated building. Two different connection principles between source and load were simulated. The first is a direct connection where the heat source is connected directly to the load. The other is an indirect connection where a buffer/storage tank is separating the source and load. RF and FCU as heat emitting systems were simulated and the results compared.

2.4.1. Super-insulated apartment building model

The typical apartment building model was revised to passive house standard by implementing thermal resistances in the wall constructions. The new U-values together with the requirements can be seen in Table 2. Window model 4001 from Fig. 4 was used. An infiltration of 0.3 h^{-1} is assumed.

Long simulation times led to a decision to omit the ventilation calculations. This is not considered to have altered the final results significantly. The rest of the model is identical to the typical apartment.

Table 2
U-values of exterior surfaces used in the revised model.

Construction	Old U-value (W/m^2K)	New U-value (W/m^2K)	Requirement (W/m^2K)
Exterior wall	0.574	0.216	0.22
Roof	0.342	0.172	0.18
Windows	0.860	0.680	0.80

The boundary wall and floor are considered adjacent surfaces and their constructions from the typical apartment are kept. Values for passive house requirements are from Byggforskserien [33].

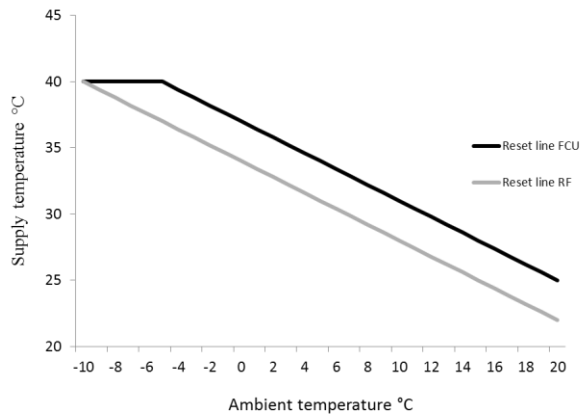

Fig. 5. The outdoor temperature reset lines used for supply temperature set-points.

2.4.2. Radiant floor

The system simulation model with an RF as the heat emitting system is depicted in Fig. 6. The ASHP model "Type 401 Compressor heat pump including frost and cycle losses" was utilized. The heat pump has a heating power of 1.2 kW at design conditions. A TRNSYS Type 4a "Stratified storage tank" with two nodes of 0.5 m each was chosen. Flow to each zone is 10 $kg/h/m^2$ and is controlled by an on/off controller, which measures the zone operational temperature. Set-point for living room is 23°C and for bedrooms 22°C. An outdoor temperature reset line (Fig. 5) decides the set-point temperature for the supply water. In the direct connection, the heat pump condenser outlet temperature is controlled by the reset line. In the indirect connection, a 3-way mixing valve is controlled by the reset line. Circulators are not simulated. A small one-node storage tank is modelled as the volume of the heating water in the system, which is approximated to 50 L. Control differential for the heat pump is $\pm$ 3°C. For the RF zone valve controllers it is $\pm$ 1°C for the direct connection and $\pm$ 0.5°C for the indirect.

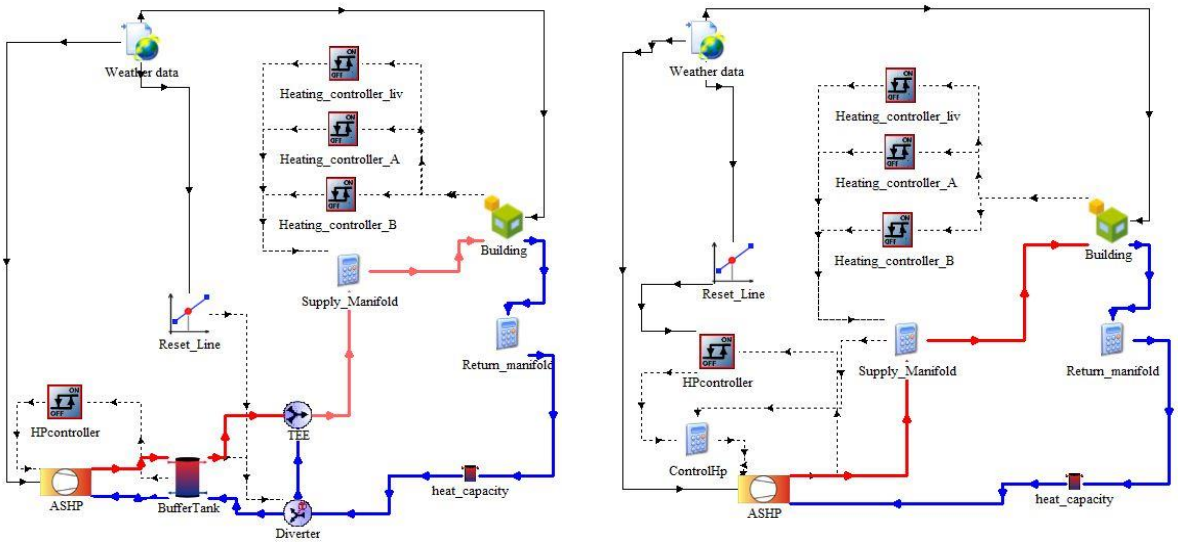

Fig. 6. Simulation studio screenshot simplified to show how the radiant floor system model is built. Left side shows the indirect connection and the right side the direct connection.

2.4.3. Fan coil unit

Modern fan coil units can be operated with lower supply temperatures, and are equipped with more silent fans. This makes them an interesting solution as a heat emitting system.

A system simulation model with an FCU as a heat emitting system was simulated, and is depicted in Fig. 7. The heat source and distributions systems are the same. The only difference is the heat emitter and the supply temperature. As FCUs have higher supply temperature requirements than RF, the upper reset line in Fig. 5 was used. An FCU from the supplier Sabiana S.p.A. [34] was modelled as a simple heat exchanger. The model was calibrated using measurements for the FCU "Carisma CRC13", as given by the supplier in the reference. A tube and shell heat exchanger model, type 5g in TRNSYS, with a constant overall heat transfer coefficient of 83.3 W/K and 1 shell pass was found to be closest to the measured values.

The FCU is controlled in 6 different stages in reality, but was simulated to operate continuously within its operative range. Four 0.9 kW FCUs were implemented into the apartment: two in the living room and one in each bed room. The total nominal heating power is 41 W/m^2, and is a purely convective gain to the zone air node. The FCUs are controlled by a P-controller with a gain constant of 1.To avoid the constant error associated with P-controllers, a hysteresis is modelled with on/off controllers connected in series with the P-controllers. When the P-controller reaches the minimum of the operative range of the FCU it usually turn the FCU off, but with this approach it keeps the FCU running at its minimum until the zone temperature reaches the upper differential of + 0.3°C. The air flow and water flow through the fan coils were interpolated between the stages according to the output signal from the controller. Flow in each stage is found in the product sheet.

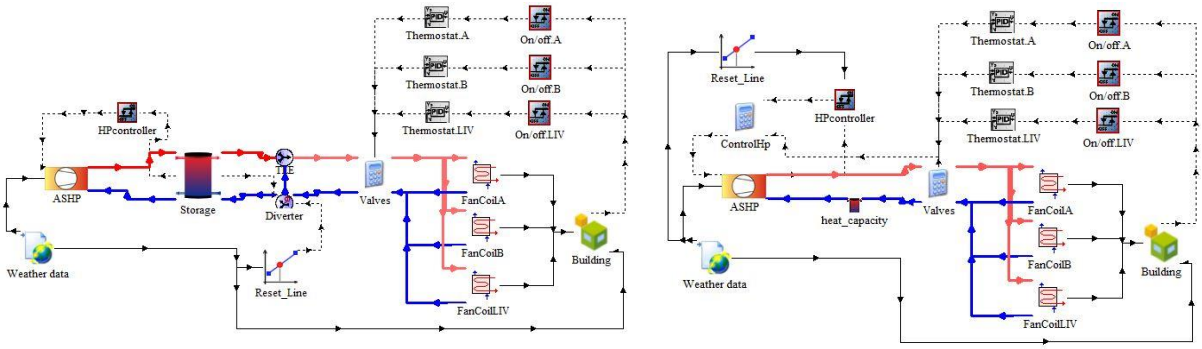

Fig. 7. Simulation studio screenshot simplified to show how the fan coil unit system model is built. Left side shows the indirect connection and the right side the direct connection. Outputs from "FanCoilLiv" are multiplied by 2 to simulate two fan coils in the living room.

3. Results

3.1. Validation

Input data is from an experiment conducted December 8th and comprises about 22 hours of operation. The validation of the calibrated radiant floor model is presented in Fig. 8. Indoor air temperature is virtually equal, and only small discrepancies are shown in floor outlet water temperature. The flow through the floor increases during the night. A small phase-shift is seen between the simulated and measured outlet temperatures.

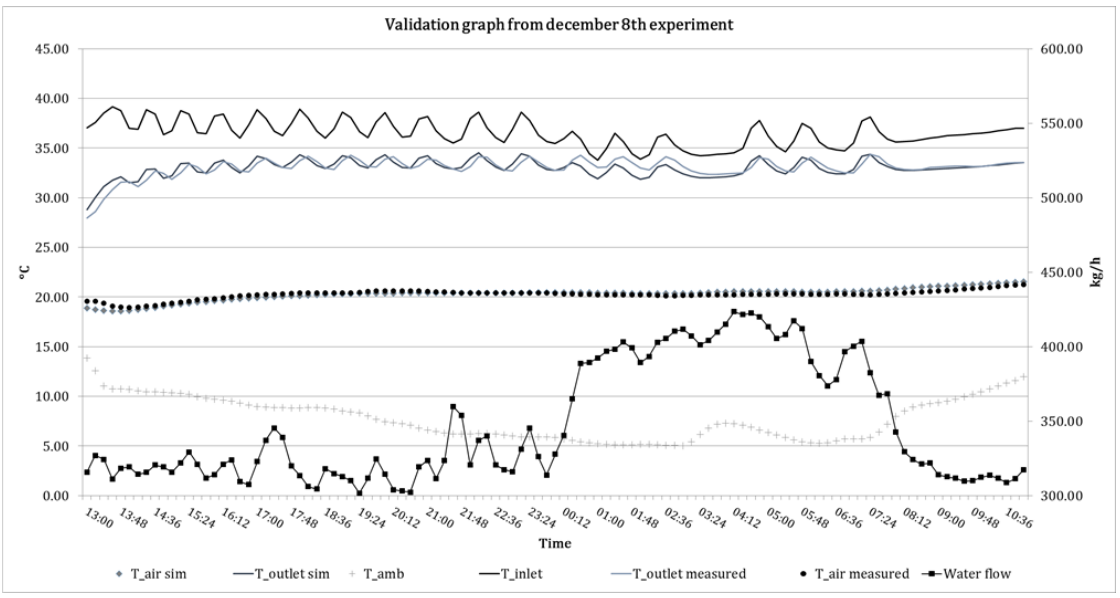

Fig. 8. Validation of the calibrated active layer model in TRNSYS Type 56 for the radiant floor at the Green Energy Laboratory.

3.2. Typical Chinese apartment model

Maximum heat load calculations were performed with two different types of windows and for two different climates. Table 3 contains the results. Windows of U-value of 0.86 is used in the analysis. In Shanghai, the maximum heat load is 41 W/m² accordingly.

Table 3
Heat loads under different climates

Window U-value [W/m²K]	Design outdoor temperature	Maximum heat load [W/m²]
2.89	-4 °C	51
	-14 °C	72
0.86	-4 °C	41
	-14 °C	57

Maximum heat loads for the model with windows installed at GEL and proposed new windows. Air temperature of the zones 22°C.

Seasonal simulation showed a heat demand of 94 kWh/m²a. Average temperatures were very close to the set-point. Very good thermal comfort (PVM) was noted. 12 kWh/m²a was lost to the boundary underneath the RF.

The performance of the floor is summarized in Table 4. Three supply temperatures and two RF designs were simulated. The two designs have different distance between tubes, otherwise they are equal. In these simulations the same distance between tubes were prescribed for all zones. A thermal comfort requirement of maximum surface temperature 27°C leads to a maximum RF heating power of 49 W/m² for the living room and 56-57 W/m² in the bedrooms. This difference is due to bigger window and external wall areas of the bedrooms. With a shorter distance between tubes, a higher heating power is achieved with the same water temperature.

Table 4
Heat transfer rates and corresponding surface temperatures.

Supply temperature	Heat transfer to zone [W/m²]			Surface temperatures [°C]		
	Liv	A	B	Liv	A	B
Distance between tubes 12 cm in all zones						
45 °C	55.0	57.4	57.2	27.8	27.1	27.3
42 °C	48.3	50.5	50.3	27.0	26.3	26.4
40 °C	43.8	46.0	45.8	26.3	25.7	25.8
Distance between tubes 15 cm in all zones						
45 °C	49.0	51.0	50.9	27.0	26.4	26.5
42 °C	43.0	45.0	44.8	26.3	25.6	25.7
40 °C	39.1	41.0	40.8	25.7	25.1	25.2

The air temperature of the room in these simulations is set to constant 21°C. Flow is at its maximum of 40 kg/hr/m². The installed radiant floor at GEL has a distance of 15 cm between tubes.

3.3. Comparison between RF and FCU for super-insulated building model

A maximum heat load of 23 W/m^2 is achieved with the revised building model. The two heat emitting systems cause different heat demands: 46 kWh/m^{2}a for the RF and 41 kWh/m^{2}a for the FCU.

Table 5 is a result summary of the total system energy analysis. Defrosting losses calculation caused the simulation to crash and was omitted. On/off cycle numbers are included as an indicator of operational stability. Least stable was the FCU with a direct connection, and cycling times at low loads were as low as 12 minutes. Total COP assumes direct electrical heating as secondary heat source and is equal to heat demand divided by total electrical energy used by compressor and electric heater. Total energy is the total electricity consumption of the system. Heat losses in storage and distribution as well as the electricity consumption of circulators are neglected. The heat demand for the RF is higher, but the total electricity consumption lower, due to a better COP.

Table 5
Total system simulation results summary

Heat emitter	Connection principle	On/off cycles	Seasonal COP	Demand coverage	Total COP	Total energy kWh/m^{2}a
RF	Direct	1856	4.3	97 %	4.0	11.6
RF	Indirect	360	4.0	98 %	3.8	12.1
FCU	Direct	4194	3.7	97 %	3.3	12.6
FCU	Indirect	445	3.5	99 %	3.4	12.1

Maximum heat load at 2 kW, total heat demand 46 kWh/m^{2}a with radiant floor and 41 kWh/m^{2}a with fan coil units. Tank volume is 300 L. Heat pump capacity is 1.2 kW for the condenser power at design conditions, which are -4°C ambient temperature and 40°C condenser outlet temperature. COP not including icing and defrosting losses.

4. Discussion and conclusion

Hydronic radiant floors are being employed in new building projects in China today. However, there are still problems with the design and operation, and the expected energy saving and comfort is not always achieved. This paper seeks to confirm the energy saving potential, and performance, of radiant floors and to compare it to another low temperature heating emitter in a total system simulation analysis.

The RF installed at the GEL is modelled in TRNSYS and calibrated to measurements. Uncertainties in the flow measurements were detected during the experiments. With a calibration of the flow, the simulation model and measurements correlated very well. The small phase-shift seen in the measured and simulated outlet temperatures is caused by the limitation of the simulation model to capture latency in the system due to low flow velocities and long pipes.

It was shown that the installed RF has a heating power of about 50-57 W/m^2, depending on the ratio of external surfaces of the zone. The standard building model has a maximum heat load of 51 W/m^2. It is at the border of what the RF can supply. Changing to better windows lowered the maximum heat load to 41 W/m^2, which is well within the heating power range of the RF. However, in a colder climate this is not a sufficient level of insulation, as the heating load with an outdoor design temperature of

-14°C is 57 W/m^2. It can be concluded that a high level of insulation is required if radiant floors are to be considered as the only heat emitter in a cold climate.

On/off mass flow control to each zone was shown to be sufficient to ensure a stable operative zone temperature. However, direct solar gains, which could lead to significant overheating, are not considered in this analysis.

Results from the total system simulations showed that a heat pump which has 60 % heat load coverage at design conditions can cover up to 99% of the heat demand. This is because the typical meteorological year model does not incorporate worst case scenarios, but rather more average climate data. Another reason is the very mild Shanghai climate, which increases the performance of the heat pump.

It is affirmed that a stable system operation can be achieved, as buffer tanks caused the number of cycles to drop significantly. This was especially evident for the FCU system. Even though there is a small reduction of heat pump COP, heat storage tanks improve the system operation.

FCUs as a heat emitting system showed an 11 % lower heat demand than the RF system. The reason is that some of the heat from the RF is lost to the boundary underneath the floor, and that higher transmission losses occur due to higher surface temperatures of external walls and windows. However, the FCU requires higher supply temperature, which decreases the performance of the heat pump. It was shown that this COP reduction counters the saved energy, and that the RF system has lower total energy consumption.

TRNSYS does not capture local thermal comfort effects like air movement, stratification and short-waved solar irradiation. A detailed computer fluid dynamics (CFD) analysis should be performed on both heat emitting systems to make a thorough thermal comfort assessment of each system.

The simulated ASHP has only one operational stage. Modern heat pumps can be continuously controlled by the means of frequency inverters. A similar analysis using this kind of heat pumps would be interesting.

Acknowledgements

The author would like to thank the master thesis supervisors at NTNU: Professor Vojislav Novakovic and Associate Professor Laurent Georges. A special gratitude is expressed to Professor Yanjun Dai at SJTU for supervising the author during the stay in Shanghai.